CENTRO INTERNACIONAL DE ESTUDOS
DE DOUTORAMENTO E AVANZADOS
DA USC (CIEDUS)

TESE DE DOUTORAMENTO

PHASE BEHAVIOUR OF SURFACE ACTIVE IONIC LIQUIDS FOR ENHANCED OIL RECOVERY

Iria Rodríguez Escontrela

ESCOLA DE DOUTORAMENTO INTERNACIONAL

PROGRAMA DE DOUTORAMENTO EN ENXEÑARÍA QUÍMICA E AMBIENTAL

SANTIAGO DE COMPOSTELA

2017

USC
UNIVERSIDADE
DE SANTIAGO
DE COMPOSTELA

DECLARACIÓN DO AUTOR DA TESE

Phase Behaviour of Surface Active Ionic Liquids for Enhanced Oil Recovery

D./Dna. Iria Rodríguez Escontrela

Presento miña tese, seguindo o procedemento adecuado ao Regulamento, e declaro que:

1) A tese abarca os resultados da elaboración do meu traballo.
2) No seu caso, na tese se fai referencia as colaboracións que tivo este traballo.
3) A tese é a versión definitiva presentada para a súa defensa e coincide ca versión enviada en formato electrónico.
4) Confirmo que a tese non incorre en ningún tipo de plaxio de outros autores nin de traballos presentados por min para a obtención de outros títulos.

En Santiago de Compostela, 27 de Outubro de 2017

Asdo. Iria Rodríguez Escontrela

USC
UNIVERSIDADE
DE SANTIAGO
DE COMPOSTELA

AUTORIZACIÓN DO DIRECTOR / TITOR DA TESE

Phase Behaviour of Surface Active Ionic Liquids for Enhanced Oil Recovery

D./Dna. Ana María Soto Campos

INFORMA/N:

Que a presente tese, correspóndese co traballo realizado por D/Dna. ***Iria Rodríguez Escontrela****, baixo a miña dirección, e autorizo a súa presentación, considerando que reúne os requisitos esixidos no Regulamento de Estudos de Doutoramento da USC, e que como director desta non incorre nas causas de abstención establecidas na Lei 40/2015.*

En Santiago de Compostela, 27 de Outubro de 2017

Asdo. Ana María Soto Campos

USC
UNIVERSIDADE
DE SANTIAGO
DE COMPOSTELA

Acknowledgements

The last four years, I had the privilege of being part of the Group of Phase Equilibria and Separation Processes of the University of Santiago de Compostela working as a PhD student. The present thesis tries to summarise the experimental work carried out in this period. Now that the work is concluded and a new cycle is coming ahead, I would like to thank all the people who helped me one way or another.

In first place I would like to thank Professors Alberto Arce and Ana Soto. They gave me the great opportunity of being part of this research group. I am particularly grateful to my supervisor Professor Ana Soto. She always offered me her valuable help and knowledge, teaching and giving me advice in every professional and personal aspect of my life and making things easier. Also thank you both for treating your PhD children as we all were members of a big family. Of course this acknowledgement is also extended to Eva Rodil for her kind dedication. In the same way, I want to thank Óscar Rodríguez, for his advice and dedication, and Héctor Rodríguez, who always was there to help and try to make things work putting his great experience in ionic liquids at the service of all group members.

The adventure started in the Master with Lidia and Santi. Thank you both for all your help, your friendship and the good times that we spent together. When I first joined the group I found the open arms of Alicia, Borja, Iago and María. I can undoubtedly say that I have found true friends in them. Although both Marlen and Raquel arrived later, we all quickly became not only good lab mates but also a great family. I would also thank Alberto, Adrián, Manu, Oussama and all the people that have been in the lab. I realised how lucky I was having such a good working environment; they were surely responsible for that.

In the last period I also had the opportunity to spend three amazing months at Rice University (Houston, TX). Professor George Hirasaki allowed me to form part of his excellent group for this period, from which I learned many things. I want to thank my supervisor, Maura Puerto, she taught me everything about surfactants, but also principles like rigor. She made me feel like home even being thousands of miles away. Thank you for being a great teacher and opening your home to me. I would like to acknowledge also Professor Clarence Miller for his help; he was always generous to share his knowledge.

I also want to thank Phases Equilibrium Calculations Group from University of Alicante. Correlations presented in this thesis were possible thanks to their help.

But the support received during these years does not only come from the work. Thus I want to thank my friends (Lucenses, Arqueros, Bovedenses and Houston Cuadrilla) for their support over the years and for being always there.

I also want to acknowledge Tristán for his understanding and patience. Thank you for your unconditional support. *Grazas lercho.*

Finally, but very, very important I want to thank my family. An especial mention is referred to my parents, Celia and José Manuel. This thesis work is now finished thanks to and for them. It wouldn't have made sense without them by my side. *Papá, Mamá gracias por estar siempre a mi lado y apoyarme incondicionalmente. Gracias también a mi tía Rosina y mis primos.*

Closing these lines, I want to express my acknowledge to the University of Santiago de Compostela, and to the Ministry of Economy and Competitiveness of the Spanish Government for financial support through project CTQ2012-33359, and for having awarded me with a FPI grant (BES-2013-062735). Thanks to Repsol and CYTEC for kindly supplying the fuel samples and some ionic liquids, respectively.

Iria Rodríguez Escontrela

Abstract in English

Chemical flooding with surfactants is well known to have huge potential in Enhanced Oil Recovery (EOR) processes. One of the main challenges for surfactant EOR is finding a surfactant or a surfactant blend able to generate a Winsor Type III microemulsion. The main objective of this thesis is to obtain optimal formulations with surface-active ionic liquids (SAILs) able to improve current surfactant EOR methods.

In the first stage, the behaviour of three SAILs ($[P_{6\ 6\ 6\ 14}][DCA]$, $[P_{6\ 6\ 6\ 14}][(iOc)_2PO_2]$ and $[P_{4\ 4\ 4\ 14}]Cl$) in the presence of water and oil was studied. Liquid-liquid equilibrium data were obtained and correlated for the ternary systems water + SAIL + *n*-alkane (*n*-dodecane or *n*-hexane) at different temperatures and atmospheric pressure. Winsor Type III systems were found in all the cases except for $[P_{4\ 4\ 4\ 14}]Cl$. The very low solubility of these surfactants in water, and a reduction of the water/oil interfacial tension far from the ultra-low required values, counts against the use of these SAILs for EOR.

Secondly, a set of water soluble SAILs, two anionic ($[P_{4\ 4\ 4\ 1}][DS]$ and $[C_4mim][AOT]$) and two cationic ($[C_{12}mim]Br$ and $[P_{4\ 4\ 4\ 14}]Cl$) were tested. Salinity scans were carried out in the presence of brine at different temperatures looking for Winsor Type III behaviour. Results indicated that, if used alone, these SAILs are too hydrophilic or too lipophilic for application in EOR.

Finally, blends containing these SAILs or a SAIL and a common EOR surfactant ($IOS_{15\text{-}18}$) were tested by means of blend scans at a fixed salinity. Based on the results obtained, a formulation containing a blend of $IOS_{15\text{-}18}$ and $[C_{12}mim]Br$ is suggested as the best option, since an ultra-low interfacial tension was achieved and an injectable optimal formulation, tolerant to divalent ions, was found at a particular salinity.

KEYWORDS: Enhanced oil recovery, surfactant, interfacial tension, ionic liquid, phase behaviour.

Resumen (Spanish)

El uso de surfactantes para la extracción mejorada de petróleo (EOR, por sus siglas en inglés) tiene un gran potencial. El principal reto es encontrar un surfactante o mezcla de surfactantes capaz de generar una microemulsion Winsor Tipo III. El objetivo principal de esta tesis es obtener formulaciones óptimas con líquidos iónicos surfactantes (SAILs, por sus siglas en inglés) capaces de mejorar los actuales métodos EOR con surfactantes.

En una primera etapa, se estudió el comportamiento de fase de tres SAILs ($[P_{6\,6\,6\,14}][DCA]$, $[P_{6\,6\,6\,14}][(iOc)_2PO_2]$ y $[P_{4\,4\,4\,14}]Cl$) en presencia de agua e hidrocarburo. Se determinaron y correlacionaron los datos de equilibrio líquido-líquido para los sistemas ternarios agua + SAIL + *n*-alcano (*n*-dodecano o *n*-hexano) a diferentes temperaturas y presión atmosférica. Se encontraron sistemas Winsor Tipo III en todos los casos, excepto con el $[P_{4\,4\,4\,14}]Cl$. La muy baja solubilidad de estos tensioactivos en agua, y una reducción de la tensión interfacial agua/hidrocarburo lejos de los valores ultra bajos exigidos, aconsejan no utilizar estos SAILs para EOR.

En segundo lugar, se evaluó un conjunto de SAILs solubles en agua, dos aniónicos ($[P_{4\,4\,4\,1}][DS]$ y $[C_4mim][AOT]$) y dos catiónicos ($[C_{12}mim]Br$ y $[P_{4\,4\,4\,14}]Cl$). Se llevaron a cabo escaneos de salinidad en la presencia de salmuera a diferentes temperaturas para encontrar un comportamiento Winsor Tipo III. Lo resultados indicaron que estos SAILs son demasiado hidrofílicos o lipofílicos para su aplicación en EOR.

Finalmente, se estudiaron mezclas de SAILs o de un SAIL con otro surfactante empleado en EOR ($IOS_{15\text{-}18}$) a una salinidad fija mediante escaneos de mezcla. Basándose en los resultados, la mejor formulación encontrada sería la hallada con una mezcla de $IOS_{15\text{-}18}$ y $[C_{12}mim]Br$, debido a que se lograron valores ultrabajos de tensión interfacial y se obtuvo una mezcla homogénea inyectable y tolerante a la presencia de iones divalentes.

PALABRAS CLAVE: Extracción mejorada de petróleo, surfactante, tensión interfacial, líquido iónico, comportamiento de fase.

Resumo (Galician)

O emprego de surfactantes nos procesos de extracción mellorada de petróleo (EOR, polas siglas en inglés) ten un gran potencial. Un dos retos principais é encontrar un surfactante ou mestura de surfactantes capaz de xerar unha microemulsion Winsor Tipo III. O obxectivo principal desta tese é obter formulacións óptimas con líquidos iónicos surfactantes (SAILs, polas siglas en inglés) capaces de mellorar os actuais métodos de EOR con surfactantes.

Nunha primeira etapa, estudouse o comportamento de fase de tres SAILs ($[P_{6\,6\,6\,14}][DCA]$, $[P_{6\,6\,6\,14}][(iOc)_2PO_2]$ e $[P_{4\,4\,4\,14}]Cl$) en presenza de auga e hidrocarburo. Os datos de equilibrio líquido-líquido para os sistemas ternarios auga + SAIL + *n*-alcano (*n*-dodecano o *n*-hexano) foron determinados e correlacionados a diferentes temperaturas e presión atmosférica. Encontráronse sistemas Winsor Tipo III en tódolos casos, excepto co $[P_{4\,4\,4\,14}]Cl$. A moi baixa solubilidade destes tensioactivos na auga, e unha redución da tensión interfacial auga-hidrocarburo lonxe dos valores ultrabaixos esixidos, aconsellan non empregar estes SAILs para EOR.

En segundo lugar, foi avaliado un conxunto de SAILs solubles en auga, dous aniónicos ($[P_{4\,4\,4\,1}][DS]$ e $[C_4mim][AOT]$) e dous catiónicos ($[C_{12}mim]Br$ e $[P_{4\,4\,4\,14}]Cl$). Leváronse a cabo escáneos de salinidade na presenza de salmoira a diferentes temperaturas para encontrar un comportamento Winsor Tipo III. Os resultados indicaron que os SAILs estudados son demasiado hidrofílicos ou lipofílicos para a súa aplicación en EOR.

Finalmente, estudáronse mesturas de dous SAILs ou dun SAIL con outro surfactante empregado en EOR ($IOS_{15\text{-}18}$) a una salinidade fixa mediante escaneos de mestura. Baseándose nos resultados, a mellor formulación encontrada sería a que contén unha mestura de $IOS_{15\text{-}18}$ e $[C_{12}mim]Br$, debido a que se lograron valores ultrabaixos de tensión interfacial e se obtivo unha disolución homoxénea, inxectable e tolerante á presenza de ións divalentes.

PALABRAS CHAVE: Extracción mellorada de petróleo, surfactante, tensión interfacial, líquido iónico, comportamento de fase.

USC
UNIVERSIDADE
DE SANTIAGO
DE COMPOSTELA

CONTENTS

1. OBJECTIVES

USC
UNIVERSIDADE
DE SANTIAGO
DE COMPOSTELA

In recent decades, Ionic Liquids (ILs) have been proposed for a great number of applications due to their interesting set of physicochemical properties. The potential for tailoring them to solve problems in Science and Technology justifies the huge number of studies where these salts are involved. For instance, specific ions can be selected in order to give a surface active character to ILs. Thus, Surface Active ILs (SAILs) can improve methods or even solve problems that traditional surfactants cannot. One of those applications where conventional surfactants fail is Enhanced Oil Recovery (EOR). Surfactant flooding is likely the most promising technique to recover difficult-to-access oil. However, it has not been easy to obtain a surfactant with the required properties: the ability to solubilise equilibrated proportions of water and oil (resulting in ultra-low interfacial tension), stability with temperature and in presence of mono and divalent ions, low cost, etc. This has led to a very limited number of applications of this EOR method in real reservoirs. So SAILs have been recently proposed to improve current EOR methods. Nonetheless, the research carried out on this topic up to now is in general not adequately oriented for practical purposes, and proposed formulations are still far from being optimal.

The main objective of this thesis is to obtain optimal formulations with SAILS able to improve current surfactant EOR methods. To accomplish that goal, two specific objectives, one with a more fundamental focus and the other with a more applied character, are defined.

The first specific objective is the study of phase equilibria, Liquid-Liquid (LLE) and Liquid-Liquid-Liquid (LLLE), for ternary systems composed of a SAIL, water and an *n*-alkane. In particular, the following systems:

- *Water + trihexyltetradecylphosphonium dicyanamide ($[P_{6\,6\,6\,14}][DCA]$) + n-hexane*
- *Water + $[P_{6\,6\,6\,14}][DCA]$ + n-dodecane*
- *Water + trihexyltetradecylphosphonium bis(2,4,4-trimethylpentyl)-phosphinate ($[P_{6\,6\,6\,14}][(iOc)_2PO_2]$) + n-dodecane*
- *Water + tributyltetradecylphosphonium chloride ($[P_{4\,4\,4\,14}]Cl$) + n-dodecane*

The determination of these equilibria will generate knowledge about the behaviour of SAILs in the presence of water and oil. These phase diagrams are of interest not only for EOR, but also for other applications like separations and reactions based on microemulsions.

Focusing on EOR, the influence of NaCl in the behaviour of these systems will be analysed. Moreover, ILs for these studies were selected to continue a previous work carried out in our research group. Thus, the influence of the number of carbon atoms in the hydrocarbon, the type of anion, and the length of the alkyl chains in the phosphonium cation will be analysed. The obtained data will be correlated in order to facilitate their use in simulation and design processes.

The second specific objective, more focused on real EOR applications, aims to find optimal formulations with SAILs. Tools traditionally used in surfactant EOR will be applied. As salinity and temperature play a definitive role in this application, visual phase behaviour tests (salinity scans) of multicomponent systems containing different salts (including divalent ions) will be carried out for a set of anionic and cationic SAILs at different temperatures. Namely, the selected anionic SAILs are: tributylmethylphosphonium dodecylsulfate ($[P_{4\,4\,4\,1}][DS]$) and 1-butyl-3-methylimidazolium dioctyl sulfosuccinate ($[C_4mim][AOT]$). Also several cationic SAILs will be tested: 1-dodecyl-3-methylimidazolium bromide ($[C_{12}mim]Br$) and tributyltetradecylphosphonium chloride ($[P_{4\,4\,4\,14}]Cl$). As some of these SAILs are designed for the application and will be synthesised for the first time, a characterisation will be carried out, determining the physical and thermal properties and studying their aggregation behaviour in an aqueous solution.

As part of the studies related to the second objective, the formulation of surfactant blends to adjust Hydrophilic-Lipophilic-Balance (HLB) or to take advantage of the synergistic behaviour in mixed systems, due to the formation of ion pairs, will be studied. The possibility of combining the previous tested SAILs or a SAIL with a common EOR surfactant ($IOS_{15\text{-}18}$) will be evaluated using blend scans to find an injectable optimal formulation, tolerant to divalent ions, at a particular salinity.

2. INTRODUCTION

USC
UNIVERSIDADE
DE SANTIAGO
DE COMPOSTELA

2.1. OIL RECOVERY

2.1.1. Energy demand

World energy consumption has quickly increased since the Industrial Revolution and, according to the U.S. Energy Information Administration [1], this consumption will grow 48% by 2040 (Figure 2.1).

In recent years there has been an increase in the exploitation of renewable and potentially renewable energy resources such as biomass, wind, solar, hydro, geothermal, etc. Accordingly, technologies have been developed and optimised to exploit these resources. Concerns about energy security, effects of fossil fuel emissions on the environment, sustainability world oil prices, etc. support expanded use of renewable energy sources and nuclear power. Renewables and nuclear power are the world's fastest-growing energy sources over the projection period shown in Figure 2.1. Renewable energy increases by an average 2.6% per year through 2040; nuclear power increases by 2.3% per year.

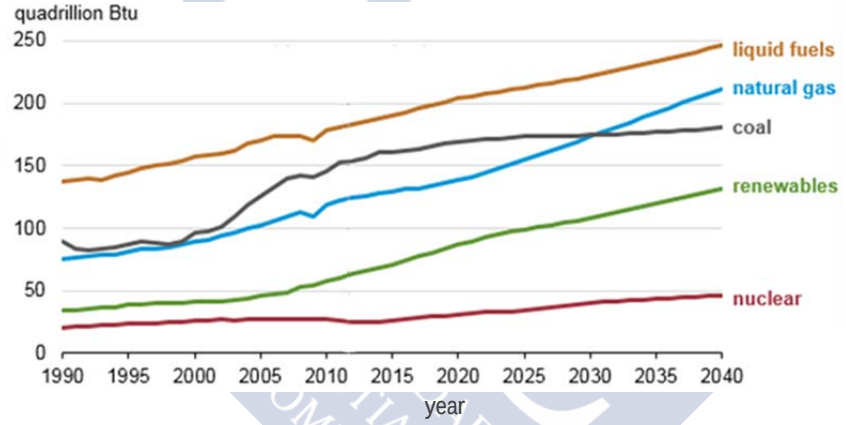

Figure 2.1. World energy consumption by source. U.S. Energy Information Administration's [1].

Even though non-fossil fuels are expected to grow faster than fossil fuels (petroleum and other liquid fuels, natural gas, and coal), fossil fuels still account for more than three-quarters of world energy consumption through 2040. Despite the need to move to renewable energies, today's dependence on fossil fuels, especially oil, as the primary energy source is a fact. Furthermore, oil is the basis of the petrochemical industry which generates thousands of chemical compounds used in the production of plastics, adhesives, detergents, dyes, fertilizers and many other products useful to society. With the

decline in oil discoveries during the last few decades, it is believed that better recovery technologies will play a key role in meeting the energy demand in years to come. If society wants to maintain its standard of living, humanity must fully exploit the oil resources at its disposal. Thus, there is considerable focus on renewed efforts to improve techniques that allow: better exploitation of wells that years ago were abandoned due to their poor output, the recovery of heavy oils, or taking advantage of tar sands.

2.1.2. Oil recovery stages

The overall process of exploitation of a reservoir is divided into three stages [2-4]. During primary recovery, extraction of oil occurs because of the pressure gradient between the interior and exterior of the reservoir. Expansion and subsequent release of the retained gas is produced. This process pushes the oil out of the well, until the pressure gradient decreases, causing a considerable decrease in the production rate. At this point, a typical production of 10-15% of the total oil reservoir is achieved, and another energy source must be applied to maintain oil production.

This "extra-energy" is applied during secondary recovery. Sometimes pumps on the surface or submerged are used to bring the oil to the surface. Other methods consist of the injection of different kinds of fluids in order to increase the pressure inside the well to maintain production. Among them, the most commonly injected fluids are water and petroleum gases. In the case of gas injection, a decrease in the fluid density inside the well occurs, while injecting water a mobilisation of the oil occurs due to viscous forces. Depending on the geological characteristics of the well and the physical properties of the crude oil, a recovery between 25-30% is achieved after the secondary recovery.

After primary and secondary recovery, approximately two thirds of the original oil remain inside the well. This is due to limitations of the processes. On one hand, the low permeability zones in the reservoir, the geometry of the well or preferential paths may cause that the injected fluid does not penetrate. On the other hand, the oil is retained discontinuously inside the pores by capillary forces.

Tertiary recovery, or EOR, consists of a set of methods in which different materials are introduced into a well in order to continue with the extraction of crude oil by exercising control over the wettability, the fluid properties and the flow in the wellbore, the interfacial tension

between oil and displacing fluid, or the pressure gradients needed to overcome the retaining forces.

When the full exploitation of reservoirs becomes economically profitable, EOR methods are the alternative to extract the difficult-to-access oil from the well. It is obvious that the economic viability of a tertiary recovery process depends on one hand on the costs of that exploitation, and on the other hand on the price of crude. A rise in oil prices implies that those wells whose production activity has ceased at the end of primary and secondary recovery processes can be subject to the application of EOR methods to continue their exploitation.

2.1.3. Enhanced Oil Recovery methods

All different EOR methods are based on at least one of the following objectives to facilitate oil extraction:

- The reduction in interfacial tension between oil and water.

- The improvement in the displacement ability of injected fluid in terms of an increase of the viscosity of the water or a decrease of the viscosity of the oil.

- The extraction of the oil by using a solvent.

EOR methods are usually classified into three groups: thermal, miscible flooding and chemical flooding methods, but also the use of microorganisms should be considered as a tertiary recovery method [4-6].

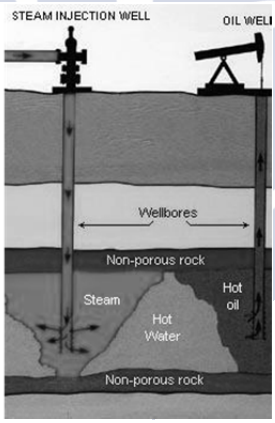

Figure 2.2. Thermal recovery by steam injection.

Thermal methods are based on reducing the oil viscosity in the wellbore. Several mechanisms are developed for that purpose. Steam injection (Figure 2.2) is the most common form of thermally EOR. Another method consists of the injection of oxygen-enriched air,

producing propagation of a combustion zone. The reduction in the viscosity of crude oil facilitates its drive towards the production wells. In general, wells containing heavy oil or sandstone reservoirs are liable to exploitation by such methods. There have also been modifications aimed to improve the process of steam injection by the addition of solvents, chemicals, gases or foams. Furthermore, several other less usual methodologies for thermal EOR have been proposed such as electric, electromagnetic and microwave heating.

Miscible flooding consists of the injection of a fluid into the reservoir at pressure levels such that it is miscible with the oil. The contact between the displacement fluid and the crude oil implies that a transfer between two phases takes place. The transport of components between phases provokes a modification of the properties of both, thus mobilising the oil. The most commonly used fluid for miscible flooding is CO_2 (Figure 2.3), but also hydrocarbons or nitrogen. The main limitation of this method lies in the reduced viscosity of the injected gas. The difference in viscosity between gas and oil implies adverse mobility ratio, and it may cause fingerings and preferential paths among the reservoir oil. The use of N_2 and hydrocarbons has been reported in several works. Nevertheless, due to the availability of inexpensive CO_2 from natural sources, CO_2 flooding has been the most common method used in miscible flooding. Alcohols have also been tested but the cost of the injected fluid becomes quite high.

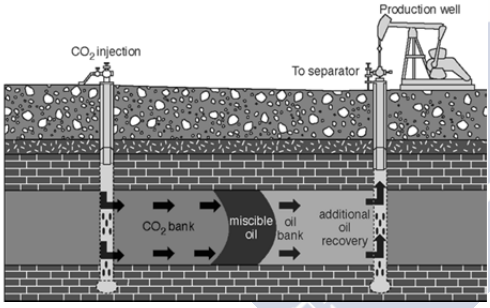

Figure 2.3. Miscible flooding using CO_2 as miscible gas.

Chemical methods [4, 7] represent an alternative to overcome the limitations that occur with the miscible flooding methods. They are based on the injection of water into the well together with chemicals of different natures. The intention with the addition of these chemicals is on one hand, to achieve a reduction in the interfacial tension between oil and water, and secondly to reduce the viscosity difference between the oil and displacing fluid through the increase of the viscosity of the

latter. In these methods, polymers, surfactants and alkaline or caustic chemicals are used.

In polymer flooding, polymers are dissolved in water, increasing its viscosity and thus reducing the difference between water and oil viscosities. This fact promotes the displacement not only of crude oil but also of water from the pores. Adsorption of polymer molecules in the surface of pores also occurs, blocking some channels and avoiding the filtration of water, increasing the effectiveness of the flooding.

Surfactant flooding (Figure 2.4) involves the use of aqueous solutions of surfactants as injection fluids, in order to achieve a significant reduction in the interfacial tension between oil and water. This reduction in the interfacial tension enhances the mobility of the oil retained in the pores, allowing it to be flushed out of the reservoir. It is necessary to take into account that a very low value of interfacial tension between displaced and displacing fluid is required for the mobilisation of the oil through the narrow capillary pores.

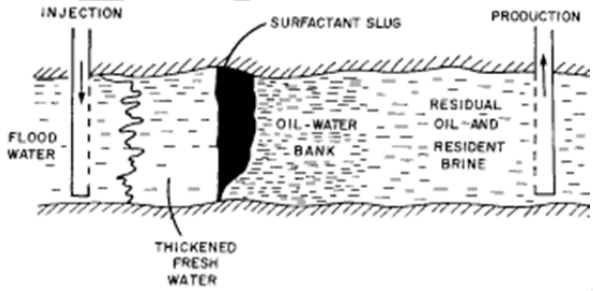

Figure 2.4. Principles of surfactant flooding [2].

Alkaline flooding is based on the formation *in situ* of surfactants by the interaction of the alkalis (from the alkaline solution flooding) with organic acids that are present in the oil. These generated surfactants reduce the interfacial tension between oil and water, and the wetting characteristics of the reservoir may also change, increasing the rate of displacement.

In most cases combined EOR methods are implemented. For instance, the Alkali/Surfactant/Polymer (ASP) flooding (Figure 2.5) combines all the advantages of the aforementioned methods.

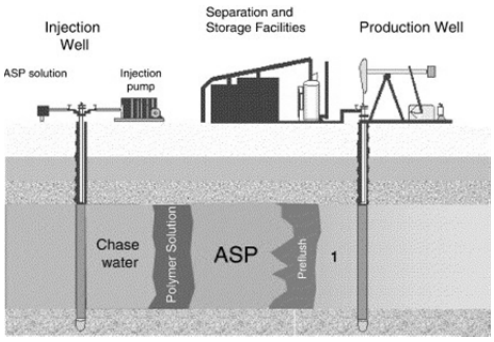

Figure 2.5. Principles of Alkali/Surfactant/Polymer (ASP) flooding.

Biological based technology can also be used in oil recovery. Microbial EOR processes involve the use of reservoir microorganisms or specially selected natural bacteria to produce specific metabolic events that lead to oil recovery. A variety of fermentation products are produced with different roles in EOR [8]: gases that reduce oil viscosity; bio-surfactants; bio-polymers; acids that improve the permeability and the porosity by dissolving carbonate precipitates; alcohols and ketones that are typical co-surfactants; and biomass that physically displace oil by growing between oil and rock/water surface. The injected bacteria and nutrients are inexpensive and easy to obtain and handle in the field, but the control over the microbial system is a serious challenge.

There are also some locally applied methods, among them the hydraulic fracturing, which are usually attributed to a special group called Oil Production Intensification methods. They increase for some period of time the current oil production (recovery) but they do not usually increase the final recovery rate as EOR methods do.

2.1.4. Surfactant flooding

Among chemical flood recovery methods, the addition of surfactants to the extraction fluid is a promising alternative.

The surface tension of a liquid changes when other substances are dissolved in it. The surface activity of a solute is its ability to change the surface tension of solvents. Solutes that reduce the surface tension of a solvent have positive surface activity, and those that do so to a significant extent are known as surface-active agents, or surfactants for short.

Surfactants are usually organic compounds that are amphiphilic, possessing both a polar hydrophilic group (the “head”) with affinity for polar solvents and a hydrophobic (lipophilic) non-polar moiety

(generally a hydrocarbon chain, the “tail”). However, amphiphiles do not have surface activity if their interactions with solvents are dominated by either their hydrophilic or their lipophilic moiety.

Surfactants are soluble in both organic solvents and water. They adsorb at a surface or fluid/fluid interface to alter the surface properties significantly; in particular, they reduce surface tension or interfacial tension.

Surfactant flooding is a multiple-slug process involving the addition of surface-active chemicals to water. These chemicals reduce the capillary forces that trap the oil in the pores of the rock. The surfactant slug displaces the oil forming a flowing oil-water bank that is propagated ahead of the surfactant slug. As surfactant contacts rock surfaces, wettability may be changed. A slug of water containing polymer, to increase viscosity, usually follows the surfactant solution to avoid digitations.

Another chemical flood recovery method that uses surfactants is the microemulsion or micellar flooding. In this case, oil and water are displaced by a microemulsion slug consisting of oil, water, surfactant, co-surfactant, electrolytes, etc. Two approaches are normally used. In the first process, a relatively low concentration (2-4%) surfactant microemulsion is injected to reduce the interfacial tension between the water and the oil. In the second process, a high concentration (8-12%) surfactant microemulsion is injected and the micelles solubilise the oil and water in the displacing microemulsion. Inside the reservoir, the process gradually reverts to a low-concentration flood. The mobility of the microemulsion can be controlled by tuning its viscosity [7].

Surfactants may be classified according to the nature of the hydrophilic group as anionic, cationic, zwitterionic and nonionic [9]. Anionic surfactants are most widely used in chemical EOR processes because they exhibit relatively low adsorption on sandstone rocks whose surface charge is negative. Nonionic surfactants primarily serve as co-surfactants to improve system phase behaviour. Although they are more tolerant of high salinity, their function to reduce interfacial tension is not as good as anionic surfactants. Quite often, a mixture of anionic and nonionic is used to increase the tolerance to salinity. Cationic surfactants can strongly adsorb in sandstone rocks; therefore, they are generally not used in sandstone reservoirs, but they can be used in carbonate rocks. Zwitterionic surfactants contain two active groups. The types of zwitterionic surfactants can be

nonionic- anionic, nonionic-cationic, or anionic-cationic. Such surfactants are temperature and salinity-tolerant, but they are expensive. A term amphoteric is also used elsewhere for such surfactants. Sometimes surfactants are grouped into low-molecular and high-molecular according to their weight. Within any class, there is a huge variety of possible surfactants [7].

Although the surfactant flooding technique is promising, its application to date has been limited due to the high cost of the surfactant and the difficulty in its recovery, as a result of its adsorption onto the oil bearing formation rocks. For these reasons, there is growing interest in finding new surfactants whose properties best fit the surfactant EOR requirements, and which optimise the process.

2.1.5. Laboratory tests for surfactant flooding

Solubilisation and reduction of the interfacial tension are two critical parameters to produce the mobilisation of the crude oil with surfactants. For that reason, after characterisation, the determination of phase behaviour and interfacial tension between the compounds involved in these EOR processes is the first step to optimise them.

2.1.5.1. Characterisation of surfactants

Critical micelle concentration

Critical micelle concentration (*cmc*) in defined as the concentration of surfactant above which micelles are spontaneously formed. Once the surfactant is introduced into the system, it will initially partition into the interface with its hydrophobic parts without contact with water, reducing the system free energy by lowering the energy of the interface. Subsequently, when the surface coverage by the surfactants increases and the surface free energy (surface tension) has decreased, the surfactants start aggregating into micelles, thus again decreasing the system-free energy by decreasing the contact area of hydrophobic parts of the surfactants with water. Upon reaching *cmc*, any further addition of surfactants will just increase the number of micelles (in the ideal case), as shown in Figure 2.6. Before reaching the *cmc*, the surface tension decreases sharply with the concentration of the surfactant. After reaching the *cmc*, the surface tension stays more or less constant and cannot be further reduced. This concentration is small, *cmc* is in the range of a few to tens of parts per million.

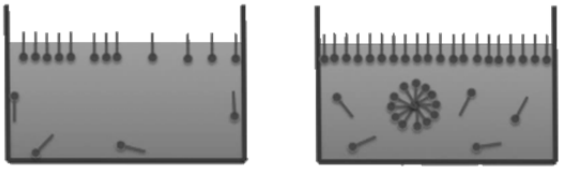

Figure 2.6. Surfactant molecules in solution at concentrations (a) below *cmc* (b) above *cmc*.

Physical properties of a surfactant solution as electrical conductivity, surface tension, light scattering or fluorescence spectroscopy exhibit a sharp concentration dependent discontinuity in the region of self-aggregation (or micellization) as shown in Figure 2.7 [10]. The applicable methods depend on the nature of the surfactant. The break indicates an increase in the mass per unit charge of the material in solution, is interpreted as evidence of the formation at that point of micelles from the unassociated molecules of surfactant, with part of the charge of the micelle neutralized by associated counterions.

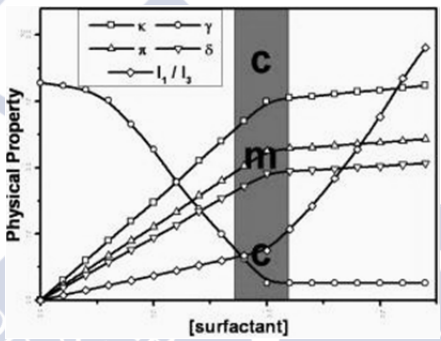

Figure 2.7. Plot of different physical properties versus log of the concentraion for an aqueous solution of a surfactant.

One parameter which relates *cmc* is Krafft temperature. The Krafft temperature, or critical micelle temperature, is the minimum temperature at which ionic surfactants form micelles. Below the Krafft point, micelles cannot form.

Adsorption at the liquid-gas (L-G) interface

The direct determination of the amount of surfactant adsorbed per unit area of liquid–gas interface is difficult. However, the amount of material adsorbed per unit area of interface can be calculated indirectly from surface tension measurements. So, usually, a plot of surface tension as a function of concentration of surfactant in the liquid phase can be used to describe adsorption at the interface. From

such a plot the amount of surfactant adsorbed per unit area of interface can readily be calculated by use of the Gibbs adsorption equation [9].

The Gibbs adsorption equation, in its most general form (Equation (2.1)), is fundamental to all adsorption processes where monolayers are formed.

$$d\gamma = -\sum_i \Gamma_i \cdot d\mu_i \tag{2.1}$$

where $d\gamma$ is the change in surface or interfacial tension of the solvent, Γ_i is the surface excess concentration of any component of the system and $d\mu_i$ is the change in chemical potential of any component of the system.

At equilibrium between the interfacial and bulk phase concentrations,

$$d\mu_i = RTdlna_i \tag{2.2}$$

where a_i is the activity of any component in the liquid phase, R is the gas constant, and T the absolute temperature. Thus

$$d\gamma = -RT\sum_i \Gamma_i \cdot dlna_i = -RT\sum_i \Gamma_i \cdot dlnx_i\gamma_i = -RT\sum_i \Gamma_i \cdot d(lnx_i + ln\gamma_i) \tag{2.3}$$

where x_i is the mole fraction of any component in the bulk phase and γ_i its activity coefficient.

For solutions consisting of solvent and only one solute:

$$d\gamma = -RT(\Gamma_0 dlna_{0+}\Gamma_1 dlna_i) \tag{2.4}$$

where subscripts 0 and 1 refer to the solvent and the solute, respectively. For dilute solutions (10^{-2} M or less) containing only one non-dissociating surface-active solute, the activity of the solvent and the activity coefficient of the solute can both be considered to be constant and the mole fraction of the solute x_1 may be replaced by its molar concentration C_1. Thus,

$$d\gamma = -RT\Gamma_1 dlnC_1 = -2.303RT\Gamma_1 dlogC_1 \tag{2.5}$$

which is the form in which the Gibbs equation is commonly used for solutions of nonionic surfactants containing no other materials. When γ is in dyn·cm^{-1} (= ergs· cm^{-2}) and R = 8.31·10^7 ergs mol^{-1} K^{-1} , then Γ_1 is in mol·cm^{-2} ; when γ is in mN·m^{-1} (=mJ·m^{-2}) and R =8.31 J·mol^{-1}·K^{-1}, then Γ_1, is in mol·m^{-2}/1000 .

For ionic surfactants,

$$d\gamma = -nRT\Gamma_1 dlnC_1 = -2.303RT\Gamma_1 dlogC_1 \quad (2.6)$$

where n is the number of solute species whose concentration at the interface changes with change in the value of C_1. Thus, for solutions of a completely dissociated surfactant of the 1:1 electrolyte type, A^+B^-, as the only solute,

$$d\gamma = RT(\Gamma_{A^+} dlna_{A^+} + \Gamma_{B^-} dlna_{B^-}) \quad (2.7)$$

Since $\Gamma_{A^+} = \Gamma_{B^-} = \Gamma_1$ to maintain electroneutrality and $a_{A^+} = a_{B^-} = C_1 \cdot \gamma_{\pm}$ without significant error,

$$d\gamma = -2RT\Gamma_1 d(lnC_1 + ln\gamma_{\pm}) \quad (2.8)$$

where $\gamma_{\pm}$ is the mean activity coefficient of the surfactant.

For dilute solutions (10^{-2} M or less) equation (2.9) can be used without significant error.

$$d\gamma = -2\,RT\,\Gamma_1\,dlnC_1 = -4.606\,RT\,\Gamma_1\,dlogC_1 \quad (2.9)$$

For surface-active solutes the surface excess concentration, Γ_1, can be considered to be equal to the actual surface concentration without significant error. The concentration of surfactant at the interface may therefore be calculated from surface or interfacial tension data by use of the appropriate Gibbs equation. Thus, for solutions of 1:1 ionic surfactant in the absence of any other solutes, from equation (2.10). When activity coefficients are used, superficial tension (γ) is plotted versus ($\log C_1 + \log \gamma_{\pm}$).

$$\Gamma_1 = -\frac{1}{4.606\,RT}\left(\frac{\partial\gamma}{\partial \log C_1}\right)_T \quad (2.10)$$

The area per molecule at the interface provides information on the degree of packing and the orientation of the adsorbed surfactant molecule when compared with the dimensions of the molecule as obtained by use of molecular models. From the surface excess concentration, the area per molecule at the interface as a_m^s, in square angstroms is calculated from the relation

$$a_m^s = \frac{10^{16}}{N\Gamma_1} \quad (2.11)$$

where N= Avogadro's number and Γ_1 is in mol·cm^{-2}.

A typical γ–log C_1, plot for a dilute solution of an individual surfactant is shown in Figure 2.7. The break in the curve occurs at the critical micelle concentration (*cmc*). Below but near the *cmc* the slope of the curve is almost constant, indicating that the surface

concentration has reached a constant maximum value. In this range the interface is considered to be saturated with surfactant and the continued reduction in the surface tension is due mainly to the increased activity of the surfactant in the bulk phase rather than at the interface.

The concentration of surfactant in the liquid phase required to produce a given amount of adsorption at the interface is a useful parameter to compare the efficiency of surfactants at the L-G interface. The efficiency of adsorption of the surfactant can be related to the free energy change involved in the adsorption.

The ideal measure of efficiency of adsorption would be some function of the minimum concentration of surfactant in the bulk phase necessary to produce the saturation at the interface. However, determining this concentration would require a complete γ–log$C$ plot for each surfactant being investigated. Observation of these plots in the literature reveals that when the surface tension of the pure solvent has been decreased about 20 $mN \cdot m^{-1}$ ($dyn \cdot cm^{-1}$) by adsorption of the surfactant, the surface (excess) concentration Γ_1 of the surfactant is close to its saturation value.

For this reason a convenient measure of the efficiency of adsorption is the negative logarithm of the concentration of surfactant in the bulk phase required to produce a 20 $mN \cdot m^{-1}$ reduction in the surface tension of the solvent, pC_{20}.

A convenient way of measuring the relative effects of some structural or microenvironmental factor on micellization and on adsorption is to determine its effect on the cmc/C_{20} ratio, where C_{20} is the concentration of surfactant in the bulk phase that produces a reduction of 20 $mN \cdot m^{-1}$ in the surface tension of the solvent. An increase in the cmc/C_{20} ratio as a result of the introduction of some factor indicates that micellization is inhibited more than adsorption or adsorption facilitated more than micellization; a decrease in the cmc/C_{20} ratio indicates that adsorption is inhibited more than micellization or micellization facilitated more than adsorption. The cmc/C_{20} ratio, therefore, affords insights into the adsorption and micellization processes. The cmc/C_{20} ratio is also an important factor in determining the value to which the surface tension of the solvent can be reduced by the presence in its solution of the surfactant.

Thermodynamic parameters of micellization

A clear understanding of the process of micellization is necessary for rational explanation of the effects of structural and environmental

factors on the value of the *cmc* and for predicting the effects on it of new structural and environmental variations. The determination of thermodynamic parameters of micellization ΔG_{mic}, ΔH_{mic}, and ΔS_{mic} has played an important role in developing such an understanding.

A standard free energy of micellization ΔG^o_{mic} may be calculated by choosing for the standard initial state of the nonmicellar surfactant species a hypothetical state at unit mole fraction x, but with the individual ions or molecules behaving as at infinite dilution, and for the standard final state, the micelle itself. For nonionic surfactants, the standard free energy of micellization is given by

$$\Delta G^o_{mic} = RTlnx_{cmc} \tag{2.12}$$

When the *cmc* is 10^{-2} or less, this can be approximated without significan error by:

$$\Delta G^o_{mic} = 2.3\ RTlog\left(\frac{cmc}{\omega}\right) \tag{2.13}$$

where the *cmc* is expressed in molar units and ω is the number of moles of water per litter of water at that absolute temperature T. For ionic surfactants, a standard free energy change of micellization, ΔG_{mic}, can be calculated by taking into account the degree of binding of the counterion to the micelle, β=*1-*α being α the degree of ionization. Thus, for ionic surfactants of the 1:1 electrolyte type:

$$\Delta G^o_{mic} = RT[1+\beta]lnx_{cmc} \tag{2.14}$$

where α is the degree of ionization of the surfactant, measured by the ratio of the slopes of the specific conductivity versus C plotted above and below the *cmc*, and x_{cmc} is the mole fraction of the surfactant in the liquid phase at the *cmc*.

Another thermodynamic parameter ΔH^o_{mic}, the standard enthalpy of micellar formation can also be determined according to the Gibbs–Helmholtz equation:

$$\Delta H^o_{mic} = \frac{\partial\left(\frac{\Delta G^o_{mic}}{T}\right)}{\partial\left(\frac{1}{T}\right)} \tag{2.15}$$

The entropy of micellization, ΔS^o_{mic}, can be obtained from the relationship as given in equation (2.16):

$$\Delta S^o_{mic} = \frac{\Delta H^o_{mic} - \Delta G^o_{mic}}{T} \tag{2.16}$$

2.1.5.2. Phase equilibria

2.1.5.2.1. Ternary systems

A valid approach for the study of the complex systems of interest in oil extraction (which consists of a mixture of water, salts, surfactant, co-surfactant, petroleum components...) is to consider them as a pseudo-ternary mixture surfactant-water-oil.

At constant temperature and pressure, Winsor (1954) [11] defined three types of basic diagrams (Figure 2.8).

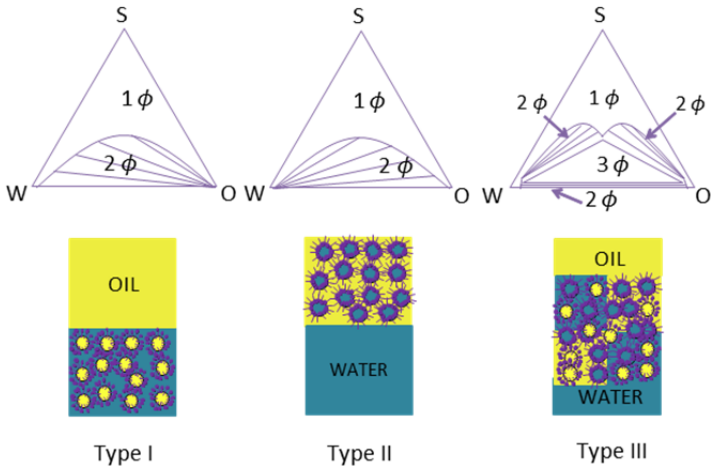

Figure 2.8. Types of Winsor diagrams. S: surfactant; W: water; O: oil.

Type I is characterised by the presence of a biphasic area (2ϕ) in the region of low concentration of surfactant, and a monophasic area (1ϕ) in which the surfactant causes miscibility between water and oil. For this type of systems, the affinity of the surfactant for the aqueous phases is greater than that for the oil. Any mixture within the interior of the immiscible area will split into an aqueous microemulsion in equilibrium with an excess phase of oil.

A microemulsion is a dispersion made of water, oil, and surfactant(s) that is an isotropic and thermodynamically stable system with dispersed domain diameter varying approximately from 1 to 100 nm, usually 10 to 50 nm. In a microemulsion the domains of the dispersed phase are either globular or interconnected (to give a bicontinuous microemulsion) [12].

In the Type II diagram, a similar situation is observed. Nevertheless, the roles of oil and water are now inverted. The affinity of the surfactant for the oil phase is the dominating one. Therefore,

the biphasic systems correspond to an oily microemulsion in equilibrium with an excess phase of water.

The Type III diagram comprises a 3-phase region (3ϕ) surrounded by three biphasic regions (2ϕ) and a monophasic region (1ϕ). Systems with global composition lying within any of the biphasic regions will split as in the previous cases. With regard to systems with global composition lying in the 3-phase region (3ϕ), these will split into three phases in equilibrium: an aqueous phase and an oily phase containing essentially water and oil respectively, plus an intermediate phase with density between those of the other two phases.

In the Type III diagram, the interactions are equilibrated and the surfactant corresponds to what the EOR researchers called in the 1970s, the optimal formulation, because such physicochemical situation corresponds to an interfacial tension extremely low and, therefore, to the almost total elimination of the capillary forces that retain the oil in the porous medium [13].

Although the real systems are multicomponent and the diagrams are much more complex, the concept of optimal formulation is maintained. The compositions of the phases can be determined by means of suitable analytical methods.

Correlation

Equilibrium conditions are deduced from the First and Second Laws of Thermodynamics. A closed system, heterogeneous and multicomponent, is at equilibrium when at constant temperature (T) and pressure (P), the Gibbs free energy (G) is a minimum. Mathematically:

$$d(G)_{T,P} = 0 \tag{2.17}$$

and this expression can be considered as a criteria or definition of equilibrium.

From this equation, equilibrium conditions can be established in terms of activities. For a multi-phasic and multi-component system, the equilibrium conditions are:

$$T^{(\mathrm{I})} = T^{(\mathrm{II})} = \cdots = T^{(j)} \tag{2.18}$$

$$P^{(\mathrm{I})} = P^{(\mathrm{II})} = \cdots = P^{(j)} \tag{2.19}$$

$$a_i{}^{(\mathrm{I})} = a_i{}^{(\mathrm{II})} = \cdots = a_i{}^{(j)} \tag{2.20}$$

where i refers to all the components of the system and the superscripts make reference to all the distinct phases. The activity is

related to composition through the activity coefficient, which is defined as the ratio of the two, hence the expression turns into:

$$(x_i.\gamma_i)^{(I)} = (x_i.\gamma_i)^{(II)} = \cdots = (x_i.\gamma_i)^{(j)} \tag{2.21}$$

which is probably the most practical expression of the equilibrium criterion.

The experimental equilibrium data can be correlated with the well-known NRTL model (*Non Random, Two-Liquid)* [14], where activity coefficient is a function of composition and temperature.

The NRTL equation was developed by Renon and Prausnitz (1968) [14]:

$$\ln\gamma_i = \frac{\sum x_i\tau_{ji}G_{ji}}{\sum x_kG_{ki}} + \sum\frac{x_jG_{ij}}{\sum x_kG_{kj}}\left(\tau_{ij} - \frac{\sum x_mG_{mj}\tau_{mj}}{\sum x_kG_{kj}}\right) \tag{2.22}$$

$$\tau_{ij} = (g_{ij} - g_{jj})/RT = \Delta g_{ij}/RT \tag{2.23}$$

$$G_{ij} = exp(-\alpha_{ij}\tau_{ij}) \tag{2.24}$$

where g_{ij} is an energy parametercharacteristic of the *i-j* interaction and $\alpha_{ij} = \alpha_{ji}$ is the parameter that takes into account the non-randomness aleatory disposition of the molecules. In principle, the non-randomness parameter can be specified (from 0.2 to 0.47) according to a set of rules, devised by the authors [14], that depend on the chemical nature of the components in the mixture, but it is usually given fixed value in an empirical way. The NRTL equation is applicable to multicomponent systems with only binary parameters (Δg_{ij}).

In the case of Winsor Type I or Winsor Type II systems, the correlation of LLE data is relatively easy. The binary interaction parameters can be obtained by using the program of Sørensen and Arlt [15]. Two objective functions are used to fit the experimental phase compositions. Firstly the experimental data are fitted using $O.F._a$ as objective function. After convergence, the obtained parameters are used in the second fit with $O.F._x$ as objective function. These funtcions are defined as:

$$O.F._a = \sum_k\sum_i[(a_{ik}^I - a_{ik}^{II})/(a_{ik}^I + a_{ik}^{II})]^2 + Q\sum_n P_n^2 \tag{2.25}$$

$$O.F._x = \sum_k\sum_i\sum_j(x_{ijk} - x_{ijk}^{cal})^2 + Q\sum_n P_n^2 \tag{2.26}$$

where a_i is the activity, x_i is the experimental composition in mole fraction, and x_i^{cal} the corresponding calculated composition for component *i*. Other subscripts and superscripts are: *j* for phases (I, II)

and k for tie-lines. With the aim of reducing the risks related to multiple solutions when using parameters of high value, a penalty term is introduced in both functions (second term). Q is set to 10^{-6} and to 10^{-10} in equations (2.25) and (2.26), respectively. P_n are the adjustable parameters.

Three-liquid-phase equilibria are more complex. Experimental data are scarce and many of them do not present a reliable model of correlation or prediction, a key engineering tool in process design.

The correlation of the Winsor Type III systems in this work, involving both LLE and LLLE, was carried out using also the NRTL model. The optimisation of the model parameters was carried out using the Generalized Reduced Gradient Nonlinear method with the objective function defined as:

$$O.F._{x,total} = O.F._{x,LL} + O.F._{x,LLL} \tag{2.27}$$

$$O.F._{x,LL} = \sum_k \sum_i \sum_j (x_{ijk} - x_{ijk}^{cal})^2 \quad \text{subject to:} \quad \sum_k \sum_i (a_{ik}^I - a_{ik}^{II})^2 < \varepsilon \tag{2.28}$$

$$O.F._{x,LLL} = \sum_i \sum_j (x_{ij} - x_{ij}^{cal})^2 \quad \text{subject to:} \quad \sum_i (a_i^I - a_i^{II})^2 + \sum_i (a_i^I - a_i^{III})^2 \sum_i (a_i^{II} - a_i^{III})^2 < \varepsilon \tag{2.29}$$

being ε is an extremely low tolerance value guaranteeing the fulfilment of the isoactivity in the phases in equilibrium.

Some additional useful strategies were applied to extend the application of the typical isoactivity algorithm for LLE correlation data from the simplest Type I and II to the complex Type III ternary systems that include one tie-triangle.

1. In the first step the correlation of the three binary subsystems was carried out independently to obtain a set of the binary parameters of the model. At this point the parameter a_{ij} was assigned the default value of 0.2. Subsequently, the parameters were allowed to change in a specific interval to simultaneously correlate the previous binary LLE data along with the LLLE tie-triangle. When for the best correlation solution found at this point any of the parameter values reached one of the established limits, this limit was extended and the correlation continued until another minimum of the objective function was

reached. Finally, the equilibrium data for all the ternary LLE regions were included in the correlation and a similar procedure to limit the changes in the parameters "step by step" was used. In this last step, a_{ij} was considered as an additional correlation parameter to give flexibility to the model. This guided procedure improves the convergence of the correlation algorithm and ensures that the best solution for the model is found. It must be taken into account that the NRTL model has six binary parameters for a ternary system. Consequently, when the three LLE binary subsystems are fitted, the values of all these parameters are already set. Only minimal changes in these interactions parameters, in addition to the variation in the non-randomness parameter, can be admitted to achieve a good representation of the ternary regions without disarranging the binary data.

2. The convergence and robustness of the algorithm was improved not by directly using the mole fractions, but by using additional parameters (which can take any positive or negative value) to optimise the correlation. The relation between the optimisation parameters used and the mole fractions are:

$$x_1 = \frac{P1}{1 + |P1| + |P2|} \tag{2.30}$$

$$x_2 = \frac{P2}{1 + |P1| + |P2|} \tag{2.31}$$

$$x_3 = 1 - x_1 - x_2 \tag{2.32}$$

This procedure guarantees that x_1, x_2 and x_3 are always positive, lower than 1 and their sum is 1.

3. It is quite common as a correlation method to set the composition of one component in one of the equilibrium phases to its experimental value, with the aim of obtaining the calculated tie-lines or tie-triangle. Compositions calculated in this way are compared with the experimental data. Unlike this usual procedure, this method looks for the minimisation of the deviations between experimental and correlated compositions of the tie-lines and tie-triangle without fixing any calculated equilibrium composition (neither x_1, x_2 nor x_3) to the corresponding experimental value. This simple strategy avoids some problems of convergence that arise when the values for the model parameters (in some step of the optimisation) take values for which no splitting is produced when the composition was fixed to the experimental value.

2.1.5.2.2. Multicomponent systems: pipette tests

The addition of tailored surfactants to the injection fluid reduces interfacial tension, and thereby increases the capillary number, decreasing the residual oil saturation [2, 7]. Healy *et al.* [16] found that the optimal formulation for surfactant oil recovery, with a minimum in the oil-water interfacial tension, is achieved when equilibrium interfacial tensions between a microemulsion phase and excess phases of oil and water become equal (Winsor Type III systems). As seen for ternary systems, achievement of the ultralow interfacial tension necessary in tertiary oil recovery processes is closely related to water and oil solubilisation by the surfactant.

Real systems in oil recovery involve more than three components. The high number of components of the oils, the presence of salts, the addition of surfactants and co-surfactants, etc. makes the rigorous study of phase equilibria very complex and useless for this application. Specifically, the presence of salt has a key influence on the phase behaviour of these multicomponent systems. Thus, salinity scans, also called pipette tests, are useful tools to determine the optimal salinity (the salinity that leads to a minimum in the interfacial tension) for EOR applications.

Figure 2.9 (up) shows a series of pseudoternary diagrams (salt and water are considered as a single component, brine). Each diagram represents a constant salinity. As the salinity is increased, the surfactant moves from the aqueous phase to the oleic phase. At a low salinity, a typical surfactant exhibits good aqueous-phase solubility with Winsor Type I phase behaviour (some oil is solubilised in the cores of micelles). The oil phase, then, is essentially free of surfactant. As salinity increases, the microemulsion changes from Winsor Type I to Type III and then to Type II.

In salinity scans (Figure 2.9, down), the temperature, oil type, water/oil ratio, and concentration of surfactant(s) are fixed, whereas the concentration for the electrolyte is varied between different test tubes. Pressure is assumed to have little effect, and it is generally atmospheric. Adding surfactant to known volumes of water and oil increases the volume of the phase where the microemulsion is formed. For hydrophilic surfactants, Winsor Type I microemulsions are formed at low salinities (the surfactant has affinity for the aqueous phase) that convert to Winsor III increasing the salinity (the surfactant solubilises water and oil) and finally to Winsor Type II (the surfactant has affinity for the oil phase).

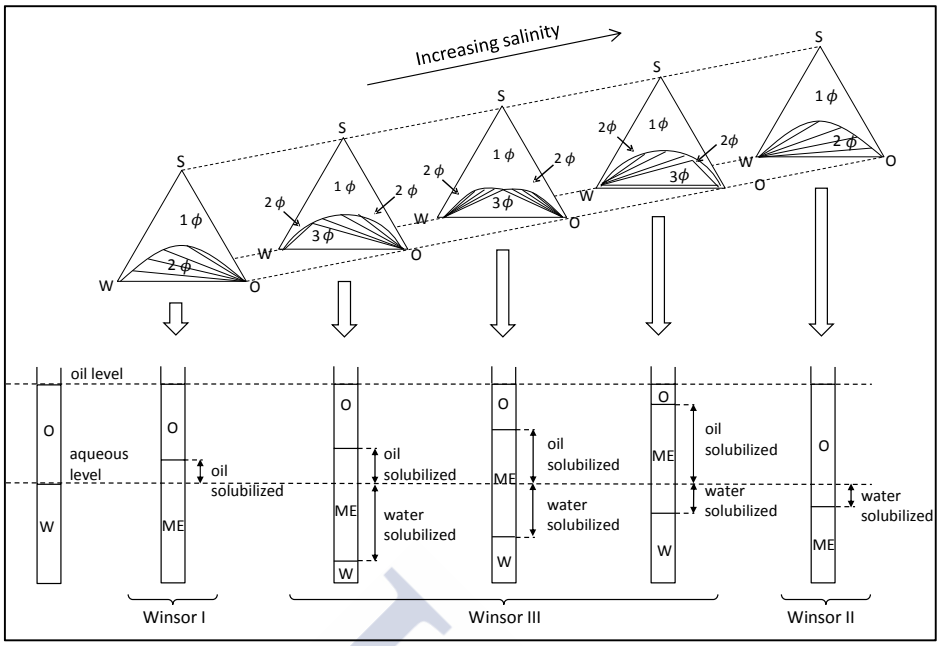

Figure 2.9. Sequence of ternary system transitions from Winsor Type I to Type II as the salinity increases (up) Salinity scan test and how to measure volumes for solubilisation ratio calculation (down).

As volumes can be measured visually, solubility plots can be made. These plots (Figure 2.10) represent volume of oil and water divided by volume of surfactant (V_o/V_s and V_w/V_s) in the microemulsion phase. To reach an ultra-low interfacial tension, solubilisation parameters must be equal and with a numerical value higher than 10 [7].

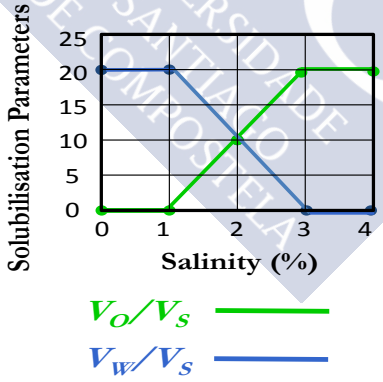

Figure 2.10. Volume fraction diagram

Frequently, it is not easy to obtain an optimal formulation with only one surfactant. The formulation of surfactant blends is useful to adjust HLB or to take advantage of the synergistic behaviour in mixed systems for surfactant flooding purposes [17]. Similarly to salinity scans, blend scans are useful tools to determine the optimal blend of two surfactants when monotonically altering only surfactant ratios at a fixed surfactant concentration, salinity, oil type and temperature.

Other important phase behaviour tests in EOR are aqueous stability tests. They allow evaluating whether the aqueous optimal solution without oil is clear (without precipitate, liquid crystals or a second liquid phase) up to or even at higher salinities than those at which the solution is intended to be injected. Such formations could lead to non-uniform distribution on injection and non-uniform transport afterwards.

2.1.5.3. Interfacial tension

The proper phase behaviour tests for screening surfactants before carrying out definitive but more expensive and time-consuming tests in EOR, core flooding experiments, are salinity (or blend) scans.

Huh's equation [18] makes it possible to estimate the value of the equilibrium interfacial tension at optimal conditions from equal values of the solubilisation parameters, $V_o/V_s = V_w/V_s$. According to that correlation:

$$\gamma = C/(\sigma_o)^2 \tag{2.33}$$

where C is a constant with a typical value of 0.3 $mN \cdot m^{-1}$, σ_o is the solubilisation parameter (V_o/V_s) and γ is the interfacial tension.

However, another method usually employed to determine optimal formulations for EOR is the direct measurement of dynamic interfacial tensions between the surfactant solution and oil. The equipment normally used is a spinning drop tensiometer that allows for the measurement of ultra-low interfacial tensions. This method requires an exhaustive screening of surfactant and salt concentration, temperature, etc. and, despite being widely used, it is clearly less effective than the pipette tests.

2.1.5.4. Core flooding tests

Before any process is considered for field testing, core flooding experiments are required. In this type of laboratory test, a fluid or combination of fluids are injected into a sample of rock to see if a significant quantity of oil can be recovered. Objectives include:

measurement of permeability, relative permeability, saturation change, formation damage caused by the fluid injection, or interactions between the fluid and the rock.

The core material often comes from an oil reservoir, but some tests use outcrop rock. The fluid in place at the start of the test is typically either a simulated formation of brine, oil (either crude oil or refined oil), or a combination of brine and oil. Injected fluids may include crude oil, simulated reservoir brine, refined fluids, drilling mud filtrate, acids, foam or other chemicals used in the oil field. Depending on the purpose of the test, conditions may be either ambient temperature and low confining pressure or high temperature and pressure of a subject reservoir. Pressures and flow rates at both ends of the core are measured, and the core can also be investigated using other measurements such as nuclear magnetic resonance (NMR) during the test. A core flood is typically used to determine the optimum injection conditions for an oil reservoir and often helps evaluate the effect of injecting fluids specifically designed to improve or enhance oil recovery [7].

2.2. IONIC LIQUIDS

There are many slightly different definitions in literature for ILs. The most widespread claims that ILs are salts composed solely of ions, having a melting point below 373.15 K [19-22]. Many of them are also liquids at room temperature, so they are called “room temperature ionic liquids” (RTILs).

The reduced coordination between the ions that form the ILs (due to the asymmetry of the cation with respect to the anion) decreases the lattice energy of the crystalline form of the salt, and it is responsible for the significantly low melting point of these compounds compared to conventional salts [23].

ILs exhibit many properties which make them potentially attractive compounds as an alternative to traditional organic solvents. Among the most important, the following should be mentioned [24, 25]:

- They are liquids below 373.15 K, by definition, and many of them at room temperature. Furthermore, in general ILs present far higher liquid range than molecular solvents.

- Their vapour pressure is negligible. This property generates a great amount of interest in ILs from the point of view of green chemistry. As non-volatile solvents, air pollution is avoided and

the upper limit of their liquid range is determined by their thermal decomposition temperature.

- In general, they are thermally stable compounds and they are usually not flammable. This means that ILs can be used at high operating temperatures without solvent degradation.

- The stability of ILs in water varies widely. Many are stable in the presence of water but there are important exceptions, such as haloaluminate-based ILs and others containing [BF_4^-] or [PF_6^-] anions.

- In general ILs present a wide electrochemical window and high conductivity values.

- ILs can dissolve substances of different natures. The existence of polar and non-polar domains in the molecule of the IL is responsible for different molecular interactions, depending on the nature of the chemical species dissolved in such medium.

In addition to these general properties, ILs may present specific properties. On one hand, different combinations of cations and anions can be used. On the other hand, the structure of the cation and/or anion can be modified by changing the length of the alkyl chain or by the introduction of different functional groups. This fundamental aspect makes that ILs are considered to be "designer solvents" [26]. An IL with physical and/or chemical specific properties can be designed depending on the requirements of the application in which it is going to be used. For instance, the miscibility of ILs in water is determined by the forming ions, being the coordination capacity of the anion a key factor in the hydrophobicity of the IL [22]. Some ILs with specific functional groups can act not only as solvents but also as catalysts in certain reactions [24]. The presence of long chain alkyl structures in the cation and/or the anion can give the ILs surfactant character [27].

2.2.1. Surface active ionic liquids

The steric mismatch that makes ILs having melting points below 373.15 K is due in large part to the attachment of alkyl side chains to the charged head-group of the cation and/or anion. At least one of the ions of an IL is thus amphiphilic, and therefore a potential surfactant. SAILs are classified as traditional ionic surfactants.

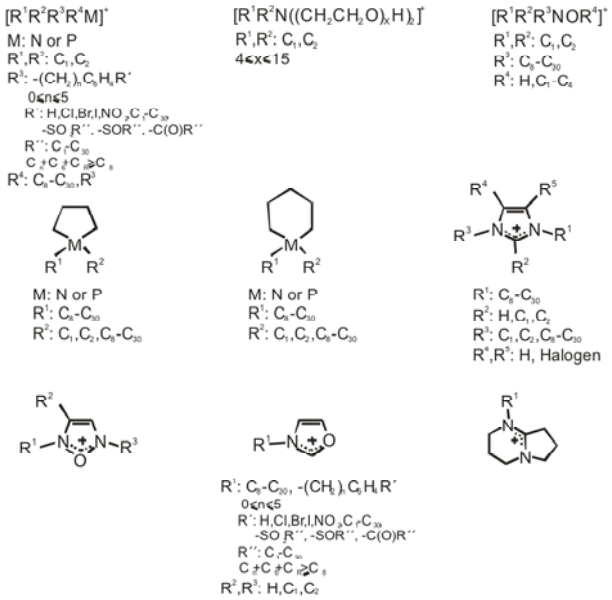

Figure 2.11. Typical cationic components of SAILs [28].

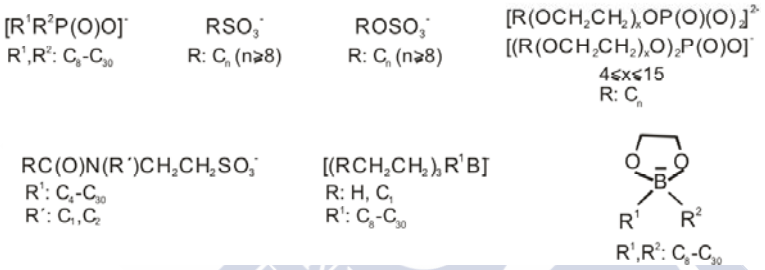

Figure 2.12. Typical anionic components of SAILs [28].

Figure 2.11 and Figure 2.12 exhibit a number of typical ions constituents of SAILs, in this case taken from a patent application that cites as an advantage of these SAILs their ability to form stable microemulsions without any need for a co-surfactant or inorganic salt [28]. Possible applications cited for these salts are presented in Table 2.1 according to their HLB.

Table 2.1. SAILs utilities corresponding to various ranges of HLB value.

HLB	Applications
1-3	Anti-foaming agents
3-8	For w/o emulsions
7-9	Wetting agents
9-18	For o/w emulsions
15-20	Solubilising agents

So far, most SAILs research has concerned ILs in which the cation is amphiphilic and the anion is not, and which are thus classifiable as cationic surfactants. However, increasing attention is being paid to SAILs with amphiphilic anions and to catanionic SAILs in which both the anion and the cation are amphiphiles. For example, Blesic *et al.* [29] reported that whereas alkylimidazolium methylsulphates, $[C_nH_{2n+1}mim]$-$[MeSO_3]$, behaves as a cationic surfactant with $n>8$, alkylimidazolium alkylsulphates SAILs of the form $[C_nH_{2n+1}mim][C_mH_{2m+1}SO_3]$ with n,m = 4,8 are catanionic and have greater surface activity.

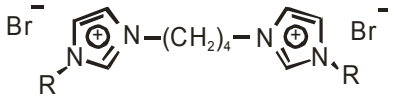

$R = C_{10}H_{21}, C_{12}H_{25}, C_{14}H_{29}$

Figure 2.13. A gemini SAIL.

Two other classes of SAILs that must be mentioned are the gemini and polymeric SAILs. Gemini SAILs feature two linked replicates of an amphiphilic moiety, like that shown in Figure 2.13. Polymerisation raises melting points. Nevertheless, the formed polyelectrolyte from a SAIL can sometimes keep both IL and surfactant behaviour, although their surface properties have not been investigated in depth [30].

Besides the already mentioned advantages of the ILs, the delocalised charges associated to the special head-groups of these compounds, can also deliver special interfacial properties to the systems [31]. Like other aspects of ILs, their micelle-forming characteristics have in fact been studied mainly in regard to $[C_nmim^+]$ salts. *cmc*s can be determined for n>6 (as can aggregation numbers, i.e. the numbers of molecules per micelle), but not for smaller molecules, although $[C_4mim^+]$ does exhibit certain signs of aggregation [32]. The aggregation number and the *cmc* are important parameters influenced by the length and shape of the alkyl chain, the type of polar head group, and the nature and size of the counter-ion [31-37].

Most applications of SAILs derive from the two fundamental properties of surface active agents in aqueous solution: adsorption at the surface or interface, and aggregation. By reducing surface tension, adsorption at the air/water interface modifies the wetting and foam-forming properties of the surfactant-containing water, while adsorption at oil/water interfaces is the first step in emulsification, and adsorption at the interface of water with suspended solids can

lead to flocculation and coagulation. The aggregation of SAILs like that of other surfactants, is the basis of applications involving the formation of micelles, microemulsions and liquid crystals.

A number of the currently most widespread applications of SAILs in fact concern conventional ionic surfactants that have only relatively recently been seen as ILs, being salts with melting points below 100˚C. Dodecyldimethylbenzyl-ammonium chloride, [C_{12}mim]Cl, for example, is widely used as a bactericide, and cetylpyridinium chloride, [C_{16}py]Cl, as a mouthwash. Other more recent examples of the applications of SAILs are: foaming and antifoaming agents [38], antimicrobials [38], solubilisation of drugs [39, 40], demulsification of crude oil [41], EOR [42], extraction of natural products [43], chromatographic and electrophoretic separations [44], synthesis of new materials (mesoporous inorganic materials, nanocomposites, nanoparticles and microcrystals) [45, 46], and microemulsion-based reactions [40].

2.2.2. SAILs in EOR

The main advantage of using SAILs in EOR is that they can be functionalised [47] according to the requirements of a specified application or reservoir. As a result, options for developing formulations are greatly expanded, especially for reservoirs at high temperatures and salinities where the choice of conventional surfactants is limited. RTILs could be shipped in neat form to the field, which is unfeasible with most conventional ionic surfactants. Furthermore, due to the characteristic rings, of many ILs, that have a high affinity to form hydrogen bonds, the Krafft temperature for SAILs is frequently lower than for similar common surfactants. For example, imidazolium SAILs have a comparatively lower Krafft temperature than alkyltrimethylammonium compounds. This would indicate that long-chained imidazolium ILs are more able to act as surfactants at lower temperature than traditional cationic surfactants with a similar chain length [48]. On the other hand, recent studies [49-51] show that aqueous solutions of ILs (with and without oil) have a high stability in extreme conditions (high salinity and/or temperature).

In the first work published in open literature where a SAIL was proposed to improve surfactant EOR methods, due to their capacity to reduce oil/water interfacial tension and solubilise oil, the phase equilibria of a ternary system involving trihexyl(tetradecyl) phosphonium chloride, [$P_{6\,6\,6\,14}$]Cl, water and *n*-dodecane (as oil) was determined and an important reduction of the interfacial tension

between water and oil was found [42]. Several advantages of SAILs over typical ionic and non-ionic surfactants were highlighted: their liquid character over a wide range of temperatures (including room temperature) which makes their handling easier; their usually high viscosity that could increase aqueous phase viscosity avoiding digitations, their design opportunities, the possibility of avoiding the use of co-surfactants because SAILs form stable aggregates due to their strong cohesive forces, their thermal stability, etc.

Since that first paper, the number of publications on this topic in scientific and technical literature has increased exponentially, which is indicative of the interest of this application.

The literature covering this research is basically focused on two aspects. There are several papers [49, 50, 52-55] where SAILs are characterised determining their surface and aggregative (micelles and higher ordered structures) properties. After this characterisation, the studies focus on the reduction of the interfacial tension between water or brine and oil. The second group of papers [56-60] involves studies more focused on the practical application of the technology, basically core flooding tests. Unfortunately, practically all those works lack previous more fundamental studies about phase behaviour and conditions to reach an optimal formulation. This is the reason why the obtained results are not optimal.

The more relevant papers are those corresponding to Benzagouta [52] and Hezave [53, 54]. These works focus on the effect of several variables (type and concentration of SAIL, temperature and salinity) in the interfacial tension between water or brine and crude oil. They reach maximum reductions of about 90% with 1-dodecylpyridinium chloride, [C_{12}py]Cl, but they are still far from the ultra-low values required. Recently, Prof. Gardas *et al.* [49, 50, 55] also presented several studies on the influence of SAILs in the interfacial tension brine/crude oil and its variation with salinity and temperature. However, only in one of the studies [55], the alkyl chains of the ILs are long enough to be surface active agents. Thus, reductions found are low (between 10 to 30%, or 40% in the case of the SAIL 1-methyl-3-octylimidazolium chloride, [C_8mim]Cl), far from the required goal.

Most of the papers found in literature are experimental. The only exception is the work of Palchowdhury and Bhargava [61]. These authors use molecular dynamics simulation to study ternary systems SAIL+ water+ *n*-alkane and their interfacial tensions. Reductions

found are always lower than 60%, again far from the ultra-low values required.

The more relevant works from a technical point of view are core flooding tests where the crude is displaced using aqueous solutions or microemulsions with SAILs. Works published by Hezave *et al.* [57] and Benzagouta *et al.* [58, 59] used ILs as surface active agents. These works present an initial study about the reduction of the interfacial tension between water or brine and oil, and some core flooding tests with the most promising SAILs. In the first work an EOR of about 13 % (total recovery 60%) was found in the best conditions of salinity with 1-dodecyl-3-methylimidazolium chloride, $[C_{12}mim]Cl$. Benzagouta's group suggest the use of Ammoeng 102 (tetra-alkyl ammonium sulfate), getting in the most favourable attempts an EOR of about 10%.

Gou *et al.* [60] used the combination of different SAILs with a co-polymer. The polymer, denoted as PAAD, was prepared with acrylamide, acrylic acid, and N,N-diallyl-2-dodecyl-benzenesulfonamide. The PAAD/$[C_8mim]Br$ complex was found more effective to reduce the interfacial tension than water/$[C_8mim]Br$ system. An EOR of about 22% was obtained with the complex brine solution. Prof. Gardas *et al.* [62] tested the combination of several methods of EOR using ILs at several temperatures and salinities. The authors carried out core-flooding experiments with sodium dodecyl sulphate (SDS), alkyl ammonium ILs, polyacrylamide and polyacrylamide after SDS/IL flood. The IL + polymer flood under high saline conditions shown significant increase in oil recovery as compared to the rest of the flooding schemes, reaching maximum recoveries of about 72% (28% EOR) with $[OHPrNH_3][CF_3COO]$.

All the previously described papers screen several SAILs for EOR, but these were not chosen by any scientific or technological reason. In some of them interfacial tension measurements have been a method proposed to evaluate SAILs for EOR applications [52, 53, 58]. These groups reported interfacial tensions between aqueous solutions of ILs and oils above 0.1 $mN \cdot m^{-1}$. However, interfacial tensions below 0.01 $mN \cdot m^{-1}$ and preferably near 0.001 $mN \cdot m^{-1}$ are needed in typical cases to mobilise trapped residual oil remaining after water flooding of an oil reservoir. Moreover, low interfacial tension is an insufficient criterion for assessing whether a surfactant is suitable for this application. For example, when the surfactant is injected into the reservoir, if ultra-low interfacial tension is from formation of a Winsor II microemulsion, this can lead to surfactant retention in the oil phase that induces

unfavourable heavy emulsification because of trapping of viscous phases within the rock.

Test results from salinity scans of SAILs are almost nonexistent in literature despite the fact that this would be the first step in evaluating, via phase behaviour, if a SAIL is suitable for EOR applications by determining oil and water solubilisation in generated microemulsions. Therefore at the same time that the works above presented were published, we also continued our research on this topic maintaining a fundamental research on phase equilibria, but also focusing on salinity scans as a fundamental tool for EOR applications. Results will be presented in the corresponding section of this Thesis.

USC
UNIVERSIDADE
DE SANTIAGO
DE COMPOSTELA

3. EXPERIMENTAL PROCEDURE

USC
UNIVERSIDADE
DE SANTIAGO
DE COMPOSTELA

3.1. CHEMICALS

Model oils, *n*-hexane (>99 wt%), *n*-octane (>99 wt%), *n*-dodecane (>99 wt%), butylbenzene (>99 wt%) and hexylbenzene (>97 wt%) were purchased from Sigma-Aldrich. They were washed six times with bi-distilled water and passed many times through a column with alumina (activated, basic Brockman I, Sigma–Aldrich), when used for determination of interfacial tension between phases in equilibrium, in order to separate any surface-active impurities that alkanes often contain [63].

The crude oil was kindly supplied by Repsol (Refinery of A Coruña, Spain). Its characterisation is shown in Table 3.1.

Table 3.1. Crude oil characterisation.

Gravity, *ºAPI*	45.3
Density, $g \cdot cm^{-3}$	0.8003
Sulphur, *wt%*	0.1
Pour Point, *ºC*	-20
Viscosity at 40 ºC, *cSt*	1.6
Acid number, $mg\ KOH \cdot g^{-1}$	0.15
Atmos. Residue 370 ºC, *wt%*	30.3

Sodium chloride was purchased from Fisher Chemical and calcium chloride dihydrate, magnesium chloride hexahydrate and sodium sulfate anhydrous were purchased from EMD chemicals. All the salts were certified ACS Reagent Grade with a purity ≥99 wt%. The brines were made by adding salt to double-distilled water.

The traditional cationic surfactant dodecyltrimethylammonium bromide (C_{12}TAB) and traditional anionic surfactants dioctyl sodium sulfosuccinate (Aerosol® OT) and sodium dodecylsulfate (SDS) were purchased from Sigma-Aldrich with purities > 98 wt%, > 97 wt% and >98 wt% respectively. The EOR surfactant ENORDET 0332, an Internal Olefin Sulfonate, is a twin-tailed or branched hydrophobe with 15–18 carbon atoms (IOS_{15-18}) and was kindly supplied by Shell Global Solutions International.

The structure of the ILs used in this work is shown in Figure 3.1. Trihexyltetradecylphosphonium bis(2,4,4-trimethylpentyl)phosphinate ($[P_{6\,6\,6\,14}][(iOc)_2PO_2]$) and trihexyltetradecylphosphonium dicyanamide ($[P_{6\,6\,6\,14}][DCA]$) were supplied, respectively, by CYTEC and IOLITEC (purity for both ILs >95 wt%). Purification was carried out by washing with double-distilled water (4 times), passing them through a column

filled with alumina (Sigma-Aldrich, activated, basic, Brockmann I) and active carbon, and finally they were placed under vacuum ($5 \cdot 10^{-3}$ mbar) and moderate temperature (~343 K) for at least 48h in order to eliminate any volatile components. 1-Dodecyl-3-methylimidazolium bromide ($[C_{12}mim]Br$) was purchased from IOLITEC and tributyl(tetradecyl)phosphonium chloride ($[P_{4\,4\,4\,14}]Cl$) was supplied by CYTEC. Both were tested as received with a purity >98 wt%. The SAILs tributylmethylphosphonium dodecylsulfate ($[P_{4\,4\,4\,1}][DS]$) and 1-butyl-3-methylimidazolium dioctyl sulfosuccinate (hereinafter $[C_4mim][AOT]$) were synthesized in our laboratory. The synthesis of each IL is detailed below.

The purity of all ILs, commercial and synthesised, was verified by ^{1}H NMR and ^{13}C NMR spectroscopy. Water content was measured by Karl-Fischer titration (Metrohm 737 KF coulometer) obtaining values below 600 ppm for all the ILs.

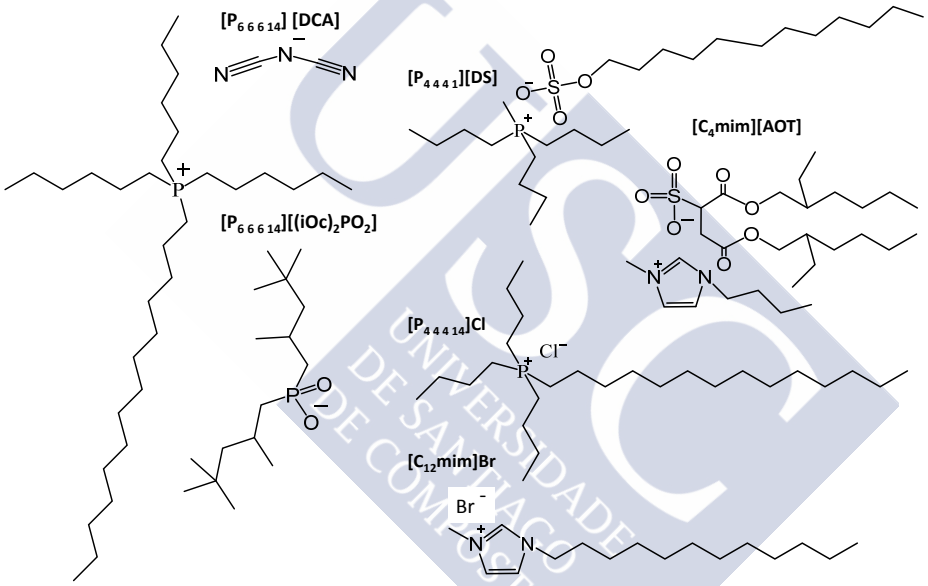

Figure 3.1. Chemical structure of the SAILs studied in this work.

The CAS number, water content, density, viscosity and surface tension of the pure compounds used in the LLE section are reported in Table 3.2 and compared with available literature data [64-73].

Table 3.2. CAS number, water content (w_{H2O}) and experimental and literature values for density (ρ), viscosity (η) and surface tension (γ) of the pure components used for the LLE determination.

Compound	w_{H2O} (ppm)	ρ (g·cm^{-3})		η (mPa·s)		γ (mN·m^{-1})	
		Exp.	Lit./[ref]	Exp.	Lit./[ref]	Exp.	Lit./[ref]
water	-	0.99706	0.99705 [64]	0.899	0.890 [64]	72.0	71.8 [64]
n-dodecane	61	0.74524	0.74518 [64]	1.359	1.378 [64]	24.9	24.9 [64]
			0.7453 [65]		1.361 [66]		
n-hexane	80	0.65487	0.65484 [64]	0.2899	0.2942 [64]	18.1	17.94 [64]
			0.65519 [73]		0.313 [74]		17.40 [75]
$[P_{6\,6\,6\,14}][DCA]$	600	0.89736	0.89886 [67]	437.8	418.33 [67]	33.1	34.85 [69]
			0.899 [68]		438.57 [68]		32.56 [70]
			0.9209 [69]				
$[P_{6\,6\,6\,14}][(iOc)_2PO_2]$	390	0.88413	0.8853 [68]	1368	1401.7 [68]	28.3	28.32 [70]
			0.8875 [71]		1004 [71]		
			0.88455 [72]		1058.22 [72]		
$[P_{4\,4\,4\,14}]$ Cl	400	-	-	-	-	-	-

3.1.1. Ionic Liquids Synthesis

The anionic SAILs $[P_{4\,4\,4\,1}][DS]$ and $[C_4mim]AOT$ were obtained by metathesis reaction.

- **$[P_{4\,4\,4\,1}][DS]$**

Equimolar amounts of tributylmethylphosphonium chloride ($[P_{4\,4\,4\,1}][Cl]$, Cytec) and sodium dodecylsulfate (SDS, Sigma Aldrich) were dissolved in water and stirred overnight at room temperature. Then, the mixture was washed with dichloromethane. Sodium chloride remains in the aqueous phase while $[P_{4\,4\,4\,1}][DS]$ is extracted to the organic phase. The organic phase was separated from the aqueous phase and washed with water and decanted several times to completely remove Cl^- ions. The washing was performed until no precipitation appeared with the addition of 0.1 M $AgNO_3$. Dichloromethane was removed using a rotary evaporator and the final product was dried under vacuum for 72 hours.

- **$[C_4mim]AOT$**

For the synthesis of $[C_4mim]AOT$, an equimolar mixture of 1-butyl-3-methylimidazolium chloride ($[C_4mim]Cl$, IOLITEC) and sodium dioctyl sulfosuccinate (hereinafter Na-AOT) was dissolved in dichloromethane and stirred overnight at room temperature. The

precipitated NaCl was filtered. This organic phase was washed with water and decanted several times to completely remove Cl^- ions. The washing was performed until no precipitation appeared with the addition of 0.1 M $AgNO_3$. Dichloromethane was removed using a rotary evaporator and the final product was dried under vacuum for 72 h [36].

For both ILs, the chemical structures were confirmed by ^1H and ^{13}C NMR. The chloride content (<800 ppm) was measured by ionic chromatography using an ion chromatograph (Metrohm 861) equipped with a suppressed conductivity detector, a sample processor (Metrohm 838) and a Metrosep A column (250 × 4.0 mm). A carbonate buffer (3.2 mM Na_2CO_3 and 1.0 mM $NaHCO_3$) was the mobile phase at a flow rate of 0.7 mL min^{-1}.

The water content of both ILs was measured by the Karl Fischer titration method in a Metrohm 737 KF coulometer being <400 ppm.

3.2. EQUIPMENT AND PROCEDURE

3.2.1. Synthesis and purification

For the synthesis of SAILs, a Velp Scientifica Arex heater and magnetic stirrer plate was used. The same equipment was also used for the purification of all the SAILs, which were dried in a glass-made vacuum line with capacity for four samples at the same time (Figure 3.2).

Figure 3.2. Velp Scientifica Arex heater in high vacuum line.

The water content of the pure compounds was measured using a Metrohm 737 KF coulometer (see Figure 3.3) by a Karl-Fischer titration method. The uncertainty in the measurements is 5 µg when the water content is lower than 10^3 µg and 0.5 wt% for higher mass of water.

Figure 3.3. Metrohm 737 coulometer.

3.2.2. Liquid-liquid equilibrium

The phase equilibrium data were obtained using specially designed jacketed glass equilibrium cells and gas chromatography as analysis method. In order to determine phase diagrams for the ternary systems (water + SAIL + *n*-alkane) a mixture of the three components, with a known composition within the biphasic or triphasic regions, was introduced in the glass jacketed equilibrium cell (see Figure 3.4, left and middle). The content of the cell was vigorously mixed for at least two hours to attain equilibrium. Stirring was carried out using a magnetic stirrer for systems with two liquid phases, and mechanical stirring (a stirrer connected to an IKA RW 16 basic motor) for systems with three liquid phases in equilibrium. Temperature was controlled by circulation of water from a Selecta Ultraterm 6000383 thermostatic bath (shown in Figure 3.4, right) through the cell jacket. The uncertainty in the temperature measurement is ± 0.05 K. The cells were then left to settle down between 24 h and 72 h until clarification, ensuring that a complete separation of the phases was achieved. Previous tests were carried out applying different stirring rates and settling-down times to ensure the suitability of selected times.

Figure 3.4. Equilibrium cell for systems with two phase (left) and three phases (middle) and thermostatic bath from Selecta (right).

Sampling ports at different heights allowed the withdrawal of samples of each phase in equilibrium using glass syringes. The two or three liquid phases were sampled for composition analysis and also

for measurement of physical properties (density, viscosity and interfacial tension).

Composition analysis was performed by gas chromatography using a Hewlett-Packard HP 6890 Series chromatograph (see Figure 3.5) equipped with a thermal conductivity detector (TCD) and an Agilent 7683B Series automatic injector. The capillary column used was a HP-FFAP (25 m x 0.2 mm x 0.33 μm) and a guard pre-column (without stationary phase) to avoid non-volatile components (ILs), not retained in the liner, reach the analytical column. Helium was used as the mobile phase. The concentrations of water and oil in the equilibrium phases were analyzed using the internal standard method. Methyl acetate was used as the internal standard for all the systems. However, 1-butanol was used as solvent for systems with *n*-dodecane as oil and isopropanol was used for systems with *n*-hexane. Samples of the equilibrium phases (ca. 0.25 mL) were diluted in the solvent (ca. 0.7 mL) and methyl acetate (ca. 0.3 mL) was added as standard. Water and oil compositions were calculated from calibration lines previously obtained using the same analytical conditions and within the same range of analyte/standard area ratios. The analysis was carried out for each sample at least four times. If a significant difference (bigger than the corresponding uncertainty) was found, the analysis was repeated. Once water and oil mass fractions were known, the IL composition was obtained by summation to unity.

Different chormathograph operation conditions were used for the analysis of the studied systems in this work: water + SAIL + n-dodecane and water + SAIL+ n-hexane. These conditions are summarised in Table 3.3 and Table 3.4, respectively, and they are the result of an optimisation process to achieve the best analytical precision.

Figure 3.5. HP 6890 Series gas chromatograph.

Table 3.3. Gas chromatograph operation conditions for the analysis of water + IL + *n*-dodecane ternary systems.

Injector	Temperature	503.15 K
	Split	1:50
	Injection volume	1 μl
Column	Type	HP-FFAP
	Flux	Constant flux of 1.1 mL ·min^{-1}
Detector	Type	TCD
	Temperature	503.15 K
Oven	Temperature program	373.15 K (2.50 min) 120 K·min^{-1} to 493.15 K (1.50 min)

Table 3.4. Gas chromatograph operation conditions for the analysis of water + IL + *n*-hexane ternary systems.

Injector	Temperature	503.15 K
	Split	1:50
	Injection volume	1 μl
Column	Type	HP-FFAP
	Flux	Constant flux of 1.1 mL ·min^{-1}
Detector	Type	TCD
	Temperature	503.15 K
Oven	Temperature program	323.15 K (1.90 min) 12 K·min^{-1} to 373.15 K (0.50 min)

When phases were practically pure *n*-alkane or water, ICP-OES (inductively coupled plasma atomic emission spectroscopy) was used to prove the IL content was <0.0005 in mass fraction. Similarly, when water content in *n*-dodecane was very low, Karl Fischer titration was used.

For the water + $[P_{6\,6\,6\,14}][(iOc)_2PO_2]$ + *n*-dodecane ternary system, fish-type phase diagrams were obtained from the rigorous LLE data and completed with data obtained by cloud-point method. The cloud-point method [76, 77] is a visual technique that determines the phase boundaries by slowly changing a variable (temperature or composition) until turbidity (the evidence of the existence of a heterogeneous system) appears or disappears. Here, samples of a given *n*-dodecane/water mass ratio were prepared by weight into a jacketed cell. Temperature was controlled circulating water from a bath thermostat (HETO model CB7) and IL was added from a burette. IL concentration and temperature were changed searching for these phase boundaries. Temperature and added volume of IL were registered for each turbidity appearance or disappearance.

All weighing was carried out by means of a Mettler Toledo AE 240 analytic balance with an uncertainty in the measurement of $\pm 10^{-4}$ g. It is shown in Figure 3.6.

Figure 3.6. Mettler Toledo AE 240 balance.

3.2.3. Physical properties

Samples of phases in equilibrium were perfectly sealed to avoid losses by evaporation or pickup of moisture, and kept at the desired temperature of measurement to avoid phase separation. Special care was put in samples at 348 K. The withdrawn of these samples was done with hot syringes and keeping vials always at this temperature, placing a thermostatic bath next to the measurement apparatus.

3.2.3.1. Density

The determination of densities was carried out at atmospheric pressure in a DMA 5000 Anton Paar oscillating U-tube density meter (Figure 3.7), with automatic viscosity correction and self-control of the temperature to ±0.01 K using the Peltier effect. Air and water were used as calibrating fluids.

Density measurements were carried out by injecting in the U-tube 1.5 mL of sample, being sure no air bubbles which would impede the stabilization of the apparatus were present. Before each new measurement, the cell was cleaned with an appropriate solvent and it was dried with air. The measurement was repeated at least three times for each sample. The uncertainty in the density measurement is $3 \cdot 10^{-5}$ g·cm^{-3}.

Figure 3.7. Anton Paar DMA densimeter.

3.2.3.2. Viscosity

A controlled stress rheometer Anton Paar Physica model MCR 301 equipped with a chamber (CTD 450, Anton Paar, Austria) was used to determine the Newtonian character or the viscosity at several temperatures of the pure ILs (Figure 3.8). A plate-plate system (diameter 50 mm and gap 2 mm) was employed. Temperature was registered with a precision of 0.01 K using a Peltier system. The uncertainty in the viscosity measurement with this equipment is 2%.

Figure 3.8. Rheometer Anton Paar Physica model MCR301.

Samples of SAIL were put between the two plates and the selected gap was adjusted. The excess of sample was carefully removed, and the rim was covered with paraffin to avoid moisture pickup from the atmosphere by the sample during the tests. A rest time of 15 minutes to release possible stresses of the sample was set before measurements.

A Newtonian behaviour was found for shear rates between 1 y 10^3 s^{-1} for all the pure ILs. For this reason, viscosities of pure ILs and equilibrium phases could be also determined using an Ubbelohde microviscosimeter.

Kinematic viscosity (υ) was determined using an Ubbelohde microviscosimeter technique (Figure 3.9). Flow time measurement was performed by Lauda Processor Viscosity system PVS1 with a resolution of 0.01 s. The temperature was controlled using a Lauda D-20-KP clear view thermostat with a through-flow cooler DLK 10. Dynamic viscosities were calculated using the equation:

$$\eta=\upsilon\cdot\rho=K\cdot(t-y)\cdot\rho \qquad (3.1)$$

where η and υ are the dynamic and kinematic viscosities, respectively, ρ is the density of the sample, K is the capillary constant provided by

the manufacturer, t is the flow time and y is the kinetic energy correction used if necessary. The measurement was repeated at least three times for each sample. The uncertainty for the dynamic viscosity is estimated to be 0.5%.

Figure 3.9. Ubbelohde microviscosimeter technique.

3.2.3.3. Interfacial tension

Interfacial tension was measured using a spinning drop tensiometer KRUSS model Site100 (Figure 3.10). Temperature is controlled circulating oil from a thermostatic bath Julabo model EH-5 with stability ±0.1 K. For measuring the interfacial tension, the capillary was filled with the heavy phase checking that no air bubbles remained inside. Since cationic surfactants adsorb onto glass [78, 79], the solution was kept into the capillary for at least 30 minutes and then it was replaced with fresh solution. The light phase was injected with a Hamilton microliter syringe at a slow speed of rotation (about 1000 rpm) and a volume varying between 2 and 8 µl. The capillary rotating speed used to carry out the measurements was the necessary to obtain a drop longitude at least 4 times bigger than its diameter. The interfacial tension was then obtained from the Vonnegut equation [80]:

$$\gamma = \frac{\Delta\rho \cdot \omega^2 \cdot r^3}{4} \tag{3.2}$$

where ω, r and $\Delta\rho$ are the capillary rotating speed, drop radius and density difference between the bulk and drop phases, respectively. The densities were experimentally measured in this work as previously explained. The measurement of each interfacial tension was repeated at least three times for each sample. The estimated uncertainty for the interfacial tension measurement is 2%.

Figure 3.10. Spinning drop KRUSS model Site100 tensiometer.

3.2.3.4. Surface tension

Surface tensions of SAILs and aqueous solutions of SAIL $[P_{4\,4\,4\,1}][DS]$ were carried out using the Wilhelmy plate method in a Krüss K11 tensiometer (Figure 3.11). A platinum Wilhelmy plate bent in a cylindrical shape to allow measurements with smaller amounts of sample was used (Krüss accessory reference PL22 with dimensions 11 mm height, 20 mm perimeter and 0.1 mm width). For each reading, the equipment rejects the first two measurements and calculates the average of 10 measurements. Data were collected in triplicate and the estimated uncertainty is 0.1 $mN \cdot m^{-1}$. An external thermostat (Selecta Frigiterm 6000382) allowed control of temperature at 298.15 K. The uncertainty in the temperature measurement is 0.05 K.

Figure 3.11. Wilhelmy plate tensiometer

3.2.3.5. Conductivity

Electric conductivity measurements were carried out using a Basis 30 Crison electric conductivimeter connected to a Selecta Ultraterm thermostatic bath. It is shown in Figure 3.12. The uncertainty in the temperature measurement is 0.1 K. Data were collected in triplicate and the estimated uncertainty is 0.1 ($\mu S \cdot cm^{-1}$).

Figure 3.12. Basis 30 Crison electric conductivimeter.

3.2.3.6. Thermal properties

Differential scanning calorimetry (DSC) experiments were run in a TA Instruments Q2000 differential scanning calorimeter (Figure 3.13, left), with an uncertainty of 1 K. Heating and cooling rates of 2 $K \cdot min^{-1}$ were used, completing three cycles, in the temperature range of 183–313 K. The samples (ca. 15–20 mg) were encapsulated in hermetic aluminium pans with lids of the same material and loaded onto the measuring chamber with an autosampler. An empty pan with its lid was used as the reference, and a 50 $mL \cdot min^{-1}$ flow of N_2 (Praxair, 99.999 %) was used as sample purge gas. It was ensured that the curves for the second and third cycle were coincident, and the results from the third cycle were used.

Figure 3.13. TA Instruments Q2000 differential scanning calorimeter (left) and TA Instruments Q500 thermogravimetric analysis apparatus (right).

The thermal stability of the samples was measured in a TA Instruments Q500 thermogravimetric analysis (TGA) apparatus (Figure 3.13, right) with a weight precision of ±0.01%. Samples (ca. 15–20 mg) were placed in open platinum measuring pans and heated at a rate of 10 $K \cdot min^{-1}$ from room temperature to 348 K, then being held isothermally at this temperature for 30 min to help removing

water and other volatile compounds that might be present. After that isothermal step, the samples were further heated, at a rate of 5 $K \cdot min^{-1}$, up to 673 K, under a constant nitrogen gas flow of 60 $mL \cdot min^{-1}$.

All DSC and TGA thermograms were evaluated using the Universal Analysis 2000 software (Version 4.5.0.5A) by TA Instruments.

3.2.3.7. Refractive index

An ATAGO RX-5000 refractometer connected to a Hetotherm CB7 thermostatic bath was used for the measurement of refractive indices. The temperature was kept constant to within ±0.1 K. The uncertainty in the refractive index measurement is 4×10^{-5}.

Figure 3.14. ATAGO RX-5000 refractometer.

3.2.4. Microscopy

Different types of microscopy were used in this work to characterise aggregates formed by the SAILs or microemulsion phases.

3.2.4.1. Transmission Electron Microscopy (TEM)

The structures formed by the surfactant $[P_{4\,4\,4\,1}][DS]$ in water were imaged at 298.15 K. Samples were prepared by putting a drop of $[P_{4\,4\,4\,1}][DS]$ solution (with concentration ca. 20 times above the *cmc*) on the carbon-coated copper grid (300 mesh). Samples were imaged under a ZEISS Libra 200 FE electron microscope at a working voltage of 200 kV (Figure 3.15, a).

3.2.4.2. Cryogenic-transmission electron microscopy (cryo-TEM)

Cryogenic-transmission electron microscopy (cryo-TEM) allows for visualization and obtention of direct, high resolution images of aggregates formed by polymers, surfactants and/or other components [81]. To obtain evidences of microemulsion formation in the middle phase of the three-phase region for the system involving $[P_{6\,6\,6\,14}][(iOc)_2PO_2]$. Experiments were carried out at CACTI services

(University of Vigo, Spain). A small amount of the sample (ca. 0.1 µl) was deposited on a carbon-coated holey polymer film in a controlled environment vitrification system, Gatan cryoplunge, where temperature and relative humidity are controlled. The excess liquid is blotted away with filter paper and quickly vitrified in liquid ethane. The vitrified sample is transferred to the electron microscope, a JEOL model JEM 2010 FEG, using a cryo-transfer system Gatan CT 3500 (Figure 3.15, c) Pictures were taken with a digital camera Gatan MSC794 at an acceleration voltage of 200 kV. The working temperature was −170 ºC.

3.2.4.3. Optical microscope

Samples of the solutions to be studied were deposited in a glass slide and covered with a cover slip. The observations were made with a Leica model TCS SP2 microscopy with polarized light (Figure 3.15, b) at room temperature. The samples were studied by conventional polarizing microscopy to prove the absence of liquid crystals by the absence of birefringence in the liquid solutions.

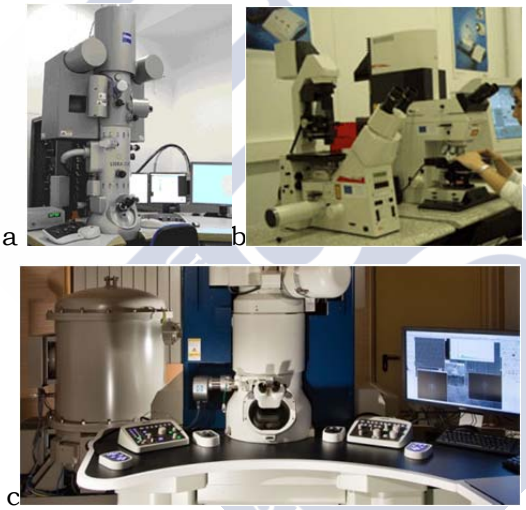

Figure 3.15. (a) ZEISS Libra 200 FE electron microscope (b) Leica model TCS SP2 optical microscope (c) JEOL model JEM 2010 FEG cryo-TEM microscope.

3.2.5. Dynamic light scattering

The hydrodynamic radius of the aggregates was measured by means of Dynamic Light Scattering (DLS). A Malvern Zen3600 ZetaSizer Nano ZS apparatus (Figure 3.16) using glass cuvettes was used to perform the DLS measurements at room temperature.

Figure 3.16. Malvern Zetasizer Nano ZS.

3.2.6. Salinity or blend scans

Salinity tests were carried out using encased glass pipettes [82]. The pipettes for the tests were made from 5-cc pipettes of borosilicate glass severed in half after sealed at the tip. Approximately 1 cm^3 of brine + surfactant and 1 cm^3 of test oil were weighed into the pipettes using an analytical balance, and the pipettes were sealed at the top with an oxygen-acetylene torch. Water oil ratio (WOR) was ~1 and the concentration of surfactant was 2 wt% overall. *n*-octane was chosen in most of the cases as oil phase because optimal salinities of various surfactants against this oil and many crude oils are somewhat similar [83]. In some cases, *n*-dodecane or butylbenzene and hexylbencene were also selected as oils to decrease the optimal salinity. Scans were carried out changing the salinity for pure surfactants, and surfactants ratio was changed in the case of blends.

Samples were mixed, at room temperature, approximately 24 hours using a rotary mixer and then they were left to equilibrate until the phase volume remained constant. Tests at higher temperatures were carried out placing the sealed pipettes inside a test tube filled with silicone oil and using a test tube dry block heater. They were removed from heater briefly several times during equilibration, shaken end-to-end by hand, and relocated. This procedure was continued until phase volumes remained constant. Photographs were taken and phase volumes read to calculate solubilisation parameters, optimal salinity or blend ratio.

USC
UNIVERSIDADE
DE SANTIAGO
DE COMPOSTELA

4. RESULTS AND DISCUSSION

USC
UNIVERSIDADE
DE SANTIAGO
DE COMPOSTELA

4.1. LIQUID-LIQUID EQUILIBRIUM

4.1.1. Water + [$P_{6\,6\,6\,14}$][DCA] + *n*-dodecane/ *n*-hexane

The LLE and LLLE data for the ternary system water + [$P_{6\,6\,6\,14}$][DCA] + *n*-dodecane were determined at 298.15 and 348.15 K and atmospheric pressure. The results are presented in Table 4.1 and Table 4.2. Figure 4.1 and Figure 4.2 show the phase equilibria diagrams. The LLLE data for the ternary system water + [$P_{6\,6\,6\,14}$][DCA] + *n*-hexane were also determined to compare the influence of the alkyl chain length of the hydrocarbon on the phase behaviour. However, when *n*-hexane was used as oil (instead previously used *n*-dodecane) the low boiling point of the hexane limited the maximum experimental temperature of the work to 323.15 K. The phase diagrams for ternary systems water + [$P_{6\,6\,6\,14}$][DCA] + *n*-hexane at 298.15 K and 323.15 K and atmospheric pressure are shown in Figure 4.3 and Figure 4.4. Experimental LLE and LLLE data are presented in Table 4.3 and Table 4.4.

It can be seen from Figures 4.1 to 4.4 that these systems are, according to Treybal classification, Type III systems because the three binary subsystems are partially miscible. Due to the surface active character of the IL, the systems could also be classified as Winsor Type III, with a triphasic region surrounded by two visible biphasic regions and one negligible biphasic region (at the bottom axis). This is common for traditional surfactants, since the height of the bottom region usually corresponds with a concentration about the critical micelle concentration in the aqueous phase [84]. Therefore, the quantity of surfactant needed to reach the triphasic region, associated with a minimum interfacial tension, is very low. The triphasic region consists of an excess oil phase, an excess water phase, and a middle phase where the IL solubilises water and oil (preferentially solubilising the hydrocarbon).

Water + [$P_{6\,6\,6\,14}$][DCA] + hydrocarbon phase diagrams at 298.15 K can be compared for *n*-hexane and *n*-dodecane. Solubility of the IL in both hydrocarbons is negligible. However, there is a bigger solubility of *n*-hexane than *n*-dodecane in [$P_{6\,6\,6\,14}$][DCA]. Analysing the three-phase region formed, both aqueous and organic phases are practically water and hydrocarbon, respectively. The apex of the tie-triangle has a higher content of the IL and minor content of the hydrocarbon in the case of *n*-dodecane. The solubility of water in [$P_{6\,6\,6\,14}$][DCA] at 298.15

K (0.029 in mass fraction) is in agreement with values reported in literature [68, 85, 86]. A comparison is provided in Table 4.5.

Similar phase diagrams have been found for other systems of the type water + phosphonium SAIL + *n*-dodecane previously studied by our research group. These ILs have the same cation but a different anion: $[P_{6\,6\,6\,14}]Cl$ [42, 87] and $[P_{6\,6\,6\,14}][NTf_2]$ [88]. All these ternary systems have been found to be Winsor Type III. However, the size of the different heterogeneous regions is different. This is due to the large influence of the anion on the water and oil miscibility in the IL. The size of the three-phase region found for the IL with the dicyanamide anion is larger than those found with the anions chloride and bis(trifluoromethylsulfonilimide.

The effect of temperature in the LLLE is small for both systems. Temperature slightly increases the solubility of water in the IL. However, for the ternary system water + $[P_{6\,6\,6\,14}][DCA]$ + *n*-dodecane, the solubility of *n*-dodecane in the IL increases from 0.195 to 0.253 (mass fraction), when temperature is raised from 298.15 K to 348.15K. This implies a small reduction in the three-phase region and the apex of the tie-triangle reduces its content of IL. In the case of the ternary system water + $[P_{6\,6\,6\,14}][DCA]$ + *n*-hexane, with the temperature, the solubility of *n*-hexane in the IL slightly increases.

Similar behaviour was found for the ILs $[P_{6\,6\,6\,14}]Cl$ [42, 87] and $[P_{6\,6\,6\,14}][NTf_2]$ [88] even when with the chloride anion the IL becomes completely miscible with *n*-dodecane at 348.15 K.

Table 4.1. LLE and LLLE data for water (1) + [P$_{6\,6\,6\,14}$][DCA] (2) + *n*-dodecane (3) ternary system at 298.15 K and 0.1 MPa. Compositions given in mass fraction.

Biphasic region 1					
Upper Phase			Lower phase		
w_1	w_2	w_3	w_1	w_2	w_3
0.029	0.971	0.000	1.000	0.000	0.000
0.029	0.918	0.053	1.000	0.000	0.000
0.028	0.878	0.094	1.000	0.000	0.000
0.026	0.839	0.135	1.000	0.000	0.000
$u(w_1)$=0.001	$u(w_2)$=0.003	$u(w_3)$=0.003	$u(w_1)$=0.001	$u(w_2)$=0.001	$u(w_3)$=0.001
Biphasic region 2					
Upper Phase			Lower phase		
w_1	w_2	w_3	w_1	w_2	w_3
0.000	0.000	1.000	0.000	0.805	0.195
0.000	0.000	1.000	0.012	0.805	0.183
$u(w_1)$=0.001	$u(w_2)$=0.003	$u(w_3)$=0.003	$u(w_1)$=0.001	$u(w_2)$=0.003	$u(w_3)$=0.003
Triphasic region					
Upper Phase			Medium Phase		
w_1	w_2	w_3	w_1	w_2	w_3
0.000	0.000	1.000	0.023	0.799	0.178
$u(w_1)$=0.001	$u(w_2)$=0.003	$u(w_3)$=0.003	$u(w_1)$=0.001	$u(w_2)$=0.003	$u(w_3)$=0.003
Lower phase					
w_1	w_2	w_3			
1.000	0.000	0.000			
$u(w_1)$=0.001	$u(w_2)$=0.001	$u(w_3)$=0.001			

Standard uncertainties: $u(P)$ = 5 kPa, $u(T)$ = 0.05 K.

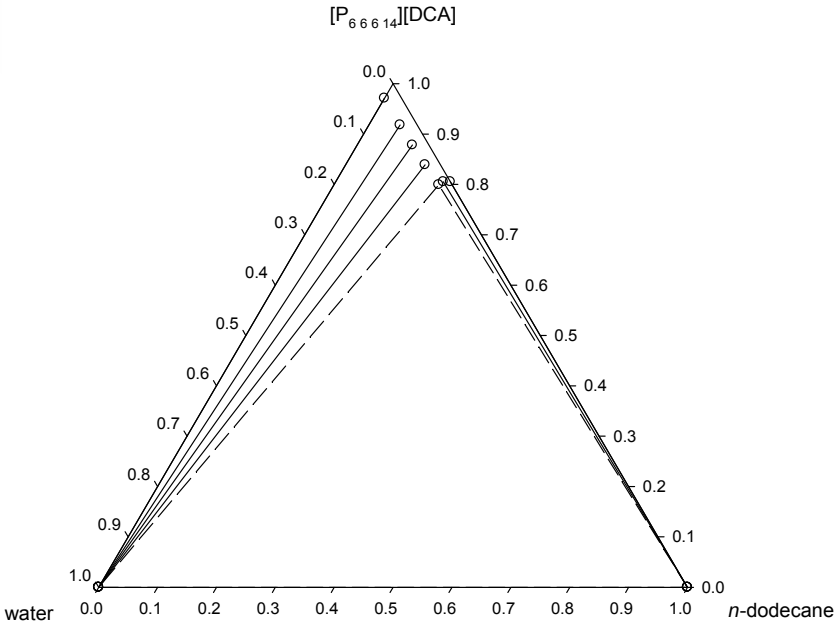

Figure 4.1. Phase diagram for water + [P$_{6\,6\,6\,14}$][DCA] + *n*-dodecane ternary system at 298.15 K and atmospheric pressure.

Table 4.2. LLE and LLLE data for water (1) + [$P_{6\,6\,6\,14}$][DCA] (2) + *n*-dodecane (3) ternary system at 348.15 K and 0.1 MPa. Compositions given in mass fraction.

Biphasic region 1					
Upper Phase			Lower phase		
w_1	w_2	w_3	w_1	w_2	w_3
0.040	0.960	0.000	1.000	0.000	0.000
0.028	0.927	0.045	1.000	0.000	0.000
0.025	0.885	0.090	1.000	0.000	0.000
0.023	0.858	0.119	1.000	0.000	0.000
0.024	0.804	0.172	1.000	0.000	0.000
$u(w_1)$=0.001	$u(w_2)$=0.003	$u(w_3)$=0.003	$u(w_1)$=0.001	$u(w_2)$=0.001	$u(w_3)$=0.001
Biphasic region 2					
Upper Phase			Lower phase		
w_1	w_2	w_3	w_1	w_2	w_3
0.000	0.000	1.000	0.000	0.747	0.253
0.000	0.000	1.000	0.008	0.756	0.237
0.000	0.000	1.000	0.014	0.762	0.224
$u(w_1)$=0.001	$u(w_2)$=0.003	$u(w_3)$=0.003	$u(w_1)$=0.001	$u(w_2)$=0.003	$u(w_3)$=0.003
Triphasic region					
Upper Phase			Medium Phase			Lower phase		
w_1	w_2	w_3	w_1	w_2	w_3	w_1	w_2	w_3
0.000	0.000	1.000	0.031	0.768	0.201	1.000	0.000	0.000
$u(w_1)$=0.001	$u(w_2)$=0.003	$u(w_3)$=0.003	$u(w_1)$=0.001	$u(w_2)$=0.003	$u(w_3)$=0.003	$u(w_1)$=0.001	$u(w_2)$=0.001	$u(w_3)$=0.001

Standard uncertainties: $u(P)$ = 5 kPa, $u(T)$ = 0.05 K.

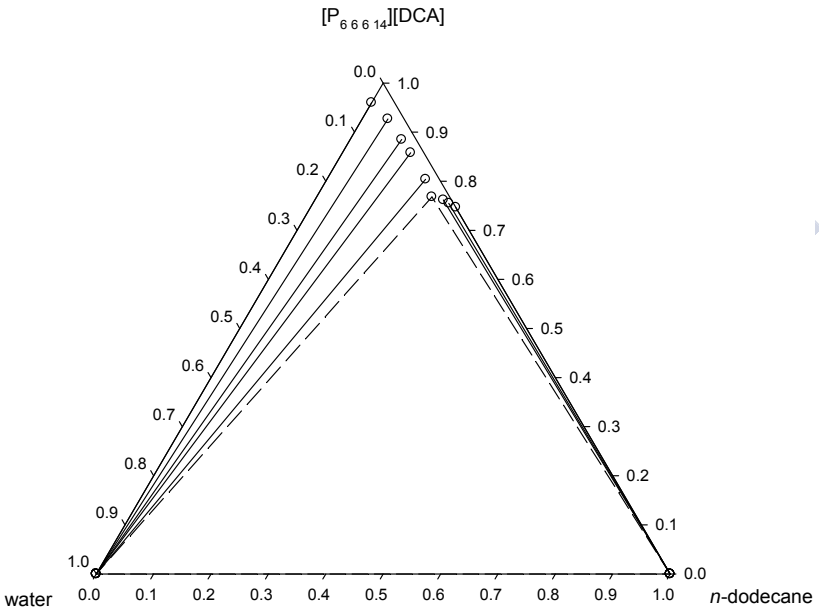

Figure 4.2. Phase diagram for water + [$P_{6\,6\,6\,14}$][DCA] + n-dodecane ternary system at 348.15 K and atmospheric pressure.

Table 4.3. LLE and LLLE data for the ternary system water + [P6 6 6 14][DCA] + hexane at T = 298.15 K and 0.1 MPa. Compositions given in mass fraction.

Biphasic region 1					
Upper Phase			Lower phase		
w_1	w_2	w_3	w_1	w_2	w_3
0.030	0.970	0.000	1.000	0.000	0.000
0.027	0.957	0.016	1.000	0.000	0.000
0.025	0.911	0.064	1.000	0.000	0.000
0.024	0.847	0.130	1.000	0.000	0.000
0.022	0.771	0.207	1.000	0.000	0.000
$u(w_1)$=0.001	$u(w_2)$=0.002	$u(w_3)$=0.002	$u(w_1)$=0.001	$u(w_2)$=0.001	$u(w_3)$=0.001
Biphasic region 2					
Upper Phase			Lower phase		
w_1	w_2	w_3	w_1	w_2	w_3
0.000	0.000	1.000	0.000	0.709	0.291
0.000	0.000	1.000	0.009	0.717	0.274
$u(w_1)$=0.001	$u(w_2)$=0.001	$u(w_3)$=0.001	$u(w_1)$=0.001	$u(w_2)$=0.002	$u(w_3)$=0.002

Triphasic region								
Upper Phase			Medium Phase			Lower phase		
w_1	w_2	w_3	w_1	w_2	w_3	w_1	w_2	w_3
0.000	0.000	1.000	0.021	0.724	0.255	1.000	0.000	0.000
$u(w_1)$=0.001	$u(w_2)$=0.001	$u(w_3)$=0.001	$u(w_1)$=0.001	$u(w_2)$=0.002	$u(w_3)$=0.002	$u(w_1)$=0.001	$u(w_2)$=0.001	$u(w_3)$=0.001

Standard uncertainties: $u(P)$ = 5 kPa, $u(T)$ = 0.05 K.

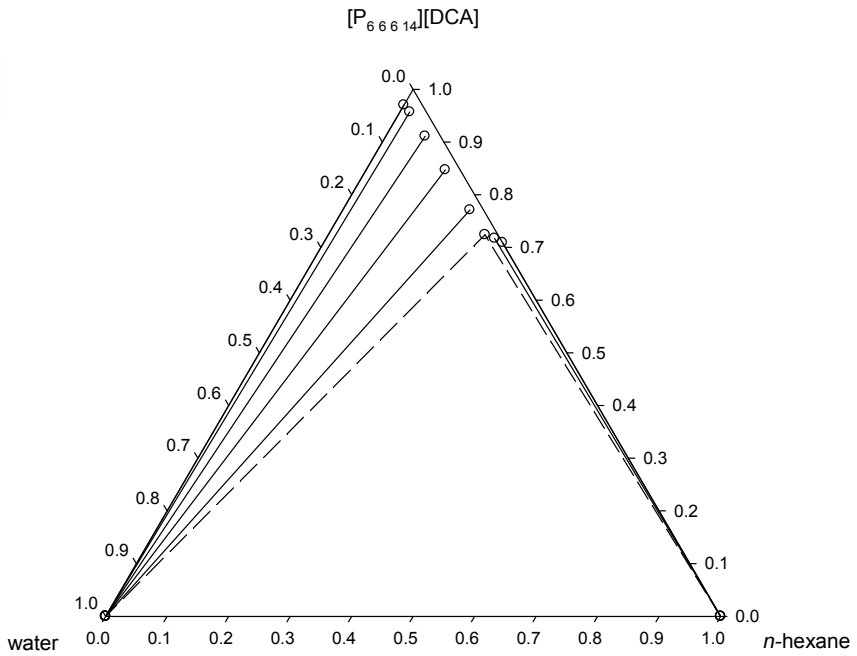

Figure 4.3. Phase diagram for water + [P6 6 6 14][DCA] + n-hexane ternary system at 298.15 K and atmospheric pressure.

Table 4.4. LLE and LLLE data for the ternary system water + [$P_{6\,6\,6\,14}$][DCA] + hexane at T = 323.15 K and 0.1 MPa. Compositions given in mass fraction.

Biphasic region 1					
Upper Phase			Lower phase		
w_1	w_2	w_3	w_1	w_2	w_3
0.032	0.968	0.000	1.000	0.000	0.000
0.025	0.953	0.022	1.000	0.000	0.000
0.020	0.891	0.089	1.000	0.000	0.000
0.019	0.830	0.151	1.000	0.000	0.000
0.020	0.730	0.250	1.000	0.000	0.000
$u(w_1)$=0.001	$u(w_2)$=0.002	$u(w_3)$=0.002	$u(w_1)$=0.001	$u(w_2)$=0.001	$u(w_3)$=0.001
Biphasic region 2					
Upper Phase			Lower phase		
w_1	w_2	w_3	w_1	w_2	w_3
0.000	0.000	1.000	0.000	0.688	0.312
0.000	0.000	1.000	0.003	0.694	0.303
0.000	0.000	1.000	0.016	0.687	0.297
$u(w_1)$=0.001	$u(w_2)$=0.001	$u(w_3)$=0.001	$u(w_1)$=0.001	$u(w_2)$=0.002	$u(w_3)$=0.002
Triphasic region					
Upper Phase			Medium Phase		
w_1	w_2	w_3	w_1	w_2	w_3
0.000	0.000	1.000	0.021	0.684	0.295
$u(w_1)$=0.001	$u(w_2)$=0.001	$u(w_3)$=0.001	$u(w_1)$=0.001	$u(w_2)$=0.002	$u(w_3)$=0.002

Lower phase		
w_1	w_2	w_3
1.000	0.000	0.000
$u(w_1)$=0.001	$u(w_2)$=0.001	$u(w_3)$=0.001

Standard uncertainties: $u(P)$ = 5 kPa, $u(T)$ = 0.05 K.

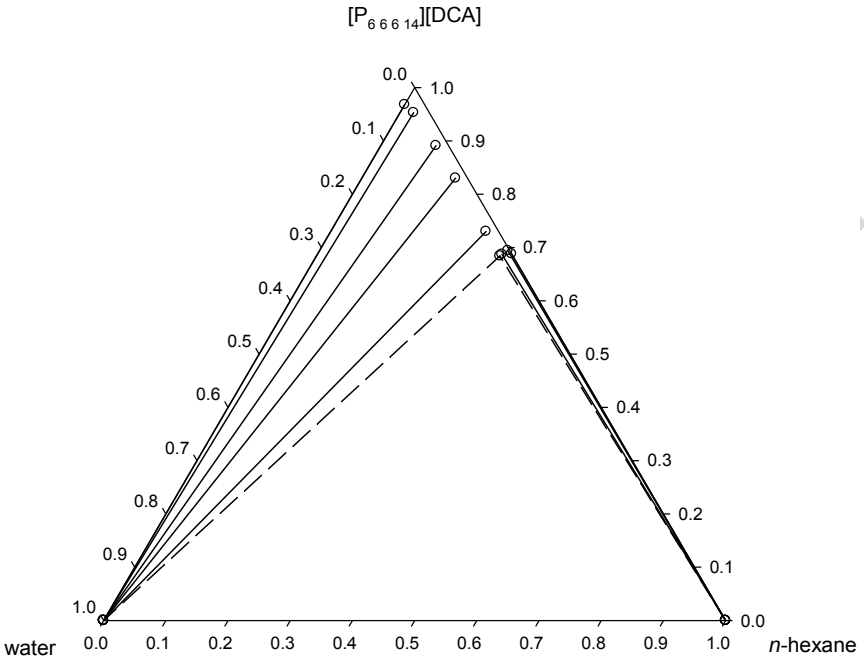

Figure 4.4. Phase diagram for water + [P6 6 6 14][DCA] + n-hexane ternary system at 323.15 K and atmospheric pressure.

Table 4.5. Comparison of water weight fraction (w_{H2O}), density (ρ), and viscosity (μ) for the IL [$P_{6\ 6\ 6\ 14}$][DCA] saturated with water, at 298.15K, obtained in this work and values available in the literature.

	This work	[68]	[85]	[86]
w_{H2O}	0.029	0.031	0.033	0.032
ρ (g·cm^{-3})	0.89860	0.9007	-	-
μ (mPa·s)	190.1	190.83	-	-

4.1.1.1. Physical properties

Interfacial tension and other physical properties like density and viscosity are of critical importance in EOR applications. The presence of salts has also to be considered due to salt content in formation and connate waters or salt dissolution effects during water flooding. Thus, physical properties for phases involved in the equilibrium were measured using both pure water and brine (4 wt% NaCl aqueous solution).

Density and viscosity were measured for phases in equilibrium of water + [$P_{6\ 6\ 6\ 14}$][DCA] + *n*-dodecane corresponding to biphasic and triphasic regions. The results are shown in Table 4.6 and Table 4.7 at 298.15 and 348.15 K, respectively, and atmospheric pressure. Previously published values [68] for these physical properties of [$P_{6\ 6\ 6\ 14}$][DCA] saturated with water are compared with our measured values in Table 4.5. Also values of these properties are shown in Table 4.6 and Table 4.7 when equilibrium is reached with brine solutions (4 wt% NaCl), that could be found in EOR applications.

Table 4.6. Physical properties (densities and viscosities) of phases in equilibrium for water/brine + [$P_{6\ 6\ 6\ 14}$][DCA] + *n*-dodecane ternary system at 298.15 K and 0.1 MPa.

		H2O		Brine	
	Phase	ρ (g·cm^{-3})	η (mPa·s)	ρ (g·cm^{-3})	η (mPa·s)
Biphasic system 1: water/brine + IL	Upper	0.89860	190.1	0.89888	172.4
	Lower	0.99705	0.890	1.02615	0.960
Biphasic system 2: *n*-dodecane + IL	Upper	0.74538	1.386	0.74538	1.386
	Lower	0.86629	102.1	0.86629	102.1
Triphasic system	Upper	0.74531	1.317	0.74535	1.347
	Middle	0.86812	78.55	0.86884	79.02
	Lower	0.99705	0.896	1.02598	0.964

Standard uncertainties: u(P) = 5 kPa. For density measurements: *u(T)* = 0.01 K. *u(ρ)* = 0.00003 g·cm^{-3}. For viscosity measurements: *u(T)* = 0.01 K. *u(η)* = 0.5%.

Table 4.7. Physical properties (densities and viscosities) of phases in equilibrium for water/brine + $[P_{6\,6\,6\,14}][DCA]$ + *n*-dodecane ternary system at 348.15 K and 0.1 MPa.

		H2O		Brine	
	Phase	ρ ($g \cdot cm^{-3}$)	η (mPa·s)	ρ ($g \cdot cm^{-3}$)	η (mPa·s)
Biphasic system 1: water/brine + IL	Upper	0.86922	24.25	0.86915	24.07
	Lower	0.97489	0.379	1.00458	0.429
Biphasic system 2: *n*-dodecane + IL	Upper	0.70890	0.667	0.70890	0.667
	Lower	0.82740	15.98	0.82740	15.98
Triphasic system	Upper	0.70874	0.649	0.70895	0.679
	Middle	0.82999	11.21	0.83105	12.15
	Lower	0.97489	0.392	0.99412	0.406

Standard uncertainties: u(P) = 5 kPa. For density measurements: $u(T)$ = 0.01 K. $u(\rho)$ = 0.00003 $g \cdot cm^{-3}$. For viscosity measurements: $u(T)$ = 0.01 K. $u(\eta)$ = 0.5%.

All measured data present values according to their compositions. As it was expected, densities and viscosities increase in the presence of salt, being more noticeable in the aqueous phases where salt preferentially solubilises, and diminish with temperature. The only exception is the case of the binary system water + IL, where the viscosity of IL-rich phase decreases in presence of salt due to a higher proportion of water solubilised in this phase.

Interfacial tension among phases in equilibrium was also determined at 298.15 and 348.15 K for the systems water/brine + $[P_{6\,6\,6\,14}][DCA]$ + *n*-dodecane. As shows Table 4.8, the addition of the SAIL implies a reduction of the interfacial tension between water and *n*-dodecane. Taking for comparative effects the interfacial tension between upper and lower phases of the three-phase system (not in contact), with $[P_{6\,6\,6\,14}][DCA]$ at 298.15 K and atmospheric pressure, an interfacial tension of 12 $mN \cdot m^{-1}$ was found, lower than the value obtained with the IL $[P_{6\,6\,6\,14}][NTf_2]$ (21.7 $mN \cdot m^{-1}$) but larger than the case of $[P_{6\,6\,6\,14}]Cl$ (1 $mN \cdot m^{-1}$) When temperature is increased, interfacial tension between phases in equilibrium decreases. A similar effect was found with the addition of salt, being more noticeable in the case of phases with appreciable content of water.

The reduction of the *n*-dodecane/water interfacial tension obtained with $[P_{6\,6\,6\,14}][DCA]$ is worse than those previously found by our research group with $[P_{6\,6\,6\,14}]Cl$ [42, 87] but better than with $[P_{6\,6\,6\,14}][NTf_2]$ [88].

Table 4.8. Interfacial tension, γ (mN·m^{-1}), between phases in equilibrium for water/brine + [$P_{6\ 6\ 6\ 14}$][DCA] + *n*-dodecane ternary system at 298.15 K and 348.15 K and 0.1 MPa.

		γ (mN·m^{-1})			
		298.15 K		348.15 K	
	Phase	Water	Brine	Water	Brine
Biphasic system 1: water/brine + IL	Upper/lower	13.3	12.5	12.4	12.0
Biphasic system 2: *n*-dodecane + IL	Upper/lower	0.93	0.93	0.76	0.76
Triphasic system	Upper/middle	0.94	0.93	0.76	0.75
	Middle/lower	12.8	12.4	11.9	11.4
	Upper/lower	12.0	11.7	10.9	10.5

Standard uncertainties: $u(P)$ = 5 kPa. $u(T)$ = 0.01 K. $u(\gamma)$ = 2%.

Interfacial tension reduction is intimately related with phase behaviour and oil solubilisation in the middle phase (0.178 in the case of the ternary system water + [$P_{6\ 6\ 6\ 14}$][DCA] + n-dodecane AT 25°C). However the interfacial tension measurements for this system are far away from the desired ultra-low values. The same small reduction in interfacial tension was expected for the system with *n*-hexane because the composition of the middle phase and the oil solubilisation parameter (0.255) was almost the same that the values found with *n*-dodecane. For this reason, physical properties for the system water + [$P_{6\ 6\ 6\ 14}$][DCA] + *n*-hexane were not determined.

4.1.1.2. Correlation

As NRTL has been widely accepted in the correlation of LLE of biphasic systems involving ILs, in this work the possibility of simultaneously correlating LLE and LLLE ternary data for systems with ILs has been analysed. To that end, the phase diagrams previously determined for water + [$P_{6\ 6\ 6\ 14}$][DCA] + *n*-hexane and *n*-dodecane were correlated using the NRTL model. The correlations were carried out by simultaneously fitting the binary and ternary LLE data together with the LLLE tie-triangle of the systems.

The NRTL interaction parameters obtained for the correlation of the system water + [$P_{6\ 6\ 6\ 14}$][DCA] + *n*-hexane at 298.15 K and 323.15 K and water + [$P_{6\ 6\ 6\ 14}$][DCA] + *n*-dodecane at 298.15 K and 348.15 K are presented in Table 4.9. This table also includes the objective function values, Equations (2.27)-(2.29), and the mean deviation between calculated and experimental concentrations in mole percentage. A inspection of deviations presented in Table 4.9 indicates that the NRTL model can be successfully used to perform a

simultaneous correlation of experimental LLE and LLLE data for these ternary systems.

Table 4.9. NRTL parameters ($J \cdot mol^{-1}$) obtained for the simultaneous correlation of LLE and LLLE data of the ternary systems previously determined. Objective function (O.F.) and mean deviation have also been included.

Water + $[P_{6\,6\,6\,14}][DCA]$+*n*-hexane						
T (K)	NRTL				O.F.*	Mean Dev. (%)**
	Parameters	Pair 1-2	Pair 1-3	Pair 2-3		
298.15	Δg_{ij}	17226.8	15940.5	-16720.1	$1.7 \cdot 10^{-3}$	0.11
	Δg_{ij}	-2123.4	13813.4	38580.1		
	$\alpha_{ij}=\alpha_{ji}$	0.2289	0.2560	0.0865		
323.15	Δg_{ij}	11493.1	14847.0	-14313.7	$1.3 \cdot 10^{-3}$	0.27
	Δg_{ij}	-537.4	13805.9	46391.9		
	$\alpha_{ij}=\alpha_{ji}$	0.2916	0.2834	0.1205		
Water + $[P_{6\,6\,6\,14}][DCA]$+ *n*-dodecane						
T (K)	NRTL				O.F.*	Mean Dev. (%)**
	Parameters	Pair 1-2	Pair 1-3	Pair 2-3		
298.15	Δg_{ij}	19101.4	35019.0	-3095.1	$3.3 \cdot 10^{-3}$	0.42
	Δg_{ij}	-3143.5	14949.5	19546.5		
	$\alpha_{ij}=\alpha_{ji}$	0,1970	0,2138	0,1929		
348.15	Δg_{ij}	26023.7	33675.8	-1470.4	$2.1 \cdot 10^{-2}$	0.99
	Δg_{ij}	-5466.5	18253.8	18169.2		
	$\alpha_{ij}=\alpha_{ji}$	0,1796	0,2309	0,2769		

* O.F. calculated by Equations (2.27)-(2.29).
** Mean dev. between cal. and exp. conc. in mol pct.

In the case of the system water + $[P_{6\,6\,6\,14}]$DCA + *n*-dodecane at 348.15 K, there is a certain deviation between the experimental and calculated tie-lines in the splitting region rich in component 1 as well as in the LLLE tie-triangle. A more precise representation of this system would require some modification of the classical activity coefficient models with the aim of increasing its flexibility, e.g adding some ternary terms.

4.1.2. Water + $[P_{6\,6\,6\,14}][(iOc)_2PO_2]$ + *n*-dodecane

In this section phase behaviour of $[P_{6\,6\,6\,14}][(iOc)_2PO_2]$ in a ternary system with water and *n*-dodecane was studied. First, the complete phase diagram was obtained at 298.15 K. The triangular phase diagram at 298.15 K is presented in Figure 4.5, and the experimental equilibrium compositions of biphasic and triphasic regions are given in Table 4.10. Blahušiak and Schlosser [72] reported the limits of the miscible region (compositions of water-saturated mixtures of

n-dodecane and $[P_{6\,6\,6\,14}][(iOc)_2PO_2]$) with good agreement with our data. However, they did not focus their work in the immiscible region, thus they did not report the existence of the three-phase region.

Table 4.10. LLE and LLLE data for the ternary system water (1) + $[P_{6\,6\,6\,14}][(iOc)_2PO_2]$ (2) + *n*-dodecane (3) at 298.15 K and 0.1 MPa. Compositions given in mass fraction.

Biphasic region 1					
Upper Phase			Lower phase		
w_1	w_2	w_3	w_1	w_2	w_3
0.147	0.853	0.000	1.000	0.000	0.000
0.142	0.828	0.030	1.000	0.000	0.000
0.126	0.734	0.140	1.000	0.000	0.000
0.103	0.623	0.274	1.000	0.000	0.000
0.093	0.522	0.384	1.000	0.000	0.000
0.079	0.440	0.482	1.000	0.000	0.000
$u(w_1)$=0.001	$u(w_2)$=0.003	$u(w_3)$=0.003	$u(w_1)$=0.001	$u(w_2)$=0.001	$u(w_3)$=0.001
Biphasic region 2					
Upper Phase			Lower phase		
w_1	w_2	w_3	w_1	w_2	w_3
0.015	0.113	0.873	0.046	0.299	0.655
$u(w_1)$=0.001	$u(w_2)$=0.003	$u(w_3)$=0.003	$u(w_1)$=0.001	$u(w_2)$=0.003	$u(w_3)$=0.003
Biphasic region 3					
Upper Phase			Lower phase		
w_1	w_2	w_3	w_1	w_2	w_3
0.006	0.040	0.954	1.000	0.000	0.000
u(w1)=0.001	u(w2)=0.003	u(w3)=0.003	u(w1)=0.001	u(w2)=0.001	u(w3)=0.001
Triphasic region					
Upper Phase			Medium Phase			Lower phase		
w_1	w_2	w_3	w_1	w_2	w_3	w_1	w_2	w_3
0.008	0.072	0.920	0.062	0.360	0.578	1.000	0.000	0.000
$u(w_1)$=0.001	$u(w_2)$=0.003	$u(w_3)$=0.003	$u(w_1)$=0.001	$u(w_2)$=0.003	$u(w_3)$=0.003	$u(w_1)$=0.001	$u(w_2)$=0.001	$u(w_3)$=0.001

Standard uncertainties: u (P) =5 kPa, u (T) = 0.05 K.

Inspection of Figure 4.5 and Table 4.10 shows up some interesting facts. The phase behaviour of the ternary system corresponds to a Winsor Type III system, with a characteristic three-phase region. $[P_{6\,6\,6\,14}][(iOc)_2PO_2]$ is only partially miscible with water, but completely miscible with n-dodecane. As a consequence, there is a large biphasic region on the left side of the diagram (see Figure 4.5) that is composed by an upper-phase microemulsion and a water excess phase. However, the biphasic region corresponding to the lower phase microemulsion and *n*-dodecane excess phase (on the right side of triangular diagram) is very small. It is also found that the three-phase triangle is separated from the water/*n*-dodecane axis. The bottom-right vertex, which is the *n*-dodecane excess phase (in equilibrium with the aqueous excess phase and the microemulsion), has a

relevant surfactant and water content (ca. 7 wt% IL and 0.8 wt% water). This effect is due to the complete miscibility of the IL and the alkane, and was not found in previously tested ILs in literature [42, 87, 88] and in this work ILs (only partially miscible with n-dodecane). Our measurements of solubility of water in $[P_{6\,6\,6\,14}][(iOc)_2PO_2]$ is in agreement with literature values (a comparison is provided in Table 4.11).

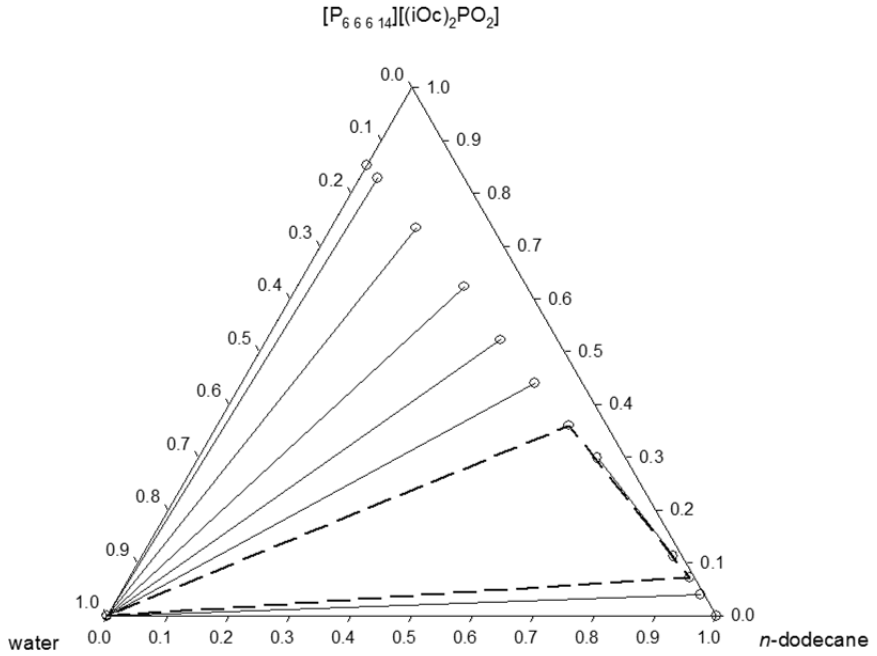

Figure 4.5. Experimental phase diagram for system water + $[P_{6\,6\,6\,14}][(iOc)_2PO_2]$ + *n*-dodecane at 298.15 K and atmospheric pressure. Tie-lines are represented by solid lines.

Table 4.11. Comparison of water weight fraction (ω_{H2O}), density (ρ), and viscosity (μ) for the IL $[P_{6\,6\,6\,14}][(iOc)_2PO_2]$ saturated with water obtained in this work and values available in the literature.

	This work	[68]	[71]	[72]
ω_{H2O}	0.147	0.1413	0.135	0.1535
ρ (g·cm^{-3})	0.91006	0.9073	0.9085	0.91440
μ (mPa·s)	135.30	173.82	139	156.74

Cryogenic transmission electron microscopy, cryo-TEM, was used to obtain evidences of microemulsion formation in the middle phase (in equilibrium with excess water and oil) of the three-phase region. Figure 4.6 shows two images of this phase taken by cryo-TEM. The

structures present in these images are similar to those of other microemulsions formed using different surfactant, co-surfactant, oil and aqueous phases [89, 90]. It is important to note that with $[P_{6\,6\,6\,14}][(iOc)_2PO_2]$ the microemulsion was obtained without the need of any other chemical (co-surfactant or a second surfactant). Blahušiak and Schlosser [72] also reported evidences of micelle formation and existence of water clusters in this ternary mixture by using Dynamic Light Scattering. For samples close to the immiscibility region and up to 80 wt% in IL, small aggregates with the mean diameter from 2 to 30 nm, reverse micelles, were found.

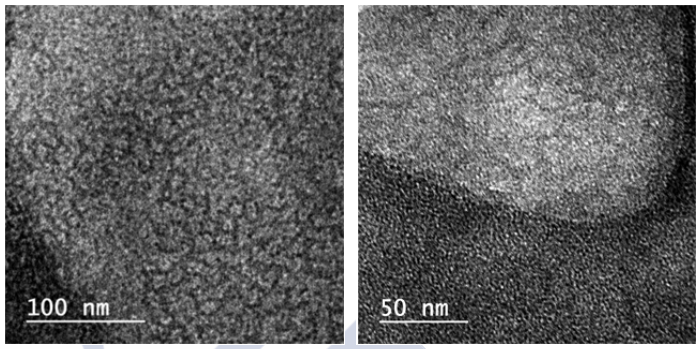

Figure 4.6. Cryo-TEM images of the microemulsion phase for the system (water+ $[P_{6\,6\,6\,14}][(iOc)_2PO_2]$+ *n*-dodecane) at 298.15 K and atmospheric pressure.

Mass compositions of the microemulsion (apex of the three-phase tie triangle) are 0.578 for *n*-dodecane and 0.360 for IL at 298.15 K (see Table 4.10). This indicates a high enrichment of the microemulsion in alkane (rather than water), which is in agreement with aggregation studies presented by Blahušiak and Schlosser [72]. This is an important issue for EOR applications, since surfactants improve oil extraction through two mechanisms [4, 91, 92]: i) Reducing the oil/water interfacial tension to increase the capillary number inside the reservoir, the so-called surfactant flooding method; and ii) Solubilizing oil into a microemulsion, called micellar flooding method. The IL $[P_{6\,6\,6\,14}][(iOc)_2PO_2]$ shows potential for both mechanisms since it shows a Winsor Type III phase diagram and is able to solubilise a large amount of the hydrocarbon into the microemulsion. However, the rich-oil microemulsion found in the three-phase system is far from the expected bicontinuous type structure, related to a minimum in the oil/water interfacial tension, with a more balanced proportion of water and oil. As other drawback, the solubilisation of n-dodecane in this middle phase requires a considerable amount of IL. This is due to the

position of the three-phase triangle in the ternary diagram a certain composition of SAIL is needed to reach the three-phase region, as can be seen in Figure 4.5, Figure 4.7 and Figure 4.8. This effect was not observed in other ternary systems involving SAILs [42, 87, 88, 93] for which very small amounts (<1 wt%) produced the three-phase system. On the other hand, this behaviour is often found with non-ionic surfactants, namely alkyl polyglycol ethers [94].

Temperature may be an important variable in the phase equilibria for systems of the type (water + surfactant + hydrocarbon or oil). Indeed, it is well known that temperature has a large influence in the phase equilibria with nonionic surfactants [95, 96]. With the few surface active ILs investigated up to date, including the first SAIL studied in this work, the effect of temperature in these systems is considered so far almost negligible [42, 87, 88]. The effect of temperature on the LLE, namely for the three-phase region, was investigated by analysing the tie-triangle compositions in the temperature range from 278.15 to 304.65 K. The same experimental procedure used to obtain the whole phase diagram at 298.15 K was used. The evolution of the three-phase region is presented in Figure 4.7 and data are shown in Table 4.12. The three-phase region size decreases as the temperature increases from 278.15 to 304.65 K. The temperature change affects the composition of the microemulsion and the oil excess phase, being the water excess phase practically pure water in all the cases. Moreover, this effect of temperature is more noticeable from 298.15 K onwards.

Table 4.12. Three-phase triangle compositions (mass fraction) for system water (1) + $[P_{6\,6\,6\,14}][(iOc)_2PO_2]$ (2) + *n*-dodecane (3) at atmospheric pressure as a function of temperature.

	Upper Phase			Medium Phase			Lower phase		
T/K	w_1	w_2	w_3	w_1	w_2	w_3	w_1	w_2	w_3
278.15	0.004	0.025	0.970	0.094	0.473	0.433	1.000	0.000	0.000
288.15	0.006	0.048	0.946	0.080	0.433	0.487	1.000	0.000	0.000
293.15	0.008	0.065	0.927	0.070	0.398	0.532	1.000	0.000	0.000
298.15	0.008	0.072	0.920	0.062	0.360	0.578	1.000	0.000	0.000
303.15	0.016	0.127	0.857	0.050	0.304	0.646	1.000	0.000	0.000
304.65	0.043	0.264	0.693	0.024	0.159	0.817	1.000	0.000	0.000
u(T)=0.05K	$u(x_1)$=0.001	$u(x_2)$=0.003	$u(x_3)$=0.003	$u(x_1)$=0.001	$u(x_2)$=0.003	$u(x_3)$=0.003	$u(x_1)$=0.001	$u(x_2)$=0.001	$u(x_3)$=0.001

Standard uncertainties: u (*P*) =5 kPa, u (*T*) = 0.05 K.

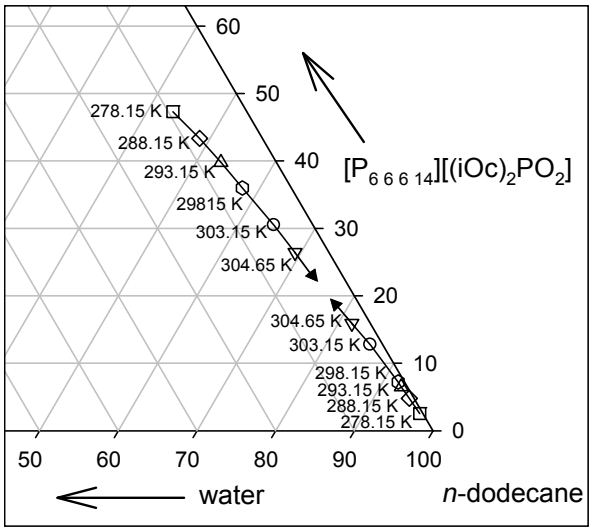

Figure 4.7. Evolution of the upper and right apices of the three-phase triangle in the liquid-liquid phase diagram at atmospheric pressure as a function of temperature. Compositions in mass fraction

The effect of temperature is more easily depicted in the so-called fish diagrams [77, 96]: phase diagram plots of temperature as a function of overall surfactant composition for a given mass ratio, α, defined as follows:

$$\alpha = \frac{m_{n-dodecane}}{m_{n-dodecane} + m_{water}} \tag{4.1}$$

where $m_{n\text{-dodecane}}$ and m_{water} represent the mass of n-dodecane and water, respectively. Such fish diagrams show in a single figure the changes in phase behaviour with temperature. Figure 4.8 shows the fish diagrams obtained for three different n-dodecane/water mass ratios, α = 0.5, 0.8 and 0.9. For α = 0.5 and α = 0.8 the typical fish shape is incomplete, but at α = 0.9 this shape is clear and the transition from three to one equilibrium phases is observed. The contact point between the fish body and tail corresponds to the temperature and composition that provide the transition from three immiscible liquid phases in equilibrium to one single phase. The strong asymmetry of the system forces this phase transition to happen only at high values of α, which can be expected from the very unsymmetrical triangle with the three liquid phases in equilibrium shown in Figure 4.5. Figure 4.8 also shows the temperature limits for the three-phase region, which can be found up to ca. 306 K.

The experimental data available for nonionic surfactants, especially for alkyl polyglycol ethers, indicate temperature ranges for

the three-phase region in the order of 5 - 20 K, with few exception going up to 40 K [77, 96]. In this work, a temperature range of about 30 K was obtained.

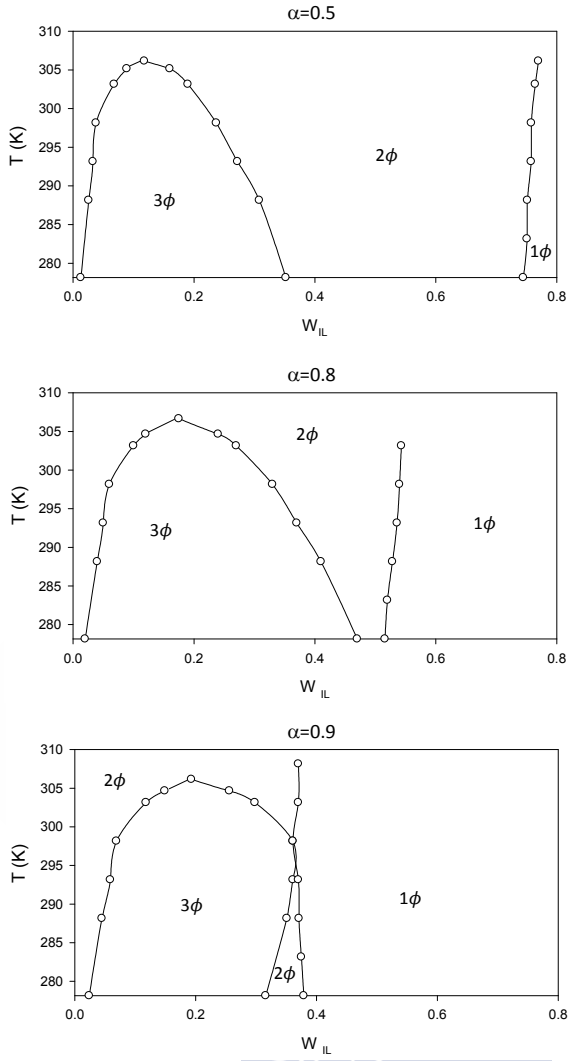

Figure 4.8. Fish diagrams for system water + $[P_{6\,6\,6\,14}][(iOc)_2PO_2]$ + *n*-dodecane at atmospheric pressure and α = 0.5 (top), 0.8 (middle) and 0.9 (bottom). Empty symbols are experimental data. 1ϕ, 2ϕ and 3ϕ denote the presence of 1, 2 or 3 liquid phases in equilibrium simultaneously. Lines are drawn to guide the eye.

4.1.2.1. Physical properties

As in the previous system, physical properties for phases involved in the studied equilibrium were measured using both pure water and

and viscosity of the equilibrium phases for the binary subsystem (water/brine + $[P_{6\,6\,6\,14}][(iOc)_2PO_2]$), and the three liquid immiscible phases obtained in the ternary system (water/brine + $[P_{6\,6\,6\,14}][(iOc)_2PO_2$ + *n*-dodecane).

Table 4.13. Densities and viscosities of involved phases in equilibrium for the system (water or brine + $[P_{6\,6\,6\,14}][(iOc)_2PO_2]$ + n-dodecane) at 298.15 K and atmospheric pressure. Brine is 4 wt% NaCl solution.

		H_2O		Brine	
	Phase	ρ *(g·cm^{-3})*	η *(mPa·s)*	ρ *(g·cm^{-3})*	η *(mPa·s)*
Biphasic system: water/brine + SAIL	Upper	0.91006	135.3	0.91633	143.7
	Lower	0.99705	0.900	1.02641	0.948
Triphasic system	Upper	0.75399	1.636	0.753506	1.652
	Middle	0.81033	11.44	0.815115	12.35
	Lower	0.99704	0.904	1.025451	0.952

Standard uncertainties: For density measurements: u(T) = 0.01 K. u(ρ) = 0.00003 g·cm^{-3}. For viscosity measurements: u(T) = 0.01 K. u(η) = 0.5%.

Densities of phases in equilibrium, for binary and ternary systems, are the consequence of their compositions, being very similar to those of the pure components when there is a major proportion of one of the compounds. In the three-phase system, the density increases from the upper *n*-dodecane-rich phase to the lower water-rich phase, with a middle IL-rich phase (the microemulsion) presenting an intermediate density. The presence of salt slightly increases densities for aqueous and IL phases, and has almost no effect in the *n*-dodecane-rich phase density. Viscosity shows a similar behaviour, with all mixtures presenting values according to their compositions, close to that of the major component and increasing in the presence of salt. In general, higher viscosities are desirable for EOR applications since that improves the capacity of the injected fluid to push the oil out of the reservoir during the flooding process [7, 97]. The viscosity obtained for the microemulsion phase is one order of magnitude higher than that of water, and increases in the presence of salt. This effect is obviously due to the presence of the IL and may avoid the addition of polymers to increase the viscosity of the injection fluid.

Coutinho and co-workers [68], Prausnitz and co-workers [71] and more recently Blahušiak and Schlosser [72] reported the solubility of water in $[P_{6\,6\,6\,14}][(iOc)_2PO_2]$ and densities and viscosities for the water-saturated IL, which are in agreement with our measurements for IL in the binary system water + $[P_{6\,6\,6\,14}][(iOc)_2PO_2]$). The small differences are, in fact, also found in the properties of the pure IL (see Table 3.2),

the binary system water + $[P_{6\,6\,6\,14}][(iOc)_2PO_2]$). The small differences are, in fact, also found in the properties of the pure IL (see Table 3.2), which are drastically affected by very low concentration of impurities. These values are compared in Table 4.11.

Interfacial tension between oil and aqueous phases is the critical property in surfactant flooding for EOR. It has been shown above that the IL $[P_{6\,6\,6\,14}][(iOc)_2PO_2]$ reduces water surface tension down to about 33.4 $mN{\cdot}m^{-1}$ with a *cmc* of $2.1{\cdot}10^{-2}$ mM. Thus, low interfacial tensions were expected for the ternary system (water + $[P_{6\,6\,6\,14}][(iOc)_2PO_2]$ + *n*-dodecane). Interfacial tensions between the equilibrium phases are shown in Table 4.14 for binary and ternary systems. The oil + water interfacial tension diminishes from 52.2 $mN{\cdot}m^{-1}$ [98, 99] down to 5.09 $mN{\cdot}m^{-1}$. That is the interfacial tension between aqueous and oil phases (not in contact) in the three-phase system. Interfacial tensions of 0.02 $mN{\cdot}m^{-1}$ for the oil/microemulsion and 5.17 $mN{\cdot}m^{-1}$ for microemulsion/aqueous interfaces were also found. Interfacial tensions between the aqueous and the oil excess phases of the same order of magnitude have been reported for other ILs using *n*-dodecane or real crude as the oil phase [42, 57, 87, 88]. For the binary (water + IL), interfacial tension decreases with the addition of sodium chloride. This effect is also noticed in the three-phase system for microemulsion/aqueous and aqueous/oil interfaces. However, the effect of the presence of salt is negligible for the oil/microemulsion interfacial tension.

Table 4.14. Interfacial tension, γ ($mN{\cdot}m^{-1}$), of involved phases in equilibrium for the system (water or brine + $[P_{6\,6\,6\,14}][(iOc)_2PO_2]$ + *n*-dodecane) at 298.15 K and atmospheric pressure. Brine is 4 wt% NaCl aqueous solution.

		γ ($mN{\cdot}m^{-1}$)	
	Phase	Water	Brine
Biphasic system: water/brine+ SAIL	Upper/lower	4.93	4.18
Triphasic	Upper/middle	0.02	0.02
	Middle/lower	5.17	4.30
	Upper/lower	5.09	4.29

Standard uncertainties: u(P) = 5 kPa. u(T) = 0.01 K. u(γ) = 2%.

There are clear differences in the phase and interfacial tension behaviour of the different ILs of the type $[P_{6\,6\,6\,14}][X]$, which are a consequence of the different anions used (measured in terms of polarity, hydrophobicity, hydration shell, etc). The ranking of solubilities of water in the studied ILs (in this work or in literature) at

298.15 K, depending on the anion is: $(iOc)_2PO_2$>Cl>DCA>NTf_2. The ranking of solubilities of *n*-dodecane in the IL is: $(iOc)_2PO_2$>Cl>NTf_2>DCA, being $[P_{6\ 6\ 6\ 14}][(iOc)_2PO_2]$ and *n*-dodecane completely miscible at 298.15 K. This leads to different sizes of the immiscible regions and different positions of the apex of the three-phase tie-triangle (composition of the middle phase in the triphasic system). Compositions of these middle phases are shown in Table 4.15 for all the systems at 298.15 K.

Table 4.15. Mass fraction compositions of the apex of the three-phase tie-triangle in systems water (1) + $[P_{6\ 6\ 6\ 14}][X]$ (2)+ *n*-dodecane (3) at 298.15 K and 0.1Mpa.

X	w_1	w_2	w_3	Lit
Cl	0.094	0.652	0.254	[42]
NTf_2	0.001	0.701	0.298	[88]
$(iOc)_2PO_2$	0.062	0.360	0.578	This work
DCA	0.023	0.799	0.178	This work

Figure 4.9 shows a plot of the interfacial tension between the upper (*n*-dodecane excess) and lower (water excess) phases and the water solubility in the pure IL as a function of water composition in the middle (IL-rich) phase for SAILs studied here ($[P_{6\ 6\ 6\ 14}]$DCA and $[P_{6\ 6\ 6\ 14}][(iOc)_2PO_2]$) and other SAILs from literature containing the same cation ($[P_{6\ 6\ 6\ 14}]$Cl and $[P_{6\ 6\ 6\ 14}][NTf_2]$). The interfacial tension decreases with the water content in the middle phase, following a second order polynomial (r_2 > 0.98). Such a simple relationship could not be found using the composition of the other components. Besides, the water solubility in the pure IL follows a linear trend (r_2 > 0.99) with the water content in the IL-rich phase. This behaviour may be a consequence of the three-phase region being formed mainly due to the immiscibility of constituent pairs. $[P_{6\ 6\ 6\ 14}][(iOc)_2PO_2]$ was not considered in the regression, despite it is shown in the graph. As mentioned above, this IL produces a different phase behaviour of the ternary system, showing complete miscibility with *n*-dodecane and a three-phase region that fades out as temperature approaches 308 K. This behaviour is usually found in non-ionic surfactants.

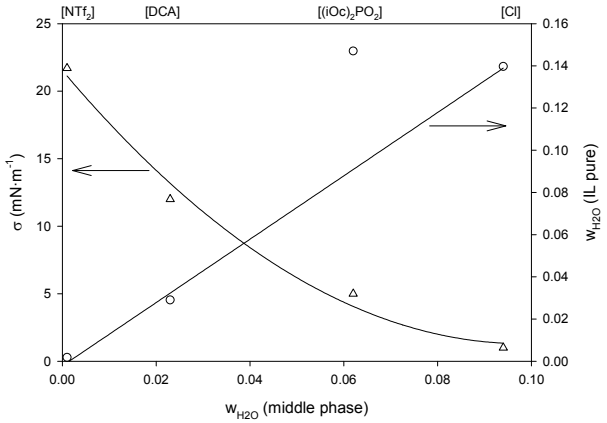

Figure 4.9. Interfacial tension between the upper and lower phases in the three-phase region and water solubility in the pure IL, as a function of water composition in the middle phase. Triangles: interfacial tension; circles: water solubility.

4.1.2.2. Correlation

The LLE and LLLE data obtained for the system water + $[P_{6\,6\,6\,14}][(iOc)_2PO_2]$ + *n*-dodecane have been correlated using the NRTL model. The NRTL interaction parameters obtained for the correlation at 298.15 K are presented in Table 4.16. This table also includes the objective function values, Equations (2.27)-(2.29), and the mean deviation between calculated and experimental concentrations in mole percentage. In this case, as in the previous studied systems, the NRTL model can be successfully used to perform a simultaneous correlation of experimental LLE and LLLE data.

Table 4.16. NRTL parameters ($J \cdot mol^{-1}$) obtained for the simultaneous correlation of LLE and LLLE data of the ternary systems previously determined in this thesis. Objective function (O.F.) and mean deviation have also been included.

Water+$[P_{6\,6\,6\,14}][(iOc)_2PO_2]$+*n*-dodecane						
T (K)	NRTL				O.F.*	Mean Dev. (%)**
	Parameters	Pair 1-2	Pair 1-3	Pair 2-3		
298.15	Δg_{ij}	67904.7	12202.3	-27790.1	$7.7 \cdot 10^{-4}$	0.27
	Δg_{ij}	-25998.7	2630.0	-8335.0		
	$\alpha_{ij}=\alpha_{ji}$	0.0938	0.1671	0.0181		

* O.F. calculated by Equations (2.27)-(2.29).
** Mean dev. between cal. and exp. conc. in mol pct.

4.1.3. Water + [$P_{4\,4\,4\,14}$]Cl + *n*-dodecane

The SAIL [$P_{4\,4\,4\,14}$]Cl is solid at 298.15 K and liquid at 348.15 K. The melting point of this IL was determined by Del Sesto *et al.* [100] and Bradaric *et al.* [101]. The reported values are 56 ºC and 60ºC, respectively. A high solubility of [$P_{4\,4\,4\,14}$]Cl in water was found at 298.15 K (ω=0.96). This is in agreement with the value previously reported by Blesic et al [102] (ω=0.94). At 348.15 K, the SAIL and water are completely miscible.

LLE data are presented in Table 4.17 and Table 4.18 and phase diagrams are shown in Figure 4.10 and Figure 4.11 at 298.15 and 348.15 K, respectively. When [$P_{4\,4\,4\,14}$]Cl, water and *n*-dodecane are mixed, biphasic systems are found. The affinity of the surfactant for the aqueous phase is greater than that for the oil. Any mixture within the interior of the immiscible area splits into an aqueous phase that contains most of the surfactant in equilibrium with an excess phase of oil (pure *n*-dodecane at 298.15 K). At the lower temperature, and due to the solid character of the IL, only very small areas of solid-liquid (SL) and solid-liquid-liquid (SLL) equilibria appear at the top of the triangular diagram and close to the SAIL + n-dodecane binary, respectively. These areas have been qualitatively determined by cloud point method and represented in Figure 4.10. At 348.15 K, a system characterised by the existence of two pairs of partially miscible liquid components was found. The immiscible region found for the ternary system diminishes with temperature.

Brine solutions were prepared with concentrations up to 4 wt% NaCl and were mixed with the surfactant at different concentrations at room temperature and atmospheric pressure. In all the cases a clear solution was found. These samples were mixed with *n*-dodecane and a biphasic system was found in all ranges of salinity. A Winsor Type III system (the goal in traditional EOR research) was not found with pure water or brine. For this reason physical properties of phases in equilibrium with pure water and brine were not determined as it was done in the previous systems.

Table 4.17. LLE equilibrium data for the ternary system water (1) + $[P_{4\,4\,4\,14}]Cl$ (2) + *n*-dodecane (3) at 298. 15 K and atmospheric pressure. Compositions given in mass fraction.

Upper Phase			Lower phase		
w_1	w_2	w_3	w_1	w_2	w_3
0.000	0.000	1.000	1.000	0.000	0.000
0.000	0.000	1.000	0.777	0.197	0.025
0.000	0.000	1.000	0.630	0.310	0.060
0.000	0.000	1.000	0.441	0.460	0.099
0.000	0.000	1.000	0.168	0.697	0.134
0.000	0.000	1.000	0.026	0.742	0.232
$u(w_1)$=0.001	$u(w_2)$=0.001	$u(w_3)$=0.001	$u(w_1)$=0.001	$u(w_2)$=0.003	$u(w_3)$=0.003

Standard uncertainties: u (P) =5 kPa, u (T) = 0.05 K.

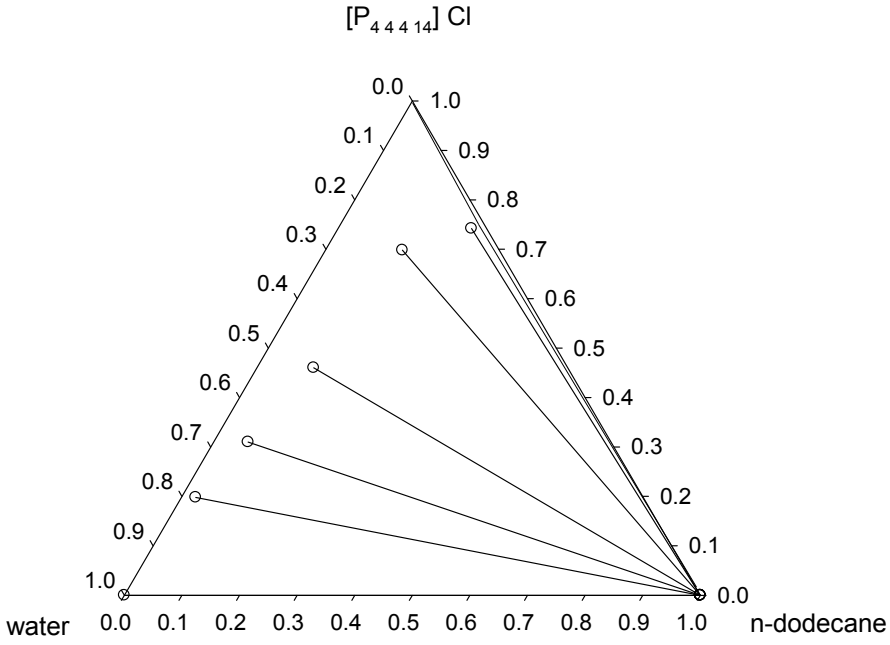

Figure 4.10. Liquid-liquid equilibrium for the ternary system water (1) + $[P_{4\,4\,4\,14}]Cl$ (2) + n-dodecane (3) at 298.15 K and atmospheric pressure

Table 4.18. LLE equilibrium data for the ternary system water (1) + $[P_{4\,4\,4\,14}]Cl$ (2) + *n*-dodecane (3) ternary system at 348.15 K and atmospheric pressure. Compositions given in mass fraction.

Upper Phase			Lower phase		
w_1	w_2	w_3	w_1	w_2	w_3
0.000	0.000	1.000	1.000	0.000	0.000
0.000	0.000	1.000	0.782	0.181	0.036
0.000	0.009	0.991	0.586	0.343	0.071
0.000	0.015	0.985	0.449	0.453	0.098
0.000	0.032	0.968	0.184	0.672	0.144
0.000	0.050	0.950	0.027	0.661	0.313
0.000	0.061	0.939	0.000	0.638	0.362
$u(w_1)$=0.001	$u(w_2)$=0.003	$u(w_3)$=0.003	$u(w_1)$=0.001	$u(w_2)$=0.003	$u(w_3)$=0.003

Standard uncertainties: u (P) =5 kPa, u (T) = 0.05 K.

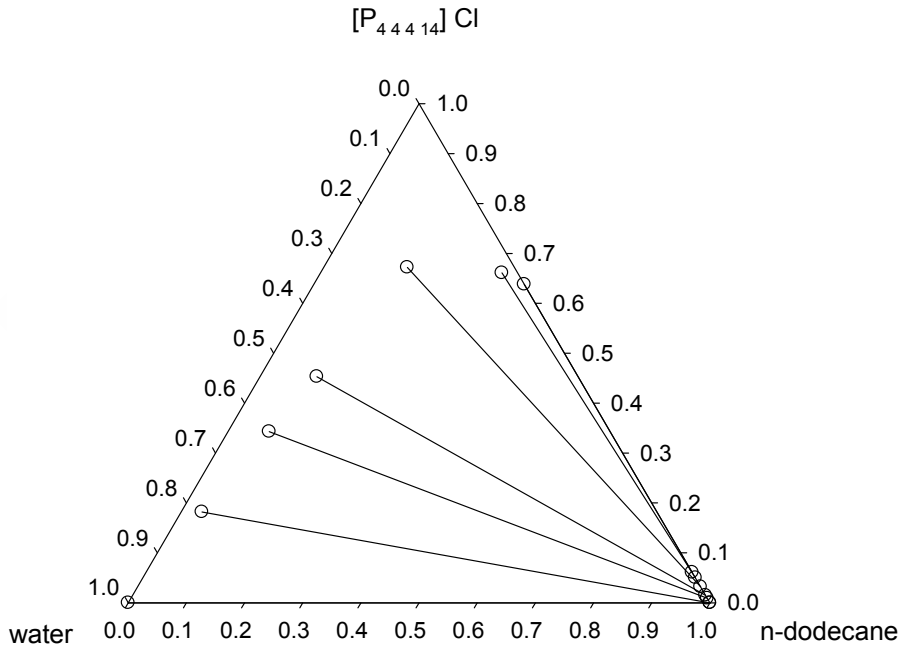

Figure 4.11. Liquid-liquid equilibrium for the ternary system water (1) + $[P_{4\,4\,4\,14}]Cl$ (2) + n-dodecane (3) at 348.15 K and atmospheric pressure.

4.1.3.1. Correlation

The correlation of the LLE data for the system water + $[P_{4\,4\,4\,14}]Cl$ + n-dodecane was carried out using the NRTL equation [14] as it has been described in section 2.1.5.2.1. In this case, the value of the non-

randomness parameter, α, was pre-fixed at 0.1, 0.2 and 0.3 values and the correlation was carried out for each of them.

The fitting parameters for NRTL are presented in Table 4.19 together with the rmsd associated with each correlation. In all cases, the best correlation was obtained with α = 0.3, while α = 0.2 provided only slightly higher deviations. A high accuracy of the NRTL correlation, as indicated by the low rmsd obtained (rmsd < 1% in all cases). The simultaneous correlation seems preferable in general since a single set of parameters would be able to describe the phase behaviour for a rather large temperature range (from 298.15 K to 348.15 K) while the loss of accuracy is rather small (an increase of about 0.3-0.5%).

Table 4.19. Binary interaction parameters and deviations (rmsd, %) of the NRTL equation (α = 0.3) for each data set (298.15 K; 348.15 K) and for the simultaneous correlation of both data sets.

	Parameters, J·mol^{-1}			
Pair i-j	Δg_{ij}	Δg_{ji}	Δg_{ij}	Δg_{ji}
1-2	-11189.6	-1174.9	878.01	4623.8
1-3	9826.0	13150.2	10667.5	11904.7
2-3	-723.08	5079.6	-1597.2	13205.0
	T=298.15K	*rmsd*=0.29%	*T*=348.15K	*rmsd*=0.52%
Simultaneous correlation (298.15 & 348.15 K)				
Pair i-j	Δg_{ij}	Δg_{ji}		
1-2	-2564.3	15914.7	*rmsd*,% (*T*,K)	
1-3	9591.6	10582.7	0.78 (298.15K)	
2-3	-1373.8	12315.4	0.88 (348.15K)	

4.2. SALINITY AND BLEND SCANS

4.2.1. Pure surfactants

Anionic surfactants are most widely used in chemical EOR processes [7]. With this in mind, the well-known traditional surfactants SDS and Na-AOT were modified changing sodium by a phosphonium or an imidazolium cation, respectively, to convert them to room-temperature SAILs. The phase behaviour of these anionic SAILs and other two cationic SAILs in mixtures with oil and brine have been evaluated. The effect of the most important reservoir parameters (salinity and temperature) has been considered for this evaluation.

4.2.1.1. Anionic SAIL: [P4 4 4 1][DS]

The SAIL tributylmethylphosphonium dodecylsulfate has been synthesized for the first time in this work. For this reason, its physical and thermal properties and its aggregation behaviour in aqueous solution were studied before testing its potential for EOR applications by means of phase behaviour tests: salinity scans.

4.2.1.1.1. Physical and thermal properties

Density and viscosity are among the most relevant properties of fluid systems for process design. Density (ρ) and viscosity (η) were measured for pure [P4 4 4 1][DS] IL from 288.15 to 348.15 K, every 10 K, and atmospheric pressure. Refractive index was also measured at the same temperatures. Values are provided in Table 4.20. The obtained results are summarised as graphical representations in Figure 4.12. As it can be observed, all the properties decrease with temperature. It was found that the IL is Newtonian within the shear rate range evaluated, from 0.1 to 100 s^{-1}, at all measured temperatures. Viscosity decreases significantly at low temperatures, achieving a moderate descent when temperature increases.

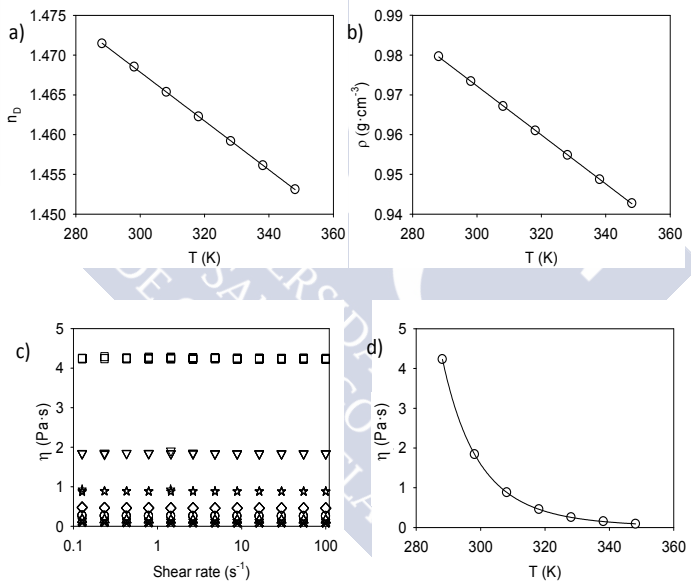

Figure 4.12. Physical properties of [P4 4 4 1][DS]: (a) Density. (b) Refractive index. (c) Viscosity as a function of shear rate at different temperatures (crosses: 348.15 K, triangles up: 338.15 K, circles: 328.15 K, diamonds: 318.15 K, stars: 308.15 K, triangles down: 298.15 K, squares: 288.15 K). (d) Viscosity of the IL as a function of temperature. Symbols: experimental data; lines: calculations by equation (4.2) for (a,b) and equation (4.4) for (d).

Table 4.20. Density (ρ), dynamic viscosity (η) and refractive index (n_D) for pure IL [$P_{4\,4\,4\,1}$][DS] at 0.1MPa.

T (K)	ρ (g·cm^{-3})	η (mPa·s)	n_D
288.15	0.97967	4240	1.47145
298.15	0.97340	1840	1.46852
308.15	0.96715	882	1.46535
318.15	0.96100	460	1.46226
328.15	0.95484	257	1.45917
338.15	0.94873	154	1.45612
348.15	0.94271	90.9	1.45311

Standard uncertainties: u(P)= 5 KPa. For density measurements: u(T) = 0.01 K. u(ρ) = 0.00003 g·cm^{-3}. For viscosity measurements: u(T) =0.01 K. u(η)<2 %. For refractive index: u(T)=0.1K. u(n_D)=0.00004.

A linear relationship was used to express the dependence with temperature for density and refractive index:

$$z = a + b \cdot T \tag{4.2}$$

where z is ρ or n_D, T is the absolute temperature, and a and b are the fitting parameters. The variation of viscosity (η) with temperature is usually correlated with the two-parameter Andrade equation:

$$\eta = \eta_\infty \cdot exp\left(-\frac{E_a}{R \cdot T}\right) \tag{4.3}$$

where R is the universal gas constant, T is the absolute temperature and the fitting parameters (characteristic constants) of the fluid are η_∞ (viscosity at infinite temperature) and E_a (a sort of "activation" energy). The Vogel–Fulcher–Tamman (VFT) equation, in particular the modified version by Cohen and Turnbull [103], was also tested for viscosities correlation:

$$\eta = A \cdot T^{0.5} \cdot exp\left(\frac{k}{T - T_0}\right) \tag{4.4}$$

where A, k and T_0 are adjustable parameters.

Relative standard deviations of the correlated variables, RSD, were calculated using following equation:

$$RSD = \left\{\frac{1}{N - v}\sum_{i}^{N}\left(\frac{z_i - z_i^{cal}}{z_i^{cal}}\right)^2\right\}^{0.5} \tag{4.5}$$

where z_i and z_i^{cal} are the values of experimental and calculated physical property, respectively, N is the number of the experimental

data points and v is the number of adjustable parameters of the equation.

Fitting parameters and RSD for density, viscosity and refractive index correlations are summarised in Table 4.21 and Table 4.22. A simple linear regression provides a good description of the temperature dependence of density and refractive index. As it was expected, due to the use of one more fitting parameter, the temperature dependence of viscosity is better described with the VFT equation.

Table 4.21. Fit parameters of the empirical polynomial correlations for density and refractive index (ρ or n_D = a + $b \cdot T$) of the surfactant IL [$P_{4\,4\,4\,1}$] [DS] as a function of temperature over the range from 288.15 to 348.15 K.

Property	Fitting parameters		RSD·10^5
	a	$b \cdot 10^4$	
ρ	1.15710	-6.16	9.9
n_D	1.56000	-3.07	6.0

Table 4.22. Fitting parameters and RSD of the Arrhenius-type and VFT equations for the correlation of viscosity as a function of temperature (in the range from 288.15 K to 348.15 K).

Equation	Fitting parameters			*RSD*
Arrhenius-type	$\eta_\infty \cdot 10^7$ (mPa·s)	Ea (kJ·mol^{-1})		0.22
	1.474	-57.68		
VFT equation	$A \cdot 10^4$ (mPa·s·K$^{0.5}$)	k (K)	T_0 (K)	0.02
	2.191	2150	134.0	

DSC analyses were carried out to identify the phase transitions in the IL. The sample was liquid at room temperature, so the heating/cooling cycles used in the DSC ranged between 183 and 313 K, at rates of 2 K·min^{-1}. Although the lower temperature used in the cycled runs was 183 K, the portions of the curves below 190 K were systematically disregarded, since loss of stability of the baseline was observed in that region (likely due to limitations of the refrigeration system of the apparatus). Two partially overlapped endothermic peaks were observed in the heating ramp, with peak temperatures of 211 and 234 K respectively. It is speculated that these signals are the result of the melting of two different types of crystals corresponding to different polymorphs of the substance, as it was previously reported in similar cases [104, 105]. For the purposes within this work, the onset temperature of the first peak, 205 K, was considered as the melting temperature of the IL. The decomposition temperature of [$P_{4\,4\,4\,1}$][DS] was determined by TGA. In the weight vs. temperature plot, a double-step decomposition was observed, with a 5% onset decomposition

temperature (onset temperature for a 5% weight loss of the original mass) of 442 K. Both the DSC and the TGA thermographs are provided in Figure 4.13.

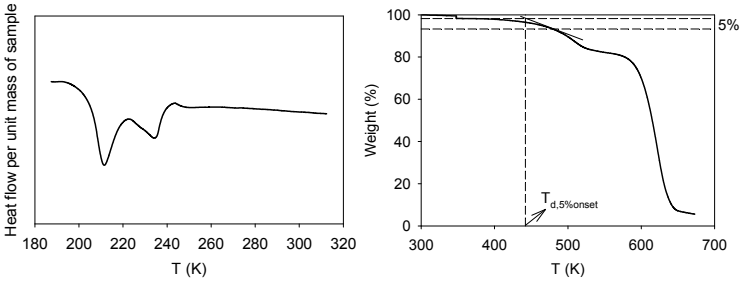

Figure 4.13**.** DSC (left) and TGA (right) thermograms of [$P_{4\,4\,4\,1}$][DS]. The TGA thermogram also shows the calculation of the 5% onset decomposition temperature, $T_{d,5\%onset}$: The crossing of the tangent at the point of 5% weight loss with the stable weight of initial sample before the starting of decomposition.

The results above indicate that the SAIL [$P_{4\,4\,4\,1}$][DS] has a liquid range of more than 200 K, from melting to decomposition. This means that [$P_{4\,4\,4\,1}$][DS] can be simply handled as a liquid not only at room temperature, but also at temperatures well above and below the ambient.

4.2.1.1.2. Aggregation behaviour in aqueous solution

Surface tension was measured to determine the critical micelle concentration (*cmc*) in aqueous solution at 298.15 K (data are available in Table 4.23). Figure 4.14 shows the change in surface tension, γ, as a function of the concentration of [$P_{4\,4\,4\,1}$][DS]. A marked break in the surface tension decrease is followed by a nearly constant value of this property. This breakpoint is the *cmc*, its value and the corresponding surface tension are given in Table 4.24.

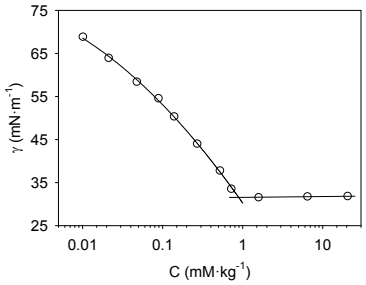

Figure 4.14. Surface tension as function of [$P_{4\,4\,4\,1}$][DS] concentration in aqueous solution at 298.15 K.

Table 4.23. Surface tension of aqueous solutions of $[P_{4\,4\,4\,1}][DS]$ at 298.15 K and 0.1MPa.

C (mmol·kg-1)	γ (mN·m^{-1})
20.60	31.8
6.50	31.7
1.59	31.5
0.73	33.5
0.52	37.7
0.27	44.0
0.14	50.3
0.09	54.5
0.05	58.4
0.02	63.9
0.01	68.8

Standard uncertainties: u(P)= 5 KPa. u(T) = 0.05 K. u(γ) = 0.1 mN·m^{-1}.

Table 4.24. Parameters derived from surface tension data for $[P_{4\,4\,4\,1}][DS]$ together with literature values for the analogous common surfactant (sodium dodecylsulfate) and different dodecylsulfate-based SAILs at 298.15 K and atmospheric pressure.

IL	*cmc* (mmol·kg^{-1})	γ_{cmc} (mN·m^{-1})	pC_{20}	*cmc*/ C_{20}	Π_{cmc} (mN·m^{-1})	Γ_m (µmol· m^{-2})	a^s_m (Å^2)	[Ref.]
$[P_{4\,4\,4\,1}]$ [DS]	0.89	31.6	3.9	7.1	40.4	2.29	72.5	-
[Na] [DS]	8.2	34.9	2.51	2.7	-	3.16	56	[9]
[C_4mim] [DS]	2.4	34.4	3.3	4.8	37.6	2.4	67.8	[106]
	1.8	31.9	3.4	4.5	40.7	2.53	66	[107]
	2.30	32.9	-	-	-	-	56	[105]
[C_6mim] [DS]	1.1	27.1	4.1	13.8	44.9	2.4	68.5	[106]
	0.8	30.0	4.0	8.0	42.6	2.08	80	[108]
[C_8mim] [DS]	0.4	26.0	4.3	8.0	46.0	2.4	68.5	[106]
	0.3	26.9	4.5	9.5	45.7	2.33	71	[108]
[C_{10}mim] [DS]	0.1	25.4	5.0	10.0	47.2	2.36	70	[108]
[C_4MP] [DS]	2.7	34.3	3.5	8.5	37.9	2.27	74	[107]
[TPA] [DS]	1.46	31.8	-	-	-	-	67	[109]
[GlyC_3] [DS]	0.74	26.0	4.4	18.6	46.0	1.14	146	[110]
[AlaC_3] [DS]	0.53	27.8	4.6	21.1	44.2	1.74	95.5	[110]
[ProC_3] [DS]	0.48	25.7	4.8	30.3	46.3	1.24	133.6	[110]
[ValC_3] [DS]	0.40	27.5	4.6	15.9	44.5	1.61	103.9	[110]
[GluC_3] [DS]	0.35	30.6	4.7	17.5	41.4	1.75	94.6	[110]

The *cmc* obtained for $[P_{4\,4\,4\,1}][DS]$ SAIL is an order of magnitude lower than its sodium analogue (the common surfactant sodium

dodecylsulfate or SDS). A comparison can also be established with other imidazolium, amino acid, ammonium and methylpyridinium analogues (see Table 4.24). The value is close to that obtained for [C_6mim][DS]. Larger chains in the cation provide lower *cmc*, however the drawback of these SAILs based on imidazolium cations is that they are not room temperature ILs. The *cmc* for [$P_{4\,4\,4\,1}$][DS] is also lower than those found for [C_4MP][DS] and [TPA][DS], but higher than values obtained by *Rao et al.* [110] for SAILs with cations based on amino acids.

The reduction produced on the surface tension is evaluated by the pC_{20}, being C_{20} the concentration required to reduce the surface tension of pure water by 20 mN·m^{-1} (see section 2.1.5.1.). The surface pressure at *cmc*, Π_{cmc}, is calculated like the difference between surface tensions of the pure solvent and the surfactant solution at the *cmc*.

Both parameters indicate the effectiveness of the surfactant to lower the surface tension of the solvent. Values reported in Table 4.24 indicate that [$P_{4\,4\,4\,1}$][DS] has larger pC_{20} and Π_{cmc} than SDS, thus being a more efficient surfactant, and are comparable to the other ILs with the same anion. The cmc/C_{20} ratio compares the tendencies of the surfactants for adsorption at interface or micellization. Dodecyl sulfate with sodium cation (SDS) has a value of this parameter significantly lower than with all the other cations. This indicates that for all the SAILs, including [$P_{4\,4\,4\,1}$][DS], adsorption is facilitated more than micellization in comparison with SDS.

The surface excess concentration, Γ_1, and the area per molecule at the interface, a_1^s, can be calculated with the Gibbs adsorption isotherm according to equation (2.10) and (2.11), respectively. C_1 is the SAIL concentration (either in mol·L^{-1} or mol·kg^{-1} since differences can be neglected in this concentration range), γ the surface tension in mN·m^{-1}, N is the Avogadro constant and all other variables have been defined above. Units for Γ_1 and a_1^s are μmol·m^{-2} and Å^2, respectively, and the derivative in equation (2.10) is obtained by fitting surface tension data up to the *cmc* to a second order polynomial. The surface excess concentration at surface saturation, Γ_m, is a useful measure of the effectiveness of adsorption of the surfactant at the interface, since it is the maximum value that adsorption can attain. This parameter, Γ_m, and the area per molecule at the interface at surface saturation, a_m^s, are presented also in Table 4.24. In comparison with all the SAILs, a lower value of the minimum area per molecule at air-

water interface is found for SDS, while amino acid-derived SAILs provide the largest values.

Electrical conductivity measurements of aqueous solutions of $[P_{4\,4\,4\,1}][DS]$ were also carried out to evaluate the thermodynamic properties of aggregation and the effect of temperature (Table 4.25). Plots of conductivity as a function of $[P_{4\,4\,4\,1}][DS]$ concentration at four different temperatures are shown in Figure 4.15. The *cmc* value is obtained as the crossing of the straight lines obtained by linear regression of the experimental data. The value obtained from conductivity measurements at 298.15 K is in good agreement with the value obtained from surface tension.

Table 4.25. Conductivity of aqueous solutions of $[P_{4\,4\,4\,1}][DS]$ at several temperatures and 0.1MPa.

C (mmol·kg^{-1})	κ (μS·cm^{-1})			
	288.15 K	298.15 K	308.15 K	318.15 K
0.06	4.8	5.7	6.3	8.5
0.18	12.0	16.0	18.0	22.1
0.25	18.1	21.9	25.7	31.3
0.38	26.0	33.0	39.0	46.1
0.55	38.1	47.0	56.0	66.0
0.72	51.3	62.1	74.2	87.1
0.91	63.9	78.4	93.7	108.3
1.05	71.0	87.0	104.1	123.0
1.16	78.0	95.0	112.0	137.0
1.29	84.9	99.8	121.3	148.0
1.45	92.0	111.0	133.0	162.0
1.63	101.6	121.0	146.0	180.3
1.81	110.0	132.0	160.0	195.0
2.00	118.5	144.2	176.1	211.0
2.20	128.7	155.0	189.0	229.0
2. 39	138.0	167.7	203.0	246.0

Standard uncertainties: u(P)= 5 KPa. u(T) = 0.1 K. u(K) = 0.1 (μS·cm^{-1}).

The *cmc* initially decreases and then increases with temperature, with the minimum in the 298-308 K range, as shown in Figure 4.16. A similar behaviour has been found with conventional surfactants and also in imidazolium-based SAILs [9, 106, 108].

Calculated values of β, ΔG^0_{mic}, ΔH^0_{mic} and ΔS^0_{mic} are given in Table 4.26. The degree of micelle ionization, α, can be calculated from the ratio of the slopes below and above the *cmc*, while the degree of counter-ion binding is obtained as $\beta = 1 - \alpha$. The micellization data at several temperatures allow the calculation of the Thermodynamic functions of the micellization process. The standard Gibbs energy of micellization, ΔG^0_{mic}, was calculated with equation (2.14). The enthalpy

of micellization, ΔH^0_{mic}, was calculated applying the Gibbs-Helmholtz equation (2.15) using the calculated free energy of micellization. The derivative in this equation is obtained by fitting the Gibbs energy previously calculated to a second order polynomial. Results from equations (2.14) and (2.15) were used to estimate the standard entropy of micellization (equation (2.16)).

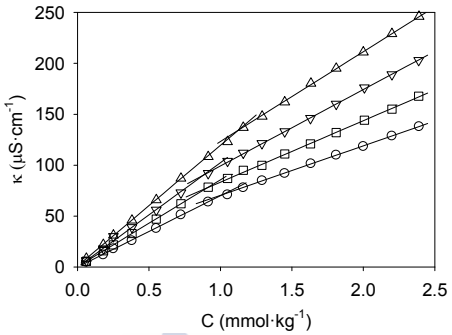

Figure 4.15**.** Conductivity as function of [P4 4 4 1][DS] concentration in aqueous solution at different temperatures and atmospheric pressure. Circles: 288.15 K, squares: 298.15 K, triangles down: 308.15 K, triangles up: 318.15 K.

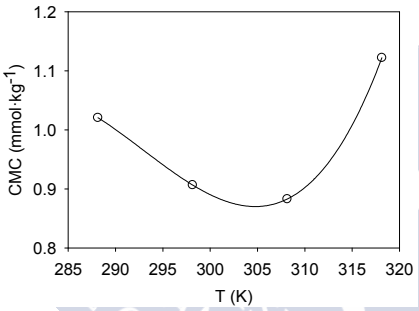

Figure 4.16. Plot of *cmc* as function of temperature for [P4 4 4 1][DS]. Line is drawn to guide the eye.

The degree of binding obtained for [P4 4 4 1][DS] is in the range 0.26-0.31, much weaker than for SDS (0.82) [9]. This was expected since the former is a much larger counter-ion than sodium. The degree of binding, β, and the Gibbs energy of micellization decrease with temperature: the micelle ionization increases with temperature and the micellization process becomes more spontaneous. Values of the degree of binding, β, are lower for [P4 4 4 1][DS] than for analogous imidazolium and tetralkylammonium dodecylsulfate ILs. Gibbs energy of micellization is also less spontaneous (less negative values) than for these other ILs [106, 108, 109] or SDS [9]. Like conventional surfactants and analogous dodecylsulfate-based ILs, ΔH^0_{mic} was found

to be positive at lower temperatures and negative at higher ones. The aggregation process is mainly entropy-driven as indicates a high value of ΔS^0_{mic} at lower temperatures, and mainly enthalpy driven at higher temperatures (see Table 4.26).

Table 4.26. Parameters derived from conductivity data for $[P_{4\,4\,4\,1}][DS]$ aqueous solution at different temperatures and atmospheric pressure.

T (K)	*cmc* (mmol·kg^{-1})	*a*	*β*	ΔG^o_{mic} (kJ·mol^{-1})	ΔH^o_{mic} (kJ·mol^{-1})	$T{\cdot}\Delta S^o_{mic}$ (kJ·mol^{-1})
288.15	1.02	0.69	0.31	-34.08	8.65	42.72
298.15	0.91	0.71	0.29	-35.26	-9.45	25.81
308.15	0.88	0.73	0.27	-35.82	-26.36	9.46
318.15	1.12	0.74	0.26	-35.89	-42.22	-6.33

The structures formed by the surfactant IL in water were analysed at 298.15 K and concentrations well above the *cmc* (20-fold). The hydrodynamic radius of the aggregates, R_h, was measured by means of Dynamic Light Scattering, with average R_h of 1.54 nm and a narrow distribution (ranging from 1 to 2 nm).The results are shown in Figure 4.17 together with a TEM image of the same sample confirming the presence of these aggregates.

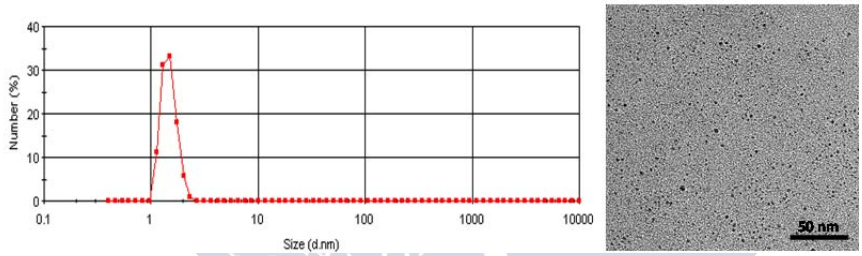

Figure 4.17. Size distribution of aggregates in water by DLS (left) and TEM image of aggregates formed by $[P_{4441}][DS]$ (right) at a concentration 20 times higher than *cmc*.

4.2.1.1.3. Salinity scans

First, phase behaviour of the modified-SDS SAIL $[P_{4\,4\,4\,1}][DS]$ was studied using *n*-dodecane as model oil. To carry out the salinity scans, temperature, concentration of surfactant and water/oil ratio (WOR=1) were fixed, whereas the concentration of salt was varied in each test tube. A salinity scan was made measuring the relative phase volumes as a function of salinity at 298.15 K. Figure 4.18 shows the obtained results. Up to 4 wt% NaCl (low salinities) there are only two phases: One excess-oil phase (top) coexists with a micro-emulsion aqueous

phase (bottom) that accumulates most of the surfactant. This type of system is called Winsor Type I with minimal solubilisation. As salinity increases a new phase appears, so there are excess-oil phase (top), excess-aqueous phase (bottom) and a middle phase (ME phase) containing most of the surfactant which solubilises water and oil. This phase had an oil solubilisation parameter (V_o/V_s, ratio of oil to surfactant volume) that was difficult to determine accurately by measuring phase volumes but was below ~1.2 up to 12 wt% NaCl – far less than for typical microemulsions. Moreover, the system never became lipophilic to form a Winsor Type II microemulsion in equilibrium with excess brine at higher salinity.

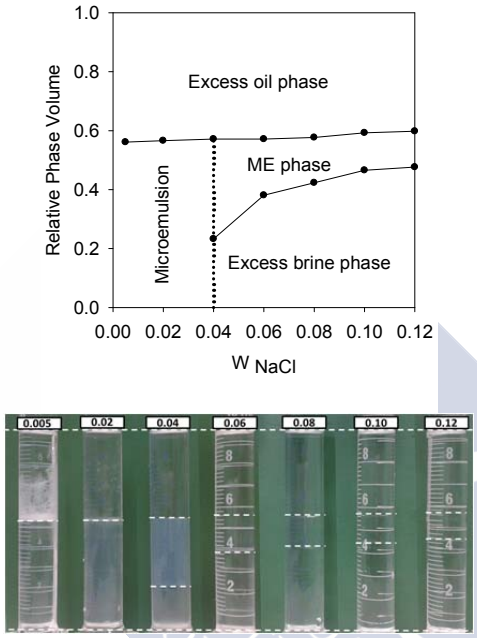

Figure 4.18. Top: Relative phase volumes at 298.15 K and different salinities. NaCl compositions for different brines are in mass fraction. Bottom: Photograph of the graduated tubes used in the measurement of phase volumes. Segmented white lines added to highlight the interfaces. Labels on top indicate the NaCl mass fraction.

The effect of temperature has been also studied at two salinities: 2 and 8 wt% NaCl. As can be seen from Figure 4.19, for low salinities (left figure, w_{NaCl} = 0.02) phase behaviour starts as Winsor Type I at low temperatures and reaches the appearance of a middle phase at *ca.* 305 K. The volume of this microemulsion phase decreases as temperature further increases. In the case of high salinities (Figure 4.19, right, w_{NaCl} = 0.08), the middle phase already exists at 25 °C and

its volume decreases as temperature increases (the same behaviour as for low salinities).

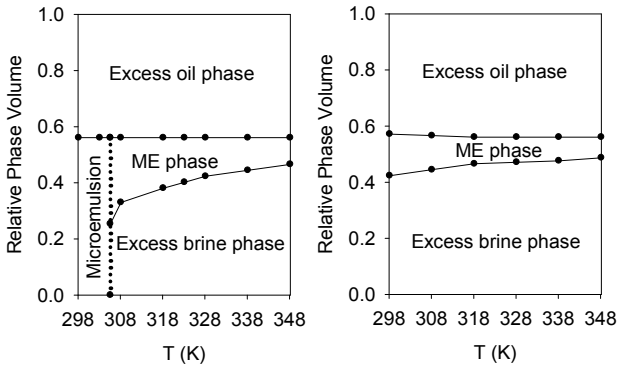

Figure 4.19. Effect of temperature on the relative phase volumes. Left: w_{NaCl}=0.02. Right: w_{NaCl}=0.08.

The volume fraction information can also be represented by a solubility plot. The solubilisation ratio for oil or water is defined as the ratio of the solubilised volume of oil or water to the surfactant volume in the microemulsion phase, assuming all the surfactant is in the microemulsion [111]. Figure 4.20 (left) shows the solubilisation parameters for the studied system at 298.15 K and different salinities. The solubilised volume of water (or oil) has been determined by difference between the initial volume of water (or oil) and the excess water (or oil) phase. The solubilisation ratio for oil (V_o/V_s) increases with salinity, while the solubilisation ratio for water (V_w/V_s) decreases. These parameters are closely related to interfacial tension, therefore its determination is important. When both solubilisation ratios for oil and for water become equal, the interfacial tension reaches its minimum, and the corresponding salinity is known as the optimal salinity (C_ϕ). The interfacial tension is also shown in Figure 4.20 (right). As the salinity is increased, the interfacial tension between the oil phase and the micro-emulsion (γ_{mo}) decreases, while the interfacial tension between the aqueous phase and the micro-emulsion (γ_{mw}) increases. Whenever the middle phase is present, both values of interfacial tension are low (in the 0.01 - 0.1 mN·m^{-1} range). However, this phase had a poor solubilisation parameter (~1) and the system never become lipophilic to form a Winsor Type II microemulsion at higher salinity. According to the literature [7] the values for the oil solubilisation ratio (V_o/V_s) should be around 10 or higher for EOR

applications. Despite this is not the case, the reduction of the interfacial tension is quite significant.

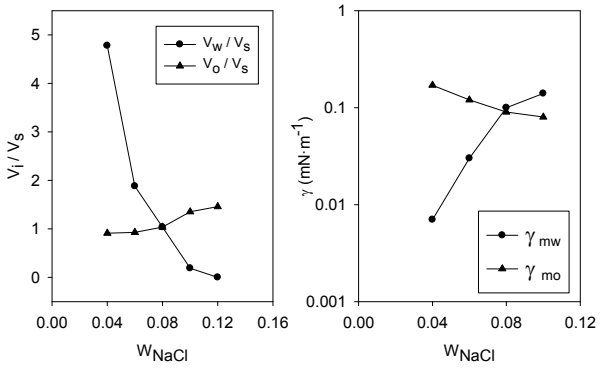

Figure 4.20. Solubilisation parameters (left) and interfacial tension (right) for the studied system at different salinities.

Table 4.27. Solubilisation parameters *(V_i/V_s)* and interfacial tensions (γ_{mi}) for the studied system at 298.15 K, 0.1MPa and several salinities.

w_{NaCl}	V_w/V_s	V_o/V_s	γ_{mw} (mN·m^{-1})	γ_{mo} (mN·m^{-1})
0.04	4.8	0.9	0.007	0.17
0.06	1.9	0.9	0.03	0.12
0.08	1.0	1.0	0.10	0.09
0.1	0.2	1.4	0.14	0.08
0.12	0.0	1.5	-	-

Standard uncertainties: u(P)= 5 KPa. For solubilisation measurements: u(T) = 0.05 K. u(Vw/Vs)=u(Vo/Vs)= 0.1.For interfacial tension measurements u(T) = 0.01 K. u(γ) = 2%.

In order to compare the ability to reduce the interfacial tension of $[P_{4\,4\,4\,1}][DS]$ with SDS and other SAILs previously tested with crude oils, the interfacial tension between a Saharan crude oil and aqueous solutions has been measured at several SDS and $[P_{4\,4\,4\,1}][DS]$ concentrations. Table 4.28 shows our results and data taken from literature [49, 50, 53-55, 57, 112, 113]. Our results and those obtained with the best SAILs, according to data presented in Table 4.28, are shown in Figure 4.21. The interfacial tension values obtained using $[P_{4\,4\,4\,1}][DS]$ significantly improve results found with the common surfactant SDS and other previously tested SAILs [49, 50, 53-55, 57, 112, 113], even when ILs are used in combination with alkalis that produce surfactants in situ [112].

Table 4.28. Interfacial tension between crude oil and surfactant aqueous solutions at 298.15K.

	γ water-oil (mN·m^{-1})						γ reduction (%)	Ref.
ppm IL	0	100	250	500	750	1000		
[$P_{4\,4\,4\,1}$] [DS]	19.20	0.18	0.08	0.10	0.11	0.11	99.43	TW
[Na][DS]	19.20	15.5	-	11.90	-	7.49	60.99	TW
[C_{12}mim][Ac]	19.20	-	-	6.14	-	4.99	77.66	[112]
[C_{12}mim] Cl	47.3	45.2	-	-	-	43.3	8.46	[53]
[C_8Py] Cl	39.98	38.49	35.82	31.68	30.21	29.53	26.14	[54]
[C_{12}Py] Cl	39.98	37.12	33.5	8.72	7.42	7.38	81.54	
[C_8mim] Cl	39.98	38.77	35.77	34.55	29.87	16.77	58.05	
[C_{12}mim] Cl	39.98	37.59	34.21	32.36	29.12	28.44	28.86	
[C_{12}mim] Cl	39.98	37.59	-	-	-	28.44	28.86	[57]
[C_{18}mim] Cl	38.8	7.59	-	-	-	1.3	96.65	[113]
[C_4mim] Cl	34.26	23.12	22.57	22.2	21.84	21.2	38.12	[55]
[C_4mim] Br	34.26	23.2	23.06	22.9	22.66	22.45	34.47	
[C_4mim][BF_4]	34.26	23.76	23.18	22.51	21.64	21.31	37.80	
[C_4mim][H_2PO_4]	34.26	23.55	23.41	23.2	22.75	22.67	33.83	
[C_4mim][HSO_4]	34.26	23.52	23.28	23.11	22.46	22.23	35.11	
[C_4mim][PF_6]	34.26	23.86	23.56	22.36	21.87	20.13	41.24	
[C_6mim] Br	34.26	22.17	21.88	21.26	20.97	20.63	39.78	
[C_6mim][HSO_4]	34.26	23.56	22.15	21.85	20.64	19.75	42.35	
[C_8mim] Cl	34.26	21.56	20.34	20.15	19.69	19.58	42.85	
[BT][HCOO]	34.26	24.12	23.96	23.44	23.18	22.74	33.63	[50]
[BT][CH_3COO]	34.26	21.75	21.13	20.65	20.18	19.71	42.47	
[BT][$C_6H_{13}COO$]	34.26	20.31	19.66	19.22	18.54	17.86	47.87	
[CP][HCOO]	34.26	20.36	19.84	19.36	18.49	17.69	48.37	
[CP][CH_3COO]	34.26	19.24	18.85	18.31	17.56	16.34	52.31	
[CP][$C_6H_{13}COO$]	34.26	17.68	16.95	16.13	15.64	14.81	56.77	
[PA][HCOO]	34.26	24.85	2381	22.51	21.77	21.05	38.56	
[PA][CH_3COO]	34.26	21.56	21.03	20.54	19.84	19.32	43.61	
[3-HPA][HCOO]	34.26	20.74	19.64	19.02	18.69	18.12	47.11	
[3-HPA][CH_3COO]	34.26	20.51	19.86	19.33	18.69	18.14	47.05	
[3-HPA][CF_3COO]	34.26	20.12	19.67	18.49	17.63	16.93	50.58	
[Et_2NH_2][H_2PO_4]	34.26	25.22	24.52	24.02	23.41	23.1	32.57	[49]
[Et_2NH_2][HSO_4]	34.26	24.06	23.8	23.27	22.61	22.13	35.41	
[Et_3NH][CH_3COO]	34.26	24.06	23.49	22.6	22.15	21.87	36.16	
[Et_3NH][BF_4]	34.26	23.77	23.15	22.49	21.9	21.07	38.50	
[Et_3NH][H_2PO_4]	34.26	23.25	22.88	22.32	21.76	21.35	37.68	
[Et_3NH][HSO_4]	34.26	23.13	22.79	22.47	21.83	21.35	37.68	
[Pr_3NH][HSO_4]	34.26	22.96	22.46	22.05	21.75	21.17	38.21	
[Bu_3NH][HSO_4]	34.26	22.05	21.85	21.25	21.01	20.52	40.11	

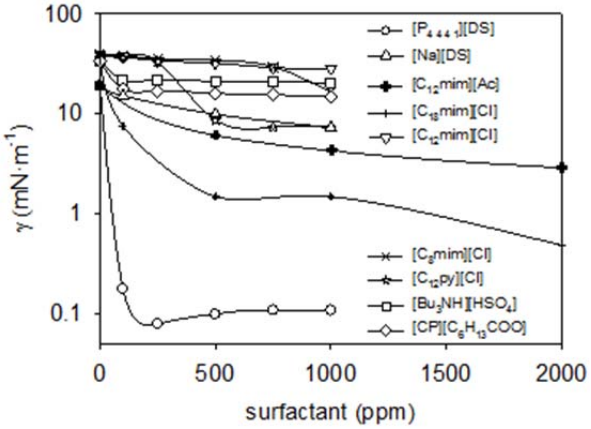

Figure 4.21. Effect of the concentration of SDS and several SAILs in water on theinterfacial tension reduction between water and crude oil.

Despite the good reduction of the water/oil interfacial tension found with [P4 4 4 1][DS], an optimal formulation associated to an ultra-low interfacial tension was not found. A similar phase behaviour was found when *n*-octane is used as oil phase. SAIL and brine form a coacervate in equilibrium with excess brine in the absence of oil or having miniscule oil solubilisation in the presence of paraffinic *n*-octane and *n*-dodecane, when the concentration of NaCl is about 4 and 4.5 wt%.

Surfactants tested with aromatic hydrocarbons have a lower optimal salinity than when tested with paraffinics of comparable oil molar volume, according to Puerto et al. [114]. Thus, salinity scans with aromatic hydrocarbons as test oils could permit to achieve an optimal salinity below that where the coacervate formed. So, butylbenzene and hexylbenzene were the test oils selected to assess the differences between [P4 4 4 1][DS] and its parent compound SDS.

In Figure 4.22 (top) the photographs of the salinity scans at 298.15 K for 2 wt% SAIL [P4 4 4 1][DS] (overall concentration) with butylbenzene (left) or hexylbenzene (right) are shown. With both oils the SAIL generated classical microemulsion phase behaviour, Winsor I-III-II transition, with optimal salinities well below 1 wt% NaCl. No coacervate was observed.

Solubilisation parameters V_o/V_s and V_w/V_s as a function of salinity are shown for both oils in Figure 4.22 (bottom). Optimal salinity, C_ϕ, increases from ~0.16 with butylbenzene to ~0.8 with hexylbenzene. This means that the optimal salinity increases when the oil molar

volume (V_{mo}) increases. In contrast, the solubilisation parameter decreases from 14 to 5. This effect of the V_{mo} in optimal salinity and solubilisation parameters (Figure 4.23) is in good agreement with the three-parameter representation of surfactant/brine/oil interaction published by Puerto *et al.* [114].

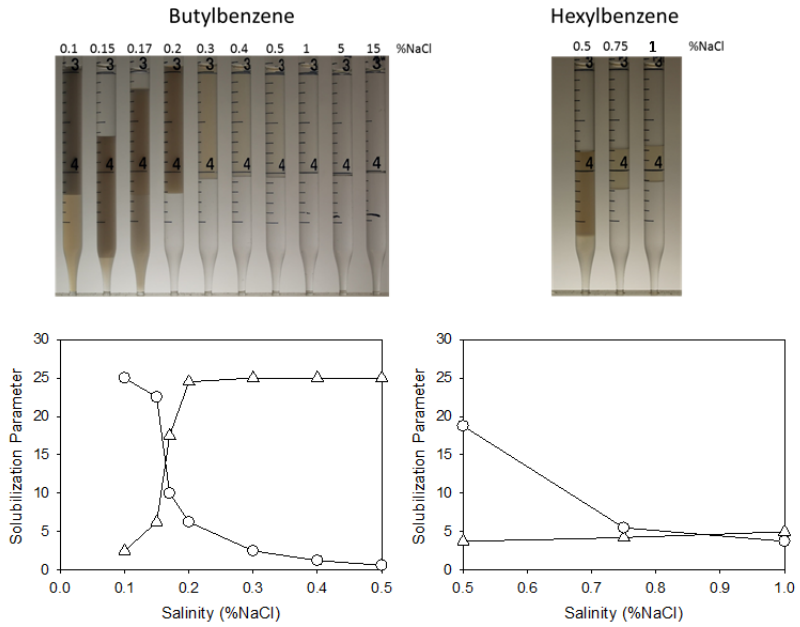

Figure 4.22. Top: Salinity scans, 2 wt% overall [$P_{4\,4\,4\,1}$][DS], butylbenzene or hexylbenzene oil, WOR~1 at 298.15 K. Bottom: Solubilisation parameters for both salinity scans.

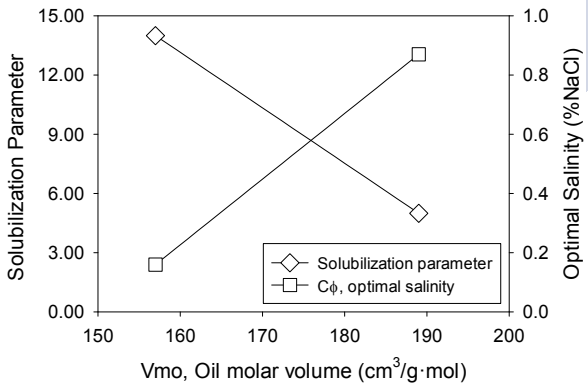

Figure 4.23 Effect of oil molar volume on optimal salinity and solubilisation parameters.

When same samples as in Figure 4.22 were tested at 323.15 K, the volume of the oleic phase was found to be greater than the initial

value for the range of salinity tested, which means the existence of an upper phase microemulsion or Winsor Type II behaviour. Therefore optimal salinity decreases when temperature increases.

Similar tests were carried with the parent compound SDS, and Winsor I behaviour was found up to 15 wt%. NaCl. Thus, in the presence of these aromatic oils, SDS-modified as a SAIL is much more lipophilic than the parent compound, as expected due to the alkyl chains of the phosphonium cation. This is in agreement with a much lower *cmc* of the SAIL (0.9 mmol·kg^{-1}) than the corresponding value for SDS (8.2 mmol·kg^{-1}).

As surfactants in EOR can be injected as a microemulsion or as an aqueous surfactant solution, the behaviour in the absence of oil at 298.15 K was also studied. The SAIL was soluble in brine up to 4.5 wt% NaCl (higher than optimal salinity), thereafter a coacervate phase formed. On the contrary, SDS that appears very hydrophilic in the presence of oil, at 1.5 wt% NaCl formed a clear solution but at 2 wt% the Krafft point was reached and a precipitate appeared, confirming that the SAIL has a lower Krafft point than SDS

4.2.1.2. Anionic SAIL: [C$_4$mim] AOT

As has been shown, the SAIL [P$_{4\ 4\ 4\ 1}$][DS] appeared unsuitable to generate Winsor III microemulsion with *n*-octane, a model oil that could mimic crude oil behaviour on optimal salinity determination for many surfactants. Lipophilic interactions can be modified in different ways [115] to adjust optimal salinity that include varying the oil, as disclosed in Figure 4.22 where n-octane was substituted by aromatic oils, or altering the lipophile. In particular, a branched lipophile would also lower optimal salinity. Accordingly, a SAIL based in the common branched surfactant Na-AOT was selected to carry out new tests.

Figure 4.25 shows solubilisation parameters as a function of salinity at 298.15, 323.15 and 356.15 K for aqueous solutions of [C$_4$mim]AOT (left) and its parent compound Na-AOT (right), equilibrated with equal volumes of *n*-octane, being the surfactant concentration 2% overall. The corresponding photographs of salinity scans are shown in Figure 4.24.

In this case, the branched SAIL [C$_4$mim]AOT generated classical phase behaviour with an optimal salinity of 0.06 wt% NaCl at 25^{o}C, while the optimal salinity for the parent compound under same conditions was 0.21 wt% NaCl. So, in the presence of n-octane, [C$_4$mim]AOT (modified-AOT) is more lipophilic than the parent

compound Na-AOT, again probably due to the alkyl chains of the imidazolium cation. This is in agreement with a lower *cmc* of the SAIL (1.78 mM) than the corresponding value for Na-AOT (2.88 mM) [105]. Furthermore, the modified compound has a solubilisation parameter at optimal salinity of ~20 at 25 and 50°C, indicating ultra-lowinterfacial tensions. This value is higher than the solubilisation parameter of the parent compound (~14 at 25°C and ~6 at 50°C), meaning that the SAIL has more potential for EOR applications at very low salinities and temperatures, conditions that are hard to satisfy with known available surfactants. In the case of the SAIL, optimal salinity increases (from ~0.06 wt% NaCl to ~0.18 wt% NaCl), and the solubilisation parameter decreases (from 20 to 8), with the increase of temperature to 83°C. In the case of the parent compound, the optimal salinity also increases with temperature (from ~0.21 wt% NaCl to ~1 wt% NaCl) and the solubilisation parameter decreases (from 14 to 5).

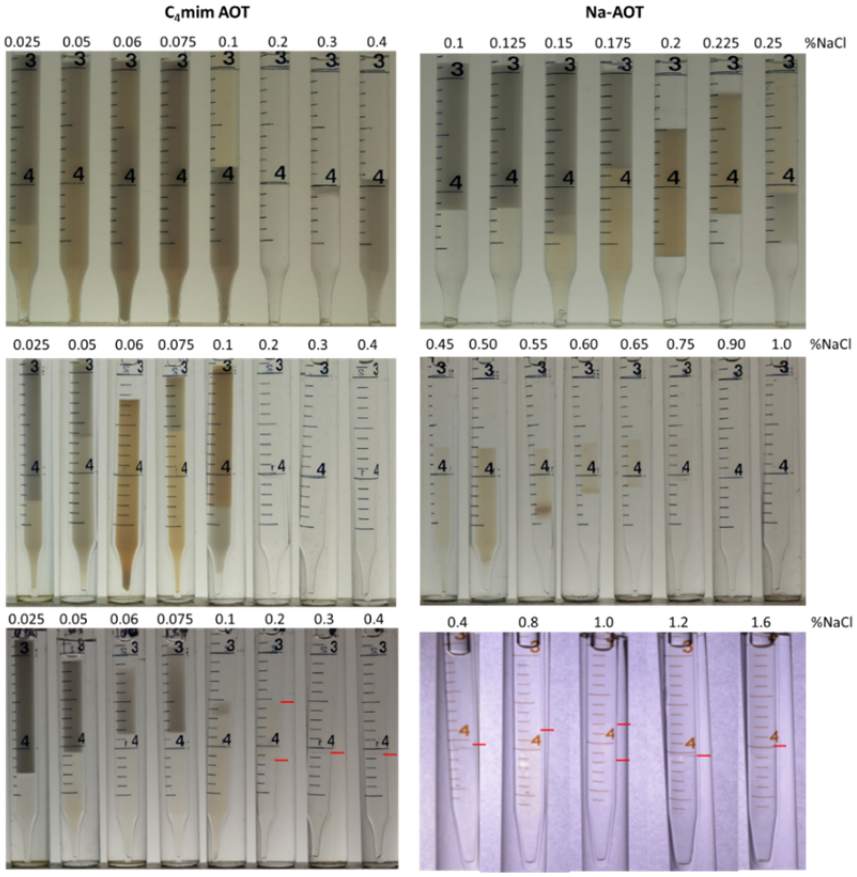

Figure 4.24. Salinity scans at 298.15 (top), 323.15 (middle) and 356.15 K (bottom) for 2% [C4mim][AOT] (left) and its parent compound Na-AOT (right), WOR~1, n-octane, NaCl brine.

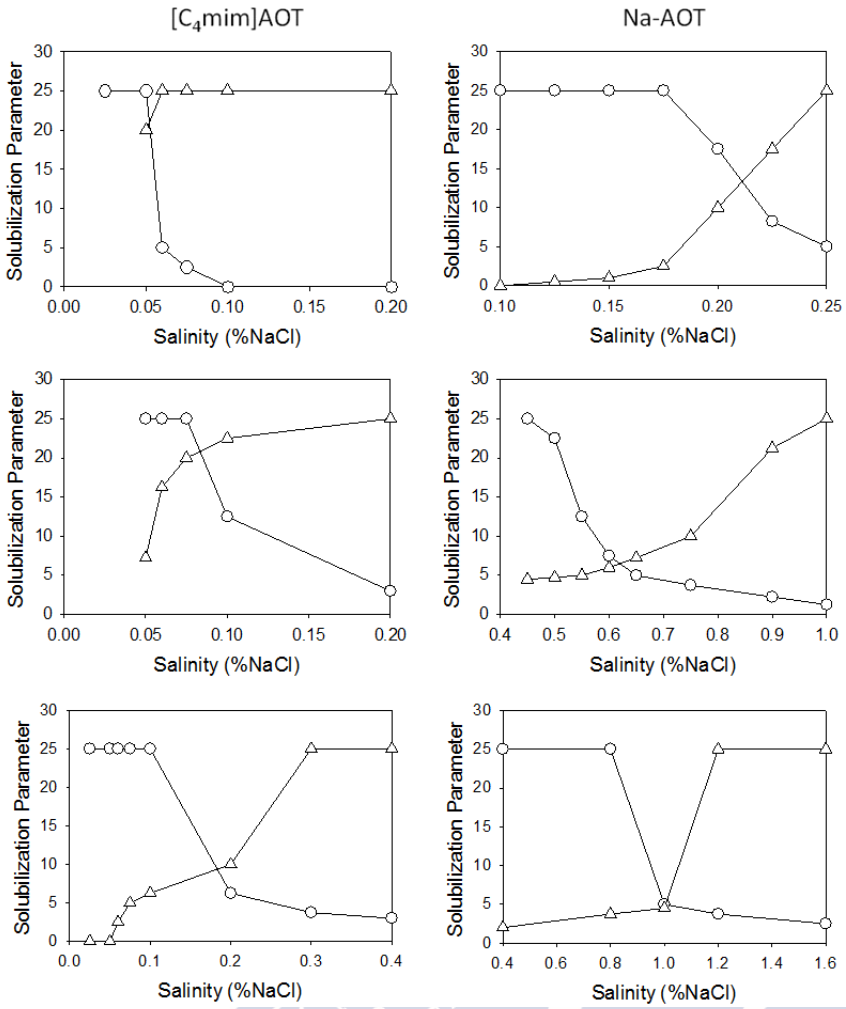

Figure 4.25. Solubilisation parameters (Vw/Vs , Vo/Vs) from salinity scans at 298.15 (top), 323.15 (middle) and 356.15 K (bottom) for 2% [C4mim]AOT (left) and its parent compound Na-AOT (right), WOR~1, *n*-octane, NaCl brine.

In the absence of oil, the behaviour of the common surfactant Na-AOT has been widely studied in literature [116], and issued test results have indicated that at the tested surfactant concentration (4 wt%) and salinity range (optimal salinities: 0.05-1 wt% NaCl), a dispersion of liquid crystalline particles exists. In the case of the modified compound, [C4mim]AOT, a similar behaviour was found. This behaviour, dominated by the nature of the surfactant anion, has been previously described in literature for other AOT compounds [109].

4.2.1.3. Cationic SAILs: [C_{12}mim]Br and [$P_{4\,4\,4\,14}$]Cl

The phase behaviour of the SAILs [C_{12}mim]Br and [$P_{4\,4\,4\,14}$]Cl as function of salinity was also studied. These cationic SAILs formed, in the presence of *n*-octane, with a WOR~1 and 2 wt% surfactant at 298.15 K, microemulsions type Winsor I up to 15 wt% NaCl and up to 356.15 K, so they could appear too hydrophilic to be used alone for many EOR applications. This behaviour for [$P_{4\,4\,4\,14}$]Cl using *n*-octane is the same that was found with n-dodecane in section 4.1.3.

Properties of several cationic SAILs have been disclosed in literature by means of time-consuming techniques (interfacial tension, core flooding experiments, etc.). For example, [C_{12}mim]Cl has been studied [53] by measuring dynamic interfacial tension and doing core flooding experiments. The test results were unfavourable because a poor tertiary oil recovery was found. [C_{12}mim] Cl is too hydrophilic (same as [C_{12}mim]Br) and microemulsions with a good solubilisation parameter (necessary for ultralow interfacial tensions) were not found. Thus, conducting salinity and blend scans of SAILs would be advisable before considering another type of experimentation

4.2.2. Blend scans

Winsor III behaviour can be achieved, not only changing salinity, but also mixing at a fixed salinity pairs of surfactants (hydrophilic + lipophilic) or (cationic + anionic, seeking ion pair formation), to adjust interactions between $\overline{W}$, $\overline{O}$, $\overline{C}$ (Water region, Oil region and amphiphilic membrane) [11] to make R=1 where R is the ratio of cohesive energy, A, per unit area between CO and CW [117].

Test results of salinity scans presented above have shown that the studied anionic SAILs were very lipophilic with the selected oils (Cø <0.8 wt% NaCl for both SAILs at all tested temperatures) while cationic ILs were the opposite, very hydrophilic (Cø >15 wt%). Therefore, the studied SAILs are unsuitable for EOR processes when used alone to cover broad salinity range. However, their blending with each other or another surfactant is a design option for application with a brine of an ionic strength similar to, for example, seawater. In this section, phase behaviour tests of blends of two SAILs or a SAIL with the well-known EOR surfactant $IOS_{15\text{-}18}$ are disclosed. The goal was to find optimal blends with n-octane as the oil phase and with a hard brine (containing divalent ions) as the aqueous phase of ionic strength similar to seawater.

4.2.2.1. [C12mim]Br / [C4mim]AOT

A first scan was done (Figure 4.26) for a 2 wt% blend of [C_{12}mim]Br/[C_4mim]AOT in 5 wt% NaCl brine with *n*-octane at 298.15 K. The cationic SAIL, [C_{12}mim]Br, is very hydrophilic with an optimal salinity higher than 15 wt% NaCl, so at 5 wt% NaCl it has a Winsor I behaviour. However the anionic SAIL, [C_4mim]AOT, with a low optimal salinity (~0.06 wt%) at the fixed test salinity has a Winsor II behaviour. When mixed, the inversion point from Winsor I to Winsor III, or optimal blend, occurred at a composition ratio between 7/3 and 6/4 of [C_{12}mim]Br/[C_4mim]AOT. The large difference in optimal salinities dominates the electrostatic anionic-cationic attraction in determining phase behaviour; this is in contrast to situations discussed below where both individual surfactants exhibited Winsor I behaviour at test conditions.

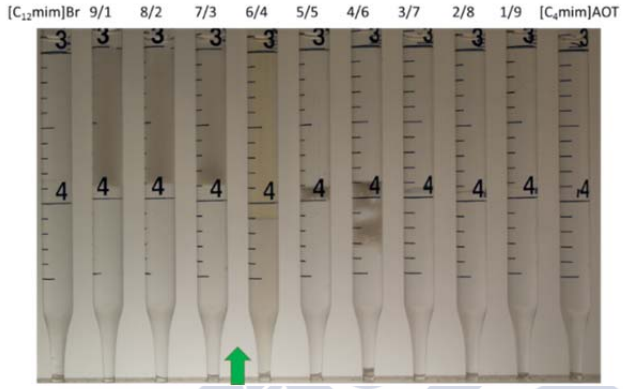

Figure 4.26. Blend scan at 298.15 K for 2 wt% [C_{12}mim]Br / [C_4mim]AOT WPR~1, n-octane, 5 wt% NaCl brine.

The chances of finding samples in the three-phase region are low when blending at 10 wt% ratio intervals for two surfactants of very dissimilar optimal salinities. Blending surfactants that are so dissimilar in optimal salinity should be a reason of concern when designing for EOR processes for obvious reason: too narrow interfacial tension region, chromatographic separation, etc. However, from a scientific point of view, this study allows for gaining insight into the behaviour of blends with SAILs. There are no data so far with IL blends screened in the manner described here.

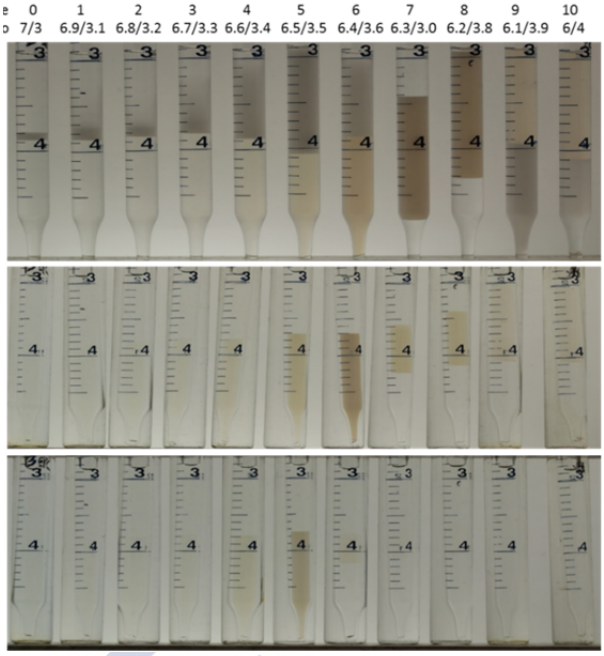

Figure 4.27. Blend scans at 298.15 (top), 323.15 (middle) and 356.15 K (bottom) for 2 wt% [C_{12}mim]Br/ [C_4mim]AOT, WOR~1, *n*-octane, 5 wt% NaCl brine.

A narrower blend scan between 7/3 and 6/4 ratios of [C_{12}mim]Br/[C_4mim]AOT was carried out at 298.15, 323.15 and 356.15 K (Figure 4.27). Solubilisation parameters are shown in Figure 4.28. The optimal Winsor III condition ($V_o/V_s=V_w/V_s$) ocurred when when cationic surfactant was in excess, and the solubilisation parameter of the optimal blend at 298.15 K was~ 18, which should produce ultralowinterfacial tension (below 0.001 mN·m^{-1}), according to Huh's correlation [18].

The classical transition, Winsor I-III-II, occurred at all tested temperatures, however a large temperature effect was found. As temperature increases the optimal blend ratio, rich in the cationic SAIL, becomes more hydrophilic and the solubilisation parameter decreases from ~20 at 298.15 K to ~5 at 356.15 K. The reason for the large temperature effect need to be further evaluated but perhaps most of formed catanionic species partition gradually into the oleic phase with increasing temperature.

To determine if these surfactants are tolerant to divalent ions, hard brine with a similar ionic strength to the previous test brine (5 wt% NaCl) was prepared and blend scan tests were conducted. Composition of hard synthetic sea water is given in Table 4.29. This

fact is really important because the presence of divalent ions (common in reservoirs and off course also in sea water) often cause precipitation of surfactants, especially if they are unalkoxylated.

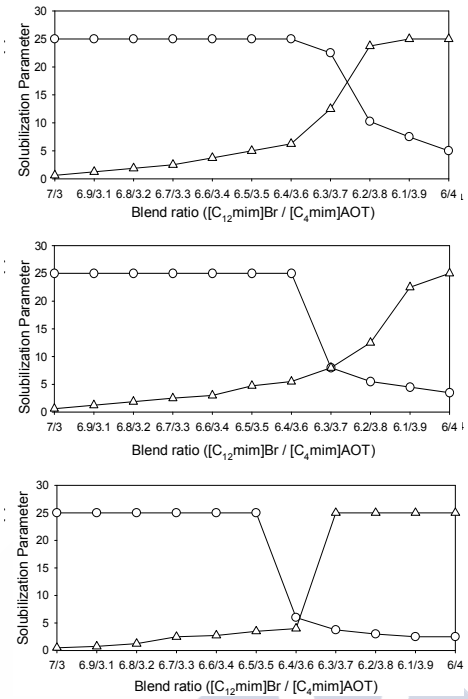

Figure 4.28. Solubilisation parameters (Vw/Vs , Vo/Vs) from blend scans at 298.15 (top), 323.15 (middle) and 356.15 K (bottom) for 2 wt% [C_{12}mim]Br/ [C_4mim]AOT, WOR~1, *n*-octane, 5 wt% NaCl brine.

Table 4.29. Sea water composition

	g/Kg solution
Na_2SO_4	4.84
$CaCl_2 \cdot 2H_2O$	1.89
$MgCl_2 \cdot 6H_2O$	15.06
NaCl	27.94

Figure 4.29 and Figure 4.30 shows the test results for this blend scan. It was found that the surfactant blend is tolerant to the presence of divalent ions, the solubilisation parameters, the optimal blend and the effect of temperature were almost equivalent to those without divalent ions.

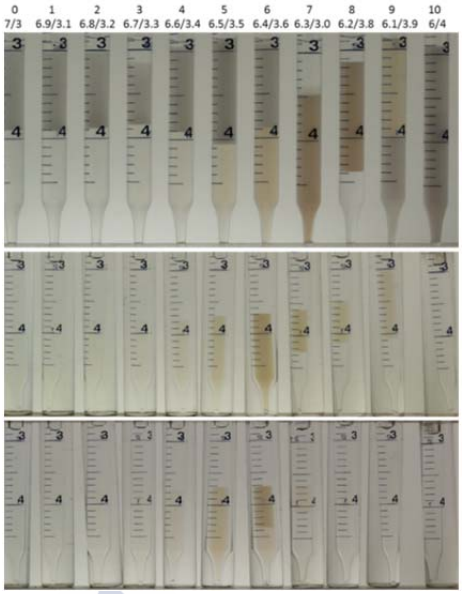

Figure 4.29. Blend scans at 298.15 (top), 323.15 (middle) and 356.15 K (bottom) for 2 wt% [C_{12}mim]Br/[C_4mim]AOT, WOR~1, *n*-octane, sea water.

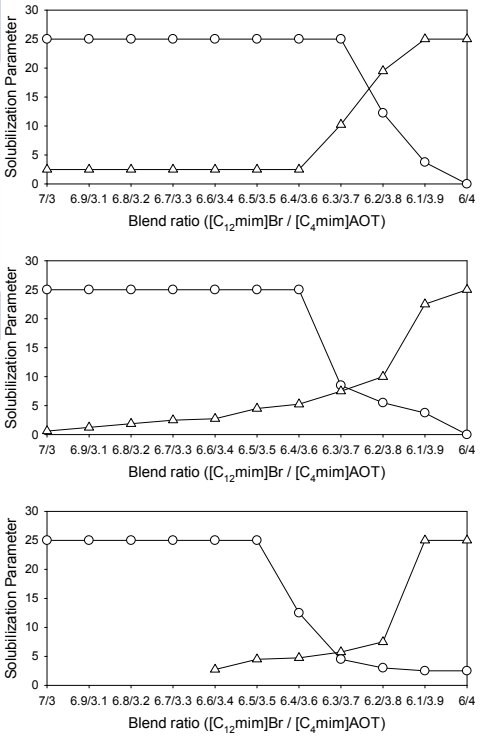

Figure 4.30. Solubilisation parameters (Vw/Vs , Vo/Vs) from blend scans at 298.15 (top), 323.15 (middle) and 356.15 K (bottom) for 2 wt% [C_{12}mim]Br/[C_4mim]AOT, WOR~1, *n*-octane, sea water.

4.2.2.2. $IOS_{15\text{-}18}$/[C_4mim]AOT and $IOS_{15\text{-}18}$/Na-AOT

One interesting feature of SAILs for creating microemulsions suitable for EOR with traditional EOR surfactants comes from its low Krafft point. Therefore, it was found as interesting option the use of $IOS_{15\text{-}18}$, as the hydrophilic surfactant, blended with [C_4mim]AOT. Blend scans were carried out for [C_4mim] AOT and Na-AOT blended with $IOS_{15\text{-}18}$, with 2% blend concentration overall, a soft 5%NaCl brine, and n-octane as oil at 298.15, 323.15 and 356.15 K (Figure 4.31). Solubilisation parameters are shown in Figure 4.32. As 5% NaCl is well above optimal salinity of [C_4mim]AOT (0.06%NaCl) and Na-AOT (0.21 %NaCl) and below optimal salinity of $IOS_{15\text{-}18}$ (~7.5 %NaCl [118]), [C_4mim]AOT and Na-AOT have Winsor II behaviour and $IOS_{15\text{-}18}$ Winsor I. The phase behaviour without divalent ions is similar for both blends. Optimal Winsor III microemulsion occurred at a mass ratio of 5/5 $IOS_{15\text{-}18}$/[C_4mim]AOT and 4/6 for $IOS_{15\text{-}18}$/Na-AOT at all tested temperatures. In both cases, when temperature increases the optimal blend is almost constant but solubilisation parameter at 298.15 K is reduced by half at 356.15 K.

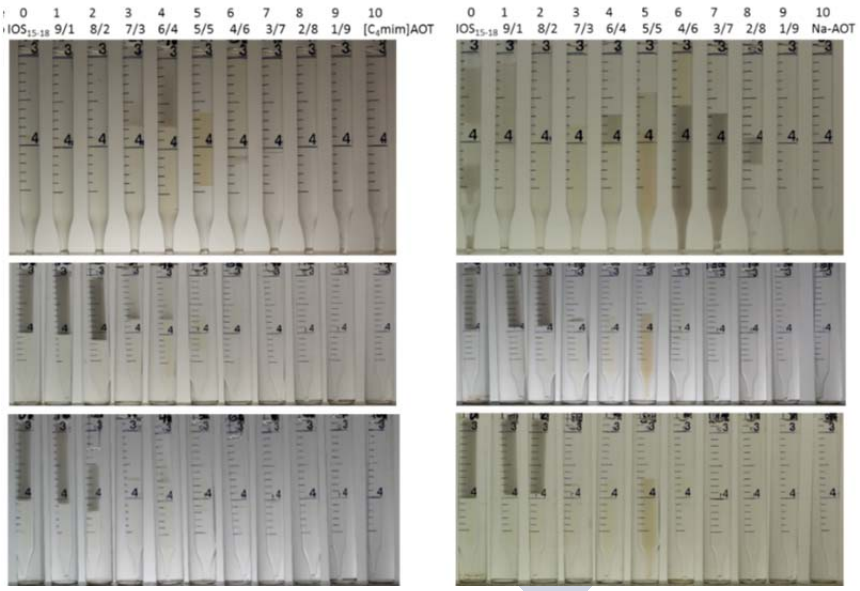

Figure 4.31. Blend scans at 298.15 (top), 323.15 (middle) and 356.15 K (bottom) for 2 wt% $IOS_{15\text{-}18}$ / [C_4mim]AOT (left) and $IOS_{15\text{-}18}$ / Na-AOT (right), WOR~1, *n*-octane, 5 wt% NaCl brine.

However, when hard sea water is used, the blend using the common surfactant Na-AOT is intolerant at 298.15 °C to divalent ions (Figure 4.33, right). Instead previous middle-phase microemulsion, a small phase (volume practically equal to volume of surfactant) appears. On the contrary, when modified-AOT SAIL ([C_4mim]AOT) is blended with IOS_{15-18}, the system presents a similar behaviour to that found with NaCl (Figure 4.33, left).

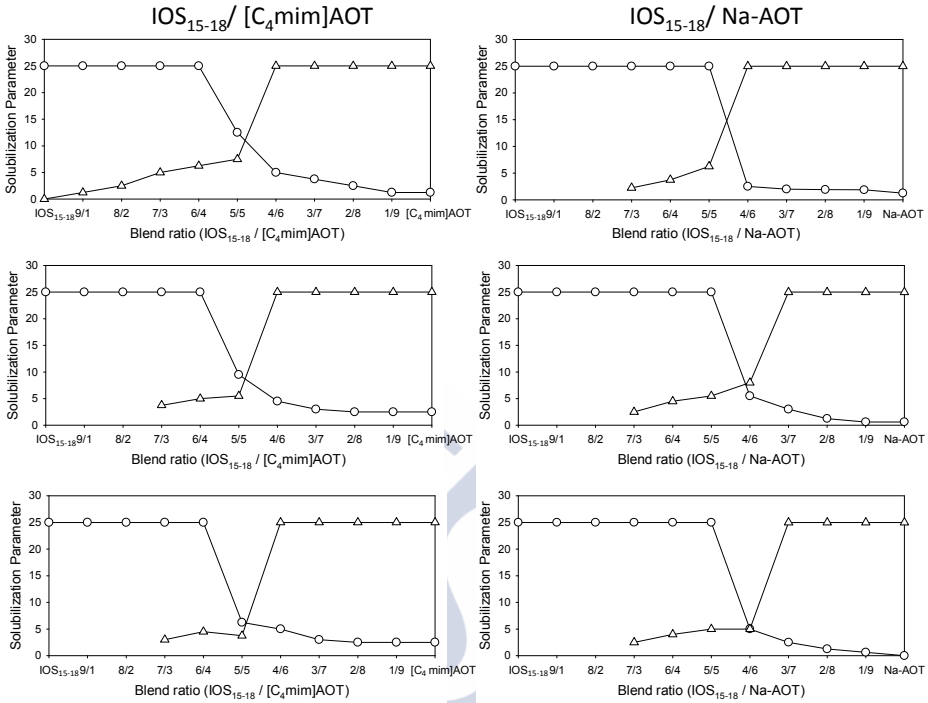

Figure 4.32. Solubilisation parameters (Vw/Vs , Vo/Vs) for blend scans at 298.15, 323.15 and 356.15 K for 2 wt% [C_4mim]AOT/IOS_{15-18} (left) and Na-AOT/IOS_{15-18} (right), WOR~1, n-octane, 5 wt% NaCl brine.

The effect of temperature in the phase behaviour was evaluated for the system tolerant to divalent ions, the one involving SAIL. Results are shown in Figure 4.34. As it can be seen, solubilisation parameters, optimal blends and the effect of temperature were almost equivalent to those without divalent ions. Solubilisation parameters are represented in Figure 4.35.

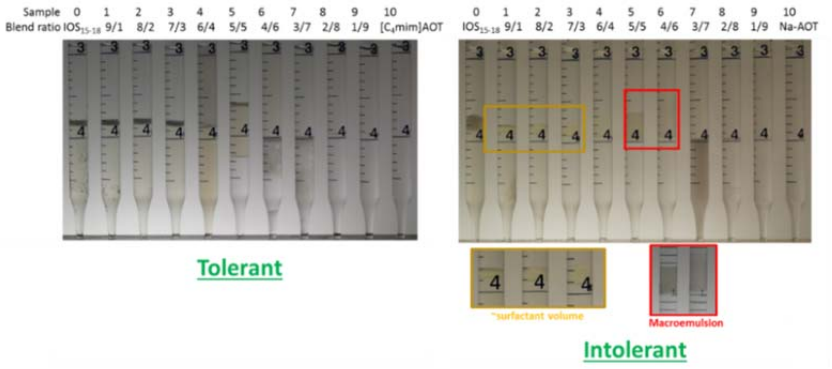

Figure 4.33. Blend scans at 298.15 K for 2 wt% $IOS_{15\text{-}18}$ /[C_4mim]AOT (left) and $IOS_{15\text{-}18}$/Na- AOT (right), WOR~1, *n*-octane, sea water.

Figure 4.34. Blend scans at 298.15 (top), 323.15 (middle) and 356.15 K (bottom) for 2 wt% $IOS_{15\text{-}18}$ /[C_4mim]AOT, WOR~1, *n*-octane, sea water.

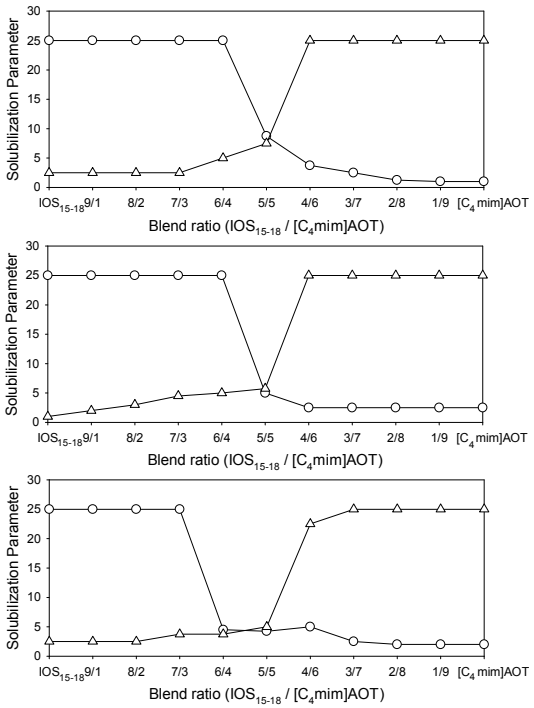

Figure 4.35. Solubilisation parameters (Vw/Vs , Vo/Vs) from blend scans at 298.15 (top), 323.15 (middle) and 356.15 K (bottom) for 2 wt% $IOS_{15\text{-}18}$/ [C_4mim]AOT, WOR~1, *n*-octane, sea water.

4.2.2.3. $IOS_{15\text{-}18}$/[$P_{4\,4\,4\,14}$] Cl

Due to the importance of surfactant or blend of surfactants to be tolerant to divalent ions, it was decided to continue the studies using the hard-synthetic sea water defined in Table 4.29 as brine.

Figure 4.37 shows the solubilisation parameters of the phase behaviour test (Figure 4.36) for a 2 wt% overall blend scan of IOS $_{15\text{-}18}$/[$P_{4\,4\,4\,14}$]Cl in hard sea water with *n*-octane at 298.15, 323.15, 356.15 and 373.15 K. In this case the situation is more complex than previously (blend of surfactants with Winsor I and Winsor II behaviour) because in this case both surfactants are in Winsor I region in hard-sea water when unblended. However, when blended they generated optimal blends in Winsor III region caused by the strong interaction between them. At 298.15 K two optimal blends appear. A monotonically change in $IOS_{15\text{-}18}$/[$P_{4\,4\,4\,14}$]Cl ratio produces Winsor I→III→II→III→I phase behaviour transition. As [$P_{4\,4\,4\,14}$]Cl proportion increases, the blend becomes more lipophilic until Winsor III behaviour appears at ~15 wt% and Winsor II behaviour at 20 wt%.

As the proportion of $[P_{4\,4\,4\,14}]Cl$ continues to increase, the formulation becomes again more hydrophilic remaining Winsor II at 70 wt% but changing to Winsor III at 80 wt% and to Winsor I again.

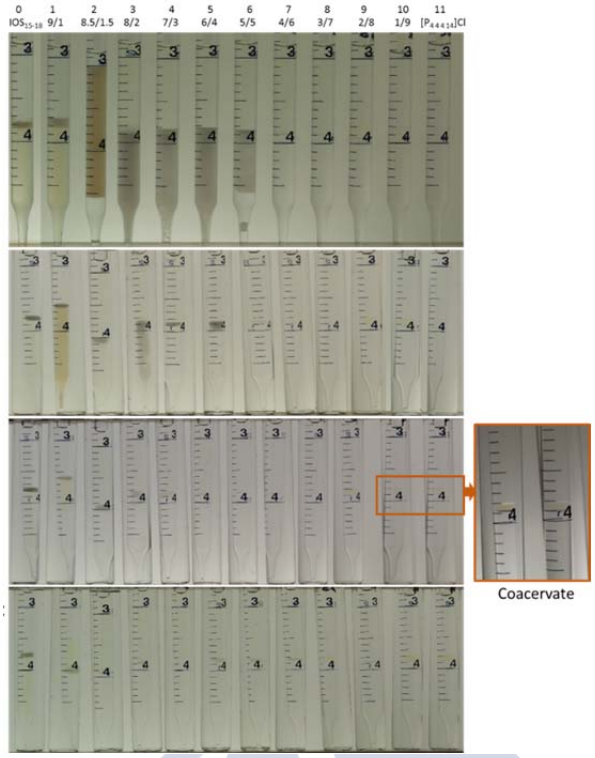

Figure 4.36. Blend scans at 298.15 (top), 323.15 (middle-top), 356.15 (middle-bottom) and 373.15 K (bottom) for 2 wt% $IOS_{15\text{-}18}$ / $[P_{4\,4\,4\,14}]Cl$, WOR~1, *n*-octane, sea water.

Two optimal blends can be seen in the plots of solubilisation parameters at 298.15 K (Figure 4.37). The first optimal is found at approximately 15 wt% $[P_{4\,4\,4\,14}]Cl$, where there is an excess of anionic surfactant, while the second is found at approximately 80 wt% with a cationic surfactant excess. Both optimal Winsor III microemulsions have very different solubilisation parameters, the first one ~15 and the second one less than 5. Therefore, only the optimum with excess of $IOS_{15\text{-}18}$ is the one perhaps with potential for EOR applications. When temperature increases, this optimal blend becomes richer in IOS with lower oil solubilisation. Since the two surfactants are Type I, the system is becoming more lipophilic. However, the optimal blend enriched in SAIL disappears and a coacervate is formed at temperatures above 298.15.

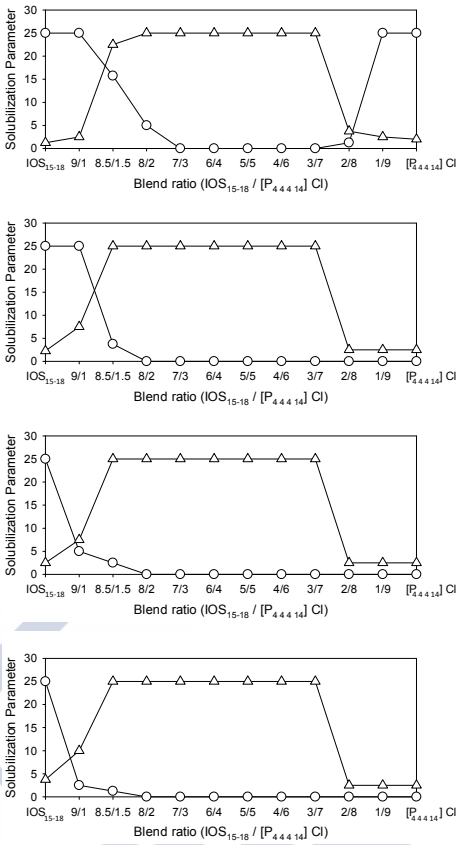

Figure 4.37. Solubilisation parameters (—○— Vw/Vs , —△— Vo/Vs) from blend scans at 298.15 (top), 323.15 (middle-top), 356.15 (middle-bottom) and 373.15 K (bottom) for 2 wt% $IOS_{15\text{-}18}$ / $[P_{4\,4\,4\,14}]Cl$, WOR~1, *n*-octane, sea water.

4.2.2.4. $IOS_{15\text{-}18}$/$[C_{12}mim]Br$ and $IOS_{15\text{-}18}$ /$C_{12}TAB$

In this test case, like in the previous one, all the individual surfactants are in Winsor I region for the given conditions. Figure 4.39 (left) shows the solubilisation parameters obtained from phase behaviour test results for a 2 wt% overall blend scan of $IOS_{15\text{-}18}$/$[C_{12}mim]Br$ in hard sea water with n-octane at 298.15, 323.15, 356.15 and 373.15 K (Figure 4.38, left). Because of the strong interactions between the surfactants, two optimal blends in the Winsor III region appear. As $[C_{12}mim]Br$ increases the blend becomes less hydrophilic until Winsor II behaviour appears at ~30 wt%. As the proportion of $[C_{12}mim]Br$ continues to increase the formulation becomes again more hydrophilic, remaining Winsor II at 60 % but changing to Winsor II at 70 wt% again.

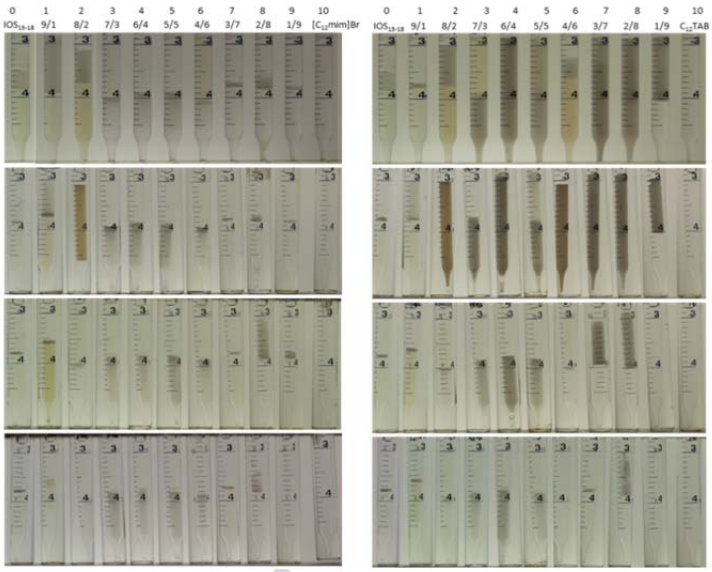

Figure 4.38. Blend scans at 298.15 (top), 323.15 (middle-top), 356.15 (middle-bottom) and 373.15 K (bottom) for 2 wt% $IOS_{15\text{-}18}$/ $[C_{12}mim]Br$ (left) and $IOS_{15\text{-}18}$/ $C_{12}TAB$ (right), WOR~1, *n*-octane, sea water.

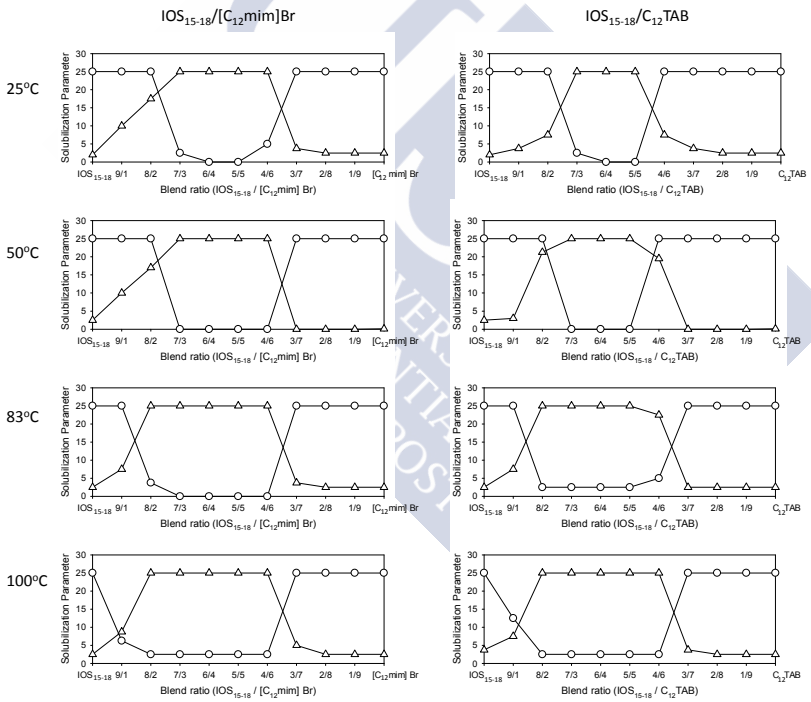

Figure 4.39. Solubilisation parameters (—○— Vw/Vs , —△— Vo/Vs) from blend scans at 298.15 (top), 323.15 (middle-top), 356.15 (middle-bottom) and 373.15 K (bottom) for 2 wt% $IOS_{15\text{-}18}$/ $[C_{12}mim]Br$ (left) and $IOS_{15\text{-}18}$/ $C_{12}TAB$ (right), WOR~1, *n*-octane, sea water.

Two optimal blends at all tested temperatures were found. The first optimal was found at approximately 25 wt% of [C_{12}mim]Br (excess of anionic surfactant), while the second was found at approximately 65 wt% (excess of cationic SAIL). Both optimal Winsor III microemulsions have good solubilisation parameters (the first ~20 and the second ~ 15), both of which should produce ultralowinterfacial tension. The optimal blend enriched in IOS_{15-18} becomes richer in IOS when temperature increases. The solubilisation parameter in this optimal remains constant when temperature increases to 323.15 K, and is reduced by half at 373.15 K. The optimal blend enriched in SAIL remains unchanged with temperature.

Figure 4.39 (right) shows the solubilisation parameters obtained from phase behaviour test results for a 2 wt% overall blend scan of IOS_{15-18}/C_{12}TAB in hard sea water with n-octane at 298.15, 323.15, 356.15 and 373.15 K. The phase behaviour when cationic surfactant C_{12}TAB is blended with IOS_{15-18} is almost the same that has been described for [C_{12}mim]Br.

The surfactant concentration in the blend scans carried out was fixed at ~2 wt% overall (or 4 wt% in the aqueous solution) for an accurate measurement of the phase volumes to calculate solubilisation parameters. However, this concentration is considered very high for injection into the well. For this reason, the phase behaviour was evaluated again for these two promising mixtures at the optimal blend containing higher concentration of IOS_{15-18} (most attractive blend from the economical point of view). Blend scans were carried out (Figure 4.40) for a 0.5 wt% overall (or 1 wt% in the aqueous solution) blend scan of IOS_{15-18}/[C_{12}mim]Br and IOS_{15-18}/C_{12}TAB in hard-sea water with n-octane (WOR~1) at 298.15 K. It was found that the phase behaviour of both blends is independent of the surfactant concentration.

Suitable aqueous solutions cannot exhibit phase separation or be turbid solutions to be injected into the reservoir. In the case of IOS_{15-18}/[C_{12}mim]Br and IOS_{15-18}/C_{12}TAB, contrarily to the previous tested blends that could be only injected as microemulsions, clear solutions were found at the optimal blend rich in IOS_{15-18} in absence of oil. The hydrodynamic radius, *Rh*, of the aggregates in these aqueous solutions was measured by means of Dynamic Light Scattering. Aggregates with average *Rh* of ~20 nm and ~12 nm were found for IOS_{15-18}/[C_{12}mim]Br and IOS_{15-18}/C_{12}TAB blends, respectively.

In absence of oil or otherwise when not formulated in microemulsion, $IOS_{15\text{-}18}$ solubility is poor in hard brine with an ionic strength similar to sea water, the presence of divalent ions causes its precipitation. Besides, this particular IOS surfactant has been extensively studied [118] and researchers concluded that because of the lack of solubility at optimal brine, it has to be injected below optimal in Winsor I with 1 wt% alcohol addition to produce injectable solutions. So it is important to highlight that in this research with SAILS, it has been found that addition of ~20 wt% of cationic surfactant (either $[C_{12}mim]Br$ or $C_{12}TAB$) to $IOS_{15\text{-}18}$, the well-known EOR surfactant generates, in the presence of divalent ions comparable to those in sea waters, clear aqueous solutions in its Winsor III region and very high solubilisation parameters (V_o/V_s~20 at 298.15 and 323.15 K) (see Figure 4.40).

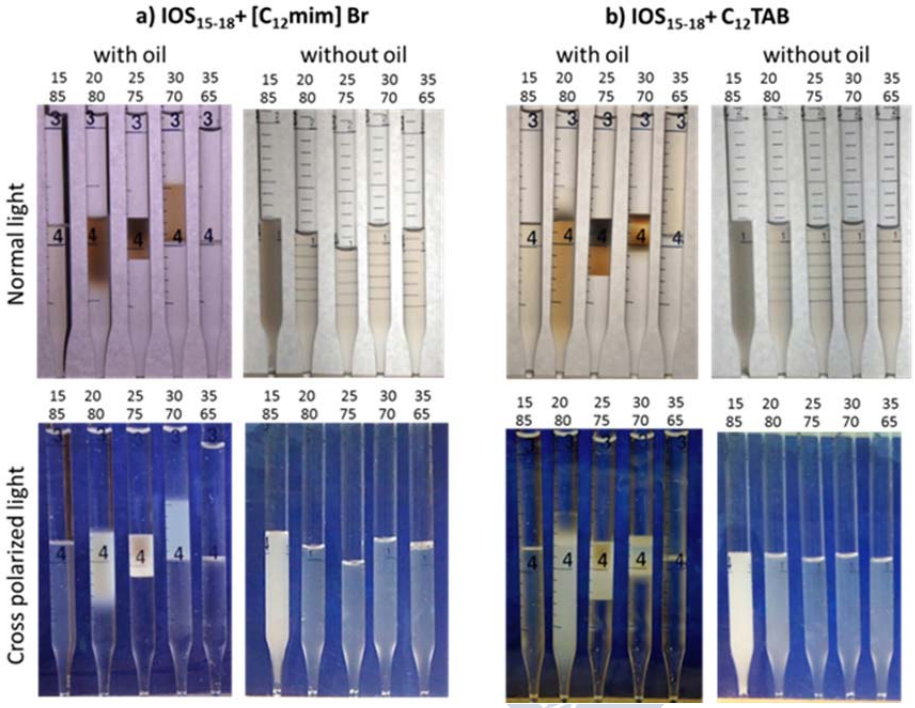

Figure 4.40. (a) 0.5 wt.% overall Blend scan $IOS_{15\text{-}18}$+ $[C_{12}mim]$ Br (left) 1wt% aqueous solution of surfactant blend in the absence of oil (right). (b) 2-cc 0.5 wt.% overall Blend scan $IOS_{15\text{-}18}$+ $C_{12}TAB$ (left) 1-cc 1wt% aqueous solution of surfactant blend in the absence of oil (right) at 298.15 K.

The existence of liquid crystals in the injecting fluid, aqueous solution or microemulsion, can lead to non-uniform distribution of the injected material and non-uniform transport owing to phase trapping

or different mobilities of coexisting phases. Therefore the existence of liquid crystals was tested for the aqueous solutions and microemulsions at optimal salinity of both blends. The samples didn´t show birefringence under polarized light. Moreover, dark pictures were obtained with polarized light microscopy what confirmed the absence of these ordered phases.

Due to the promising results obtained with these blends, dynamic interfacial tensions between the optimal formulations and oil were determined. Aqueous solutions in the Winsor Type I region, but just before the optimal blend (mass ratio=8/2 of $IOS_{15\text{-}18}$ /[C_{12}mim]Br or C_{12}TAB) with a solubilisation parameter high enough to produce lowinterfacial tension were prepared. Surfactant blend concentration was 1 wt%. The capillary tube of the tensiometer was filled with this surfactant solution and set in rotation. A fresh drop of *n*-octane was injected and its radius, that varied by centrifugal force, measured until equilibrium (successive equal values). The interfacial tensions obtained were $2{\cdot}10^{-3}$ mN·m^{-1} and $1{\cdot}10^{-2}$ mN·m^{-1} for $IOS_{15\text{-}18}$ / [C_{12}mim]Br and $IOS_{15\text{-}18}$ /C_{12}TAB, respectively. Both interfacial tensions are probably low enough to displace substantial oil.

Huh correlation [18] was used to calculate interfacial tension from the solubilisation parameters. Interfacial tensions experimentally determined and those obtained with Huh correlation are shown in Figure 4.41. A good agreement was found between calculated and measured interfacial tensions.

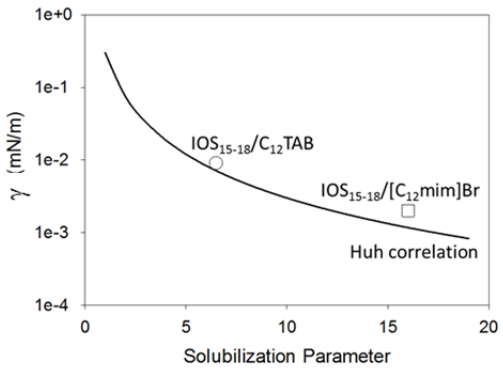

Figure 4.41.interfacial tension versus solubilisation parameter. Huh correlation (solid line) and experimental values for blends containing 80% $IOS_{15\text{-}18}$ and 20% cationic surfactant (circle) or cationic SAIL (square).

USC
UNIVERSIDADE
DE SANTIAGO
DE COMPOSTELA

5. CONCLUSIONS

USC
UNIVERSIDADE
DE SANTIAGO
DE COMPOSTELA

In this thesis, in order to evaluate the ability of SAILs to obtain optimal formulations aimed at improving current surfactant EOR methods, a set of cationic and anionic SAILs were evaluated by determining their phase equilibria with water and an alkane, and by means of salinity and blend scans.

To achieve the first specific objective of this work, the phase equilibria for the systems (water + $[P_{6\,6\,6\,14}][DCA]$ + *n*-dodecane), (water + $[P_{6\,6\,6\,14}][DCA]$ + *n*-hexane), (water + $[P_{6\,6\,6\,14}][(iOc)_2PO_2]$) + *n*-dodecane) and (water + $[P_{4\,4\,4\,14}]Cl$ + *n*-dodecane) were obtained at different temperatures and atmospheric pressure, and the interfacial tension between the equilibrium phases was determined.

The phase diagrams for the ternary systems water + $[P_{6\,6\,6\,14}][DCA]$ + *n*-dodecane or *n*-hexane at 298.15 K and atmospheric pressure show a liquid-liquid-liquid region, which is bigger in the case of *n*-dodecane due to the higher immiscibility of this hydrocarbon with the IL. This phase diagram shares many common features, in principle very interesting for EOR, with other water + $[P_{6\,6\,6\,14}][X]$ + *n*-dodecane systems, being X: Cl or NTf_2. All these systems can be classified as Winsor Type III, and the triphasic systems are formed without the need of any co-surfactant. In all these systems, a small amount of surfactant is required to reach the three-phase region, and this region is maintained over a wide range of temperatures or in the presence of salt. However, the very low solubility of these ILs in water constitutes a problem for EOR applications: they can only be injected into the well as microemulsions. Moreover, the three phases appear in the ternary systems as a consequence of the immiscibility of the three binaries; the obtained microemulsion has a really high concentration of IL and a low solubilisation of water and oil. This behaviour, associated with a limited interfacial tension reduction, allows us to conclude that these ILs are not adequate for EOR purposes.

When the anion is exchanged for bis(2,4,4-trimethylpentyl)phosphinate, the SAIL ($[P_{6\,6\,6\,14}][(iOc)_2PO_2]$) becomes completely miscible with *n*-dodecane. The phase diagram obtained with this SAIL, water and *n*-dodecane at 298.15 K can also be classified as a Winsor Type III system and is stable in the presence of salt. The behaviour found in this system is different from the previously studied $[P_{6\,6\,6\,14}][X]$ SAILs. Two significant differences were found in comparison with previously determined (water + SAIL + *n*-dodecane) phase diagrams. In the case of $[P_{6\,6\,6\,14}][(iOc)_2PO_2]$, the biphasic region close to the (water + *n*-dodecane) binary is not negligible, and the three-phase region size (almost unaffected by

temperature in the previous systems) is dramatically influenced by temperature, and decreases as the temperature increases (disappearing for temperatures over 308 K). This behaviour is typically found with non-ionic rather than ionic surfactants. However, the hydrophobic character of the IL leads to a microemulsion with a significantly higher proportion of oil than water, far from the classic bicontinuous structures required in EOR. The high hydrophobicity of the IL leads to low oil-microemulsion but high water-microemulsion interfacial tensions. For economic reasons, after the surfactant solution is introduced, water injection is required, and these differences in interfacial tension could make the process unsuccessful.

To study the effect of the length of the alkyl chains in the phosphonium cation, the phase behaviour of $[P_{4\ 4\ 4\ 14}]Cl$ with water and *n*-dodecane was determined. Reducing the alkyl chains length of the phosphonium cation, the SAIL becomes completely miscible with water (desirable for EOR applications). However, phase diagrams obtained at 298.15 and 348.15 K are Winsor Type I. At 298.15 K, because of the solid character of the IL, small regions of SL and SLL equilibrium were also found. The addition of NaCl showed that this biphasic system is maintained throughout a wide range of salinities. A Winsor Type III system with a bicontinuous microemulsion, desired in EOR, was not found.

Despite the fact that the SAILs studied cannot be presented as a promising alternative for EOR, the three-phase region found when mixed with water and oil makes these ILs candidates to be used for microemulsion applications (chemical reactions, drug delivery, nanoparticle synthesis, etc.). It can also be concluded that the simultaneous correlation of LLE and LLLE data can be satisfactorily carried out with the NRTL model. This facilitates the manipulation of the equilibrium data for any application.

Focusing on EOR, salinity is an essential variable in obtaining optimal formulations. The absence of salinity scans with SAILs has led to studies at conditions where interfacial tensions are far from the required ultra-low values. To accomplish the second specific objective of this thesis, salinity scans with SAILs and blends containing SAILs were carried out for the first time.

Salinity scans for two cationic SAILs $[P_{4\ 4\ 4\ 14}]Cl$ and $[C_{12}mim]Br$, with *n*-octane as the oil and a NaCl solution as brine, indicated that if used alone they are too hydrophilic for use in EOR except perhaps at

high salinities exceeding 15 %wt NaCl. In the case of $[P_{4\,4\,4\,14}]Cl$, these conclusions were previously obtained through rigorous phase equilibria determinations.

Replacement of Na+ as counterion by the less polar $[C_4mim]^+$ and $[P_{4\,4\,4\,1}]^+$ for common anionic surfactants, Aerosol OT (Na-AOT) and sodium dodecyl sulfate (SDS), yielded anionic room-temperature SAILs ($[C_4mim]AOT$ and $[P_{4\,4\,4\,1}]DS$) which were much less hydrophilic than the original surfactants. Salinity scans with several oils showed that they are too lipophilic to be used alone in EOR.

Blend scans for mixtures of anionic and cationic SAILs, $[C_4mim]AOT$ and $[C_{12}mim]Br$, were carried out using *n*-octane as oil and synthetic hard sea water as brine. An optimal blend ratio was found at which a microemulsion phase (with high solubilisation of both oil and brine) was formed, an indication of low enough interfacial tension to recover substantial quantities of oil. However, the large difference in hydrophilicity between the SAILs dominated the electrostatic anionic/cationic interactions in influencing phase behaviour, making it very sensitive to blend ratio and consequently of little interest for EOR.

Blend scans for mixtures of the anionic surfactant $IOS_{15\text{-}18}$ and anionic SAIL $[C_4mim]AOT$ revealed that they had nearly equal weight fractions for the optimal blend ratio. Almost the same optimal blend ratio was found when $[C_4mim]AOT$ was replaced by Na-AOT. The $IOS_{15\text{-}18}/[C_4mim]AOT$ mixture was superior to $IOS_{15\text{-}18}$/Na-AOT in sea water because highly viscous phases were seen near the interface in Na-AOT samples near the optimal condition. However, good solubilisation parameters were only obtained at 298.15 K, limiting the range of temperatures for practical application.

Blend scans for mixtures of anionic $IOS_{15\text{-}18}$ with cationic SAILs $[P_{4\,4\,4\,14}]Cl$ and $[C_{12}mim]Br$ exhibited optimal behaviour with high oil and brine solubilisation for blends containing about 10-20% of the respective SAILs. Because anionic and cationic surfactants were both hydrophilic, the uncharged “catanionic” surfactant produced by their electrostatic interaction made phase behaviour with the mixed surfactants less hydrophilic than the individual surfactants.

The optimal blend of the $IOS_{15\text{-}18}/[C_{12}mim]Br$ system with *n*-octane and sea water was the most promising of blends tested containing a SAIL. Interfacial tension as measured in a spinning drop tensiometer was ~0.002 $mN{\cdot}m^{-1}$ after equilibrium was reached, following injection of a drop of fresh *n*-octane into an aqueous sea water solution having

1 %wt total surfactant content with optimal blend ratio. Such low interfacial tension, lower than that obtained with the blend $IOS_{15\text{-}18}/C_{12}TAB$, suggests high oil recovery potential. The aqueous solution (without oil) appeared suitable for injection in an EOR process because it exhibited no phase separation and contained micelles or vesicles with a hydrodynamic radius of ~20 nm, much smaller than typical pore sizes. This result is of interest because blends of other surfactants with such high proportions of $IOS_{15\text{-}18}$ usually exhibit precipitation in hard brines at low temperatures. Core flooding tests should be conducted for the $IOS_{15\text{-}18}/[C_{12}mim]Br$ systems to assure injectivity of the aqueous solution, surfactant transport through the core, and oil displacement without excessive surfactant retention or pressure drops.

Research on the use of SAILs in EOR is still in its infancy but results obtained here are promising. The ability to design and synthesise a wide variety of SAILs should be utilised in the search for optimal formulations, especially for high temperatures and salinities where the choice of conventional surfactants is limited. The study of SAIL-SAIL and surfactant-SAIL blends, with improved properties compared with those of individual surfactants or SAILs, should lead future research.

LIST OF SYMBOLS

USC
UNIVERSIDADE
DE SANTIAGO
DE COMPOSTELA

Symbols

a	activity
a	empirical fit parameter in equation (4.2)
$a^s{}_m$	area per surfactant molecule at saturated interface
A	adjustable parameter in equation (4.4)
A	cohesive energy
ASP	Alkaline/Surfactant/Polymer flooding
b	empirical fit parameter in equation (4.2)
B_ϕ	optimal blend
C	constant in Huh's equation (2.33)
C	molar concentration
$\bar{C}$	amphiphilic membrane
C_{20}	concentration needed to reduce surface tension of the solvent in 20 mNm
C_ϕ	Optimal salinity
CAS	Chemical Abstracts Service
cmc	critical micelle concentration
DLS	Dynamic Light Scattering
DSC	Differential Scanning Calorimetry
Ea	activation energy
EOR	Enhanced Oil Recovery
G	Gibbs free energy
g_{ij}	binary energy interaction parameters in the NRTL model
H	enthalpy
HLB	Hydrophilic-Lipophilic Balance
IL	Ionic Liquid
k	adjustable parameter in equation (4.4)
K	capillary constant
L-G	liquid-gas
LLE	liquid-liquid equilibrium
LLLE	liquid-liquid-liquid equilibrium
ME	microemulsion phase
n	number of solute species
n_D	refractive index
N	Avogadro's number
N	number of experimental data points in equation (4.5)
NMR	Nuclear Magnetic Resonance
NRTL	Non Randon Two-Liquid Activity Coefficient Model
O	oil
$\bar{O}$	oil region
$O.F.$	objective function
P	optimisation parameter in equations (2.30) and (2.31)
P	pressure
pC_{20}	negative logarithm of the concentration needed to reduce surface tension in 20 $mN{\cdot}m^{-1}$ of the solvent
P_n	adjustable parameter in Equations (2.25) and (2.26)
Q	10^{-6} in Equation (2.25) and 10^{-10} in Equation (2.24)
r	drop radius

R	gas constant
R	ratio of cohesive energy
RSD	relative standard deviation
RTIL	Room Temperature Ionic Liquid
S	entropy
S	surfactant
SAIL	Surface Active Ionic Liquid
SL	solid-liquid
SLL	solid-liquid-liquid
t	time
T	temperature
T_o	adjustable parameter in equation (4.4)
TEM	Transmission Electron Microscopy
TGA	Thermogravimetric Analysis
u	standard uncertainty
V	volume
ω	mass fraction
W	water
$\bar{W}$	water region
x	mole fraction
X	anion
y	kinetic energy correction
z	generic physical property

Greek letters

α	degree of micelle ionization
α	Non-randomness parameter in the NRTL equation
α	*n*-dodecane/water mass ratio
β	degree of counter-ion binding to the micelle
γ	activity coefficient
γ	surface or interfacial tension
Γ	surface excess concentration
Δ	variation of property
ε	low tolerance value
η	dynamic viscosity
κ	conductivity
μ	chemical potential
Π	surface pressure
ρ	density
σ_o	solubilisation parameter for the oil (V_o/V_s)
τ_{ij}	parameter in the NRTL model
υ	kinematic viscosity
υ	number adjustable parameters in equation (4.5)
ϕ	phase
ω	capillary rotating speed
ω	number of moles of water per litter of water

Subscripts

$\pm$	mean
0	solvent
1	solute

1,2,3…	components
a	activity
A^+	electrolyte cation
B^-	electrolyte anion
cmc	critical micelle concentration
i, j, k	components
i	component
j	phase
k	tie-line
LL	liquid- liquid
LLL	liquid- liquid- liquid
mic	micellization
n	counter
o	oil
P	constant pressure
s	surfactant
T	constant temperature
w	water
x	composition
∞	infinite dilution

Superscripts

0	standard state
I, II, III	phases in equilibrium
cal	calculated value

USC
UNIVERSIDADE
DE SANTIAGO
DE COMPOSTELA

REFERENCES

USC
UNIVERSIDADE
DE SANTIAGO
DE COMPOSTELA

[1] International Energy Outlook 2016 (IEO2016), *U.S. Energy Information Administration*, May 11, 2016. Available from: https://www.eia.gov/outlooks/ieo/pdf/0484(2016).pdf [accessed 18 October 2017].

[2] E.C. Donaldson, G.V. Chilingarian and T.F. Yen, *Enhanced oil recovery, II: Processes and operations*, Elsevier, Amsterdan, 1989.

[3] J.L. Salager, *Recuperación mejorada del petróleo*, (Cuaderno FIRP S357-C), Universidad de los Andes, Mérida-Venezuela, 2005.

[4] J.G. Speight, *Enhanced recovery methods for heavy oil and tar sands*, Elsevier, Houston-TX, 2013.

[5] V. Alvarado and E. Manrique, Enhanced Oil Recovery: An Update Review, *Energies*, 3 (2010) 1529-1575.

[6] A. Shah, R. Fishwick, J. Wood, G. Leeke, S. Rigby and M. Greaves, A review of novel techniques for heavy oil and bitumen extraction and upgrading, *Energy Environ. Sci.*, 3 (2010) 700-714.

[7] J. Sheng, *Modern chemical enhanced oil recovery: theory and practice*, Gulf Professional Publishing (Elsevier), Amsterdam, 2011.

[8] I. Lazar, I.G. Petrisor and T.F. Yen, Microbial Enhanced Oil Recovery (MEOR), *Pet. Sci. Technol.*, 25 (2007) 1353-1366.

[9] M.J. Rosen, *Surfactants and interfacial phenomena*, John Wiley & Sons, Inc., New Jersey, 2004.

[10] T. Chakraborty, I. Chakraborty and S. Ghosh, The methods of determination of critical micellar concentrations of the amphiphilic systems in aqueous medium, *Arabian J. Chem.*, 4 (2011) 265-270.

[11] P.A. Winsor, *Solvent properties of amphiphilic compounds*, Butterworths Scientific Publications, London, 1954.

[12] M. Fanun, *Microemulsions: properties and applications*, CRC Press (Taylor & Francis Group), Boca Ratón-FL, 2008.

[13] J. Salager, J. Morgan, R. Schechter, W. Wade and E. Vasquez, Optimum formulation of surfactant/water/oil systems for minimum interfacial tension or phase behavior, *SPEJ*, 19 (1979) 107-115.

[14] H. Renon and J.M. Prausnitz, Local compositions in thermodynamic excess functions for liquid mixtures, *AlChE J.*, 14 (1968) 135-144.

[15] J.M. Sørensen and W. Arlt, *Liquid-liquid Equilibrium Data Collection: Ternary and Quaternary Systems*, DECHEMA, Chemistry Data Series, Frankfurt, 1980.

[16] R.N. Healy, R.L. Reed and D.G. Stenmark, Multiphase Microemulsion Systems, *SPEJ*, 16 (1976) 147-160.

[17] M. Puerto, G.J. Hirasaki, C.A. Miller and J.R. Barnes, Surfactant systems for EOR in high-temperature, high-salinity environments, *SPEJ*, 17 (2012) 11-19.

[18] C. Huh, Interfacial tensions and solubilizing ability of a microemulsion phase that coexists with oil and brine, *J. Colloid Interface Sci.*, 71 (1979) 408-426.

[19] R.D. Rogers and K.R. Seddon, Ionic liquids- solvents of the future?, *Science*, 302 (2003) 792-793.

[20] J.F. Brennecke and E.J. Maginn, Ionic liquids: innovative fluids for chemical processing, *AlChE J.*, 47 (2001) 2384-2389.

[21] R.D. Rogers and K.R. Seddon, Preface to *Ionic Liquids as Green Solvents - Progress and Prospects* (Eds. R.D. Rogers, and K.R. Seddon), ACS Symposium Series, vol. 856, American Chemical Society, Washington DC, 2003.

[22] M. Freemantle, *An introduction to ionic liquids*, Royal Society of chemistry, Cambridge, 2010.

[23] M.J. Earle and K.R. Seddon, Ionic liquids. Green solvents for the future, *Pure Appl. Chem.*, 72 (2000) 1391-1398.

[24] T. Welton, Room-temperature ionic liquids. Solvents for synthesis and catalysis, *Chem. Rev.*, 99 (1999) 2071-2084.

[25] K.R. Seddon, Ionic liquids for clean technology, *J. Chem. Technol. Biotechnol.*, 68 (1997) 351-356.

[26] K.R. Seddon, *Ionic liquids: Designer solvents?*, in The International George Papatheodorou Symposium: Proceedings (Eds. S. Boghosian, V. Dracopoulos, C.G. Kontoyannis and G.A. Voyiatzis), 131-135, Institute of Chemical Engineering and High Temperature Chemical Processes, Patras, 1999.

[27] K.S. Rao, P. Bharmoria, T.J. Trivedi and A. Kumar, Self-Assembly of Surface-Active Ionic Liquids in Aqueous Medium, in: *Ionic Liquid-Based Surfactant Science: Formulation, Characterization, and Applications* (Eds. B.K. Paul, S.P. Moulik and W. Kunz), Jonh Wiley & Sons, New Jersey, 2015, 175-192.

[28] I. Collins, M. Earle, S. Exton, N. Plechkova and K. Seddon, Ionic liquids and uses thereof, *WO Patent*, 111712 (2006) A2.

[29] M. Blesic, M. Swadźba-Kwaśny, J.D. Holbrey, J.N.C. Lopes, K.R. Seddon and L.P.N. Rebelo, New catanionic surfactants based on 1-alkyl-3-methylimidazolium alkylsulfonates,$[C_nH_{2n+1}mim][C_mH_{2m+1}SO_3]$: mesomorphism and aggregation, *Phys. Chem. Chem. Phys.*, 11 (2009) 4260-4268.

[30] J. Lu, F. Yan and J. Texter, Advanced applications of ionic liquids in polymer science, *Prog. Polym. Sci.*, 34 (2009) 431-448.

[31] M. Blesic, A. Lopes, E. Melo, Z. Petrovski, N.V. Plechkova, J.N. Canongia Lopes, K.R. Seddon and L.s.P.N. Rebelo, On the self-aggregation and fluorescence quenching aptitude of surfactant ionic liquids, *J. Phys. Chem. B*, 112 (2008) 8645-8650.

[32] N. Smirnova and E. Safonova, Micellization in solutions of ionic liquids, *Colloid J.*, 74 (2012) 254-265.

[33] M. Blesic, M.H. Marques, N.V. Plechkova, K.R. Seddon, L.P.N. Rebelo and A. Lopes, Self-aggregation of ionic liquids: micelle formation in aqueous solution, *Green Chem.*, 9 (2007) 481-490.

[34] N. Cheng, P. Yu, T. Wang, X. Sheng, Y. Bi, Y. Gong and L. Yu, Self-Aggregation of New Alkylcarboxylate-Based Anionic Surface Active Ionic Liquids: Experimental and Theoretical Investigations, *J. Phys. Chem. B*, 118 (2014) 2758-2768.

[35] J. Bowers, C.P. Butts, P.J. Martin, M.C. Vergara-Gutierrez and R.K. Heenan, Aggregation Behavior of Aqueous Solutions of Ionic Liquids, *Langmuir*, 20 (2004) 2191-2198.

[36] K. Srinivasa Rao, P.S. Gehlot, T.J. Trivedi and A. Kumar, Self-assembly of new surface active ionic liquids based on Aerosol-OT in aqueous media, *J. Colloid Interface Sci.*, 428 (2014) 267-275.

[37] P.D. Galgano and O.A. El Seoud, Synthesis, Molecular Structure, Micellar Properties and Applications, in: *Ionic Liquid-Based Surfactant Science: Formulation, Characterization and Applications* (Eds. B.K. Paul, S.P. Moulik and W. Kunz), John Wiley & Sons, New Jersey, 2015, 63-99.

[38] H. Li, C. Yu, R. Chen, J. Li and J. Li, Novel ionic liquid-type Gemini surfactants: Synthesis, surface property and antimicrobial activity, *Colloids Surf., A*, 395 (2012) 116-124.

[39] C. Ghatak, V.G. Rao, S. Mandal, S. Ghosh and N. Sarkar, An Understanding of the Modulation of Photophysical Properties of

Curcumin inside a Micelle Formed by an Ionic Liquid: A New Possibility of Tunable Drug Delivery System, *J. Phys. Chem. B*, 116 (2012) 3369-3379.

[40] X.Q. An and J. Shen, Ionic Liquid Microemulsions and Applications: Formulation, Characterization, and Applications, in: *Ionic Liquid-Based Surfactant Science: Formulation, Characterization and Applications* (Eds. B.K. Paul, S.P. Moulik and W. Kunz), John Wiley & Sons, New Jersey, 2015, 359-374.

[41] D. Guzmán-Lucero, P. Flores, T. Rojo and R. Martínez-Palou, Ionic Liquids as Demulsifiers of Water-in-Crude Oil Emulsions: Study of the Microwave Effect, *Energy Fuels*, 24 (2010) 3610-3615.

[42] S. Lago, H. Rodriguez, M.K. Khoshkbarchi, A. Soto and A. Arce, Enhanced oil recovery using the ionic liquid trihexyl(tetradecyl)phosphonium chloride: phase behaviour and properties, *RSC Adv.*, 2 (2012) 9392-9397.

[43] H. Xia, J. Yu, Y. Jiang, I. Mahmood and H. Liu, Physicochemical Features of Ionic Liquid Solutions in the Phase Separation of Penicillin(II): Winsor II Reversed Micelle, *Ind. Eng. Chem. Res.*, 46 (2007) 2112-2116.

[44] M.J. Trujillo-Rodríguez, P. González-Hernández and V. Pino, Analytical Applications of Ionic Liquid-Based Surfactants in Separation Science, in: *Ionic Liquid-Based Surfactant Science: Formulation, Characterization and Applications* (Eds. B.K. Paul, S.P. Moulik and W. Kunz), John Wiley & Sons, New Jersey, 2015, 475-501.

[45] J. Zhang, Ionic Liquid-Based Microemulsions, in: *Ionic Liquid-Based Surfactant Science: Formulation, Characterization and Applications* (Eds. B.K. Paul, S.P. Moulik and W. Kunz), John Wiley & Sons, New Jersey, 2015, 325-341.

[46] S. Livi, J.-f. Gérard and J. Duchet-Rumeau, Ionic Liquids, in: *Ionic Liquid-Based Surfactant Science: Formulation, Characterization and Applications* (Eds. B.K. Paul, S.P. Moulik and W. Kunz), John Wiley & Sons, New Jersey, 2015, 503-515.

[47] M. Freemantle, Designer solvents: ionic liquids may boost clean technology development, *Chem. Eng. News*, 76 (1998) 32-37.

[48] J. Łuczak, C. Jungnickel, M. Joskowska, J. Thöming and J. Hupka, Thermodynamics of micellization of imidazolium ionic liquids in aqueous solutions, *J. Colloid Interface Sci.*, 336 (2009) 111-116.

[49] S. Sakthivel, S. Velusamy, R.L. Gardas and J.S. Sangwai, Adsorption of aliphatic ionic liquids at low waxy crude oil–water interfaces and the effect of brine, *Colloids Surf., A*, 468 (2015) 62-75.

[50] S. Sakthivel, P.K. Chhotaray, S. Velusamy, R.L. Gardas and J.S. Sangwai, Synergistic effect of lactam, ammonium and hydroxyl ammonium based ionic liquids with and without NaCl on the surface phenomena of crude oil/water system, *Fluid Phase Equilib.*, 398 (2015) 80-97.

[51] S. Sakthivel, S. Velusamy, V.C. Nair, T. Sharma and J.S. Sangwai, Interfacial tension of crude oil-water system with imidazolium and lactam-based ionic liquids and their evaluation for enhanced oil recovery under high saline environment, *Fuel*, 191 (2017) 239-250.

[52] M.S. Benzagouta, I.M. AlNashef, W. Karnanda and K. Al-Khidir, Ionic liquids as novel surfactants for potential use in enhanced oil recovery, *Korean J. Chem. Eng*, 30 (2013) 2108-2117.

[53] A.Z. Hezave, S. Dorostkar, S. Ayatollahi, M. Nabipour and B. Hemmateenejad, Dynamic interfacial tension behavior between heavy crude oil and ionic liquid solution (1-dodecyl-3-methylimidazolium chloride ([C_{12}mim][Cl] + distilled or saline water/heavy crude oil)) as a new surfactant, *J. Mol. Liq.*, 187 (2013) 83-89.

[54] A. Z. Hezave, S. Dorostkar, S. Ayatollahi, M. Nabipour and B. Hemmateenejad, Effect of different families (imidazolium and pyridinium) of ionic liquids-based surfactants on interfacial tension of water/crude oil system, *Fluid Phase Equilib.*, 360 (2013) 139-145.

[55] S. Sakthivel, S. Velusamy, R.L. Gardas and J.S. Sangwai, Use of Aromatic Ionic Liquids in the Reduction of Surface Phenomena of Crude Oil–Water System and their Synergism with Brine, *Ind. Eng. Chem. Res.*, 54 (2015) 968-978.

[56] J.F. Pereira, R. Costa, N. Foios and J.A. Coutinho, Ionic liquid enhanced oil recovery in sand-pack columns, *Fuel*, 134 (2014) 196-200.

[57] A.Z. Hezave, S. Dorostkar, S. Ayatollahi, M. Nabipour and B. Hemmateenejad, Investigating the effect of ionic liquid (1-dodecyl-3-methylimidazolium chloride ([C_{12}mim] [Cl])) on the water/oil interfacial tension as a novel surfactant, *Colloids Surf., A*, 421 (2013) 63-71.

[58] M.S. Bin-Dahbag, A.A. Al Quraishi, M.S. Benzagouta, M.M. Kinawy, I.M. Al Nashef and E. AI-Mushaegeh, Experimental study of

use of ionic liquids in enhanced oil recovery, *J Pet Environ Biotechnol*, 4 (2014) 1-7.

[59] M.B. Dahbag, A. AlQuraishi and M. Benzagouta, Efficiency of ionic liquids for chemical enhanced oil recovery, *J. Pet. Explor. Prod. Technol.*, 5 (2015) 353-361.

[60] S. Gou, T. Yin, L. Yan and Q. Guo, Water-soluble complexes of hydrophobically modified polymer and surface active imidazolium-based ionic liquids for enhancing oil recovery, *Colloids Surf., A*, 471 (2015) 45-53.

[61] S. Palchowdhury and B. Bhargava, Ionic Liquids at Nonane–Water Interfaces: Molecular Dynamics Studies, *J. Phys. Chem. B*, 118 (2014) 13930-13939.

[62] S. Sakthivel, R.L. Gardas and J.S. Sangwai, Effect of alkyl ammonium ionic liquids on the interfacial tension of the crude oil–water system and their use for the enhanced oil recovery using ionic liquid-polymer flooding, *Energy Fuels*, 30 (2016) 2514-2523.

[63] K. Lunkenheimer, R. Miller, G. Kretzschmar, K.H. Lerche and J. Becht, Investigations on the possibility of purifying surfactant solutions by adsorption on solids, *Colloid. Polym. Sci.*, 262 (1984) 662-666.

[64] J.A. Riddick, W.B. Bunger and T.K. Sakano, *Organic solvents: physical properties and methods of purification*, Wiley, New York, 1986.

[65] T.M. Aminabhavi and V.B. Patil, Density, Refractive Index, Viscosity, and Speed of Sound in Binary Mixtures of Ethenylbenzene with Hexane, Heptane, Octane, Nonane, Decane, and Dodecane, *J. Chem. Eng. Data*, 42 (1997) 641-646.

[66] Y. Liu, R. DiFoggio, K. Sanderlin, L. Perez and J. Zhao, Measurement of density and viscosity of dodecane and decane with a piezoelectric tuning fork over 298–448 K and 0.1–137.9 MPa, *Sens. Actuators, A*, 167 (2011) 347-353.

[67] A.B. Pereiro, H.I.M. Veiga, J.M.S.S. Esperança and A. Rodríguez, Effect of temperature on the physical properties of two ionic liquids, *J. Chem. Thermodyn.*, 41 (2009) 1419-1423.

[68] C.M.S.S. Neves, P.J. Carvalho, M.G. Freire and J.A.P. Coutinho, Thermophysical properties of pure and water-saturated tetradecyltrihexylphosphonium-based ionic liquids, *J. Chem. Thermodyn.*, 43 (2011) 948-957.

[69] P. Kilaru, G.A. Baker and P. Scovazzo, Density and Surface Tension Measurements of Imidazolium-, Quaternary Phosphonium-, and Ammonium-Based Room-Temperature Ionic Liquids: Data and Correlations, *J. Chem. Eng. Data*, 52 (2007) 2306-2314.

[70] H.F.D. Almeida, J.A. Lopes-da-Silva, M.G. Freire and J.A.P. Coutinho, Surface tension and refractive index of pure and water-saturated tetradecyltrihexylphosphonium-based ionic liquids, *J. Chem. Thermodyn.*, 57 (2013) 372-379.

[71] B. Yoo, W. Afzal and M. J. Prausnitz, Effect of Water on the Densities and Viscosities of Some Ionic Liquids Containing a Phosphonium Cation, *Z. Phys. Chem.*, 227 (2013) 157-166.

[72] M. Blahušiak and Š. Schlosser, Physical properties of phosphonium ionic liquid and its mixtures with dodecane and water, *J. Chem. Thermodyn.*, 72 (2014) 54-64.

[73] E.J. González, N. Calvar, B. González and Á. Domínguez, Liquid−Liquid Equilibrium for Ternary Mixtures of Hexane + Aromatic Compounds + [EMpy][ESO_4] at T = 298.15 K, *J. Chem. Eng. Data*, 55 (2010) 633-638.

[74] G.P. Dubey, M. Sharma and N. Dubey, Study of densities, viscosities, and speeds of sound of binary liquid mixtures of butan-1-ol with n-alkanes (C_6, C_8, and C_{10}) at T = (298.15, 303.15, and 308.15) K, *J. Chem. Thermodyn.*, 40 (2008) 309-320.

[75] A. Mejía, H. Segura, M. Cartes and J.R. Pérez-Correa, Experimental determination and theoretical modeling of the vapor–liquid equilibrium and surface tensions of hexane + tetrahydro-2H-pyran, *Fluid Phase Equilib.*, 316 (2012) 55-65.

[76] S.C. Silvério, O. Rodríguez, J.A. Teixeira and E.A. Macedo, Liquid−Liquid Equilibria of UCON + (Sodium or Potassium) Phosphate Salt Aqueous Two-Phase Systems at 23 °C, *J. Chem. Eng. Data*, 55 (2010) 1285-1288.

[77] S. Burauer, T. Sachert, T. Sottmann and R. Strey, On microemulsion phase behavior and the monomeric solubility of surfactant, *Phys. Chem. Chem. Phys.*, 1 (1999) 4299-4306.

[78] T. Sottmann and R. Strey, Ultralow interfacial tensions in water–n-alkane–surfactant systems, *J. Chem. Phys.*, 106 (1997) 8606-8615.

[79] M.J. Rosen, H. Wang, P. Shen and Y. Zhu, Ultralow Interfacial Tension for Enhanced Oil Recovery at Very Low Surfactant Concentrations, *Langmuir*, 21 (2005) 3749-3756.

[80] B. Vonnegut, Rotating Bubble Method for the Determination of Surface and Interfacial Tensions, *Rev. Sci. Instrum.*, 13 (1942) 6-9.

[81] H. Cui, T.K. Hodgdon, E.W. Kaler, L. Abezgauz, D. Danino, M. Lubovsky, Y. Talmon and D.J. Pochan, Elucidating the assembled structure of amphiphiles in solution via cryogenic transmission electron microscopy, *Soft Matter*, 3 (2007) 945-955.

[82] J.R. Barnes, J. Smit, J. Smit, G. Shpakoff, K.H. Raney and M. Puerto, *Development of Surfactants for Chemical Flooding at Difficult Reservoir Conditions*, in: SPE Symposium on Improved Oil Recovery, Society of Petroleum Engineers, Tulsa, 2008.

[83] R.C. Nelson, The Effect of Live Crude on Phase Behavior and Oil-Recovery Efficiency of Surfactant Flooding Systems, *SPEJ*, 23 (1983) 501-510.

[84] J.L. Salager, Microemulsions, in: *Handbook of Detergents - part A: Properties, Surfactant Science Series* (Ed. B. Guy), Marcel Dekker, New York, 1999, 253-302.

[85] J. Marták and Š. Schlosser, Extraction of lactic acid by phosphonium ionic liquids, *Sep. Purif. Technol.*, 57 (2007) 483-494.

[86] M.G. Freire, P.J. Carvalho, R.L. Gardas, L.M.N.B.F. Santos, I.M. Marrucho and J.A.P. Coutinho, Solubility of Water in Tetradecyltrihexylphosphonium-Based Ionic Liquids, *J. Chem. Eng. Data*, 53 (2008) 2378-2382.

[87] S. Lago, M. Francisco, A. Arce and A. Soto, Enhanced Oil Recovery with the Ionic Liquid Trihexyl(tetradecyl)phosphonium Chloride: A Phase Equilibria Study at 75 °C, *Energy Fuels*, 27 (2013) 5806-5810.

[88] S. Lago, B. Rodríguez-Cabo, A. Arce and A. Soto, Water/oil/[$P_{6,6,6,14}$][NTf_2] phase equilibria, *J. Chem. Thermodyn.*, 75 (2014) 63-68.

[89] L. Wolf, H. Hoffmann, Y. Talmon, T. Teshigawara and K. Watanabe, Cryo-TEM imaging of a novel microemulsion system of silicone oil with an anionic/nonionic surfactant mixture, *Soft Matter*, 6 (2010) 5367-5374.

[90] K. Margulis-Goshen, M.C. di Gregorio, N.V. Pavel, L. Abezgauz, D. Danino, J. Vazquez Tato, V.H. Soto Tellini, S. Magdassi and L. Galantini, Drug-loaded nanoparticles and supramolecular nanotubes formed from a volatile microemulsion with bile salt derivatives, *Phys. Chem. Chem. Phys.*, 15 (2013) 6016-6024.

[91] R.E. Terry, Enhanced Oil Recovery, in: *Encyclopedia of Physical Science and Technology* (Ed. R.A. Meyers), Academic Press, New York, 2003, 503-518.

[92] V.C. Santanna, A.C.M. Silva, H.M. Lopes and F.A. Sampaio Neto, Microemulsion flow in porous medium for enhanced oil recovery, *J. Pet. Sci. Eng.*, 105 (2013) 116-120.

[93] C. Qin, J. Chai, J. Chen, Y. Xia, X. Yu and J. Liu, Studies on the phase behavior and solubilization of the microemulsion formed by surfactant-like ionic liquids with ε–β-fish-like phase diagram, *Colloid. Polym. Sci.*, 286 (2008) 579-586.

[94] J.L. Anderson, V. Pino, E.C. Hagberg, V.V. Sheares and D.W. Armstrong, Surfactant solvation effects and micelle formation in ionic liquids, *Chem. Commun.*, (2003) 2444-2445.

[95] B.-J. Lin and L.-J. Chen, Liquid–liquid equilibria for the ternary system water + tetradecane + 2-butyloxyethanol, *Fluid Phase Equilib.*, 216 (2004) 13-20.

[96] C. Browarzik, D. Browarzik and J. Winkelmann, Modeling of the three-phase equilibrium in systems of the type water + nonionic surfactant + alkane, *Fluid Phase Equilib.*, 296 (2010) 82-87.

[97] A. Bera and A. Mandal, Microemulsions: a novel approach to enhanced oil recovery: a review, *J. Pet. Explor. Prod. Technol.*, 5 (2015) 255-268.

[98] D.M. Mitrinovic, A.M. Tikhonov, M. Li, Z. Huang and M.L. Schlossman, Noncapillary-wave structure at the water-alkane interface, *Phys. Rev. Lett.*, 85 (2000) 582-585.

[99] S. Zeppieri, J. Rodríguez and A.L. López de Ramos, Interfacial Tension of Alkane + Water Systems, *J. Chem. Eng. Data*, 46 (2001) 1086-1088.

[100] R.E. Del Sesto, C. Corley, A. Robertson and J.S. Wilkes, Tetraalkylphosphonium-based ionic liquids, *J. Organomet. Chem.*, 690 (2005) 2536-2542.

[101] C.J. Bradaric, A. Downard, C. Kennedy, A.J. Robertson and Y. Zhou, Industrial preparation of phosphonium ionic liquids, *Green Chem.*, 5 (2003) 143-152.

[102] M. Blesic, J.N.C. Lopes, M.F.C. Gomes and L.P.N. Rebelo, Solubility of alkanes, alkanols and their fluorinated counterparts in tetraalkylphosphonium ionic liquids, *Phys. Chem. Chem. Phys.*, 12 (2010) 9685-9692.

[103] M.H. Cohen and D. Turnbull, Molecular Transport in Liquids and Glasses, *J. Chem. Phys.*, 31 (1959) 1164-1169.

[104] E. Gómez, N. Calvar and A. Domínguez, Thermal Behaviour of Pure Ionic Liquids, in: *Ionic Liquids - Current State of the Art* (Ed. P.S. Handy), InTech, 2015, 199-228. Available from: https://www.intechopen.com/books/ionic-liquids-current-state-of-the-art/thermal-behaviour-of-pure-ionic-liquids [accessed 18 October 2017].

[105] P. Brown, C.P. Butts, J. Eastoe, D. Fermin, I. Grillo, H.-C. Lee, D. Parker, D. Plana and R.M. Richardson, Anionic Surfactant Ionic Liquids with 1-Butyl-3-methyl-imidazolium Cations: Characterization and Application, *Langmuir*, 28 (2012) 2502-2509.

[106] K.S. Rao, T.J. Trivedi and A. Kumar, Aqueous-Biamphiphilic Ionic Liquid Systems: Self-Assembly and Synthesis of Gold Nanocrystals/Microplates, *J. Phys. Chem. B*, 116 (2012) 14363-14374.

[107] J. Jiao, B. Dong, H. Zhang, Y. Zhao, X. Wang, R. Wang and L. Yu, Aggregation Behaviors of Dodecyl Sulfate-Based Anionic Surface Active Ionic Liquids in Water, *J. Phys. Chem. B*, 116 (2012) 958-965.

[108] J. Jiao, B. Han, M. Lin, N. Cheng, L. Yu and M. Liu, Salt-free catanionic surface active ionic liquids 1-alkyl-3-methylimidazolium alkylsulfate: Aggregation behavior in aqueous solution, *J. Colloid Interface Sci.*, 412 (2013) 24-30.

[109] P. Brown, C. Butts, R. Dyer, J. Eastoe, I. Grillo, F. Guittard, S. Rogers and R. Heenan, Anionic Surfactants and Surfactant Ionic Liquids with Quaternary Ammonium Counterions, *Langmuir*, 27 (2011) 4563-4571.

[110] K. Srinivasa Rao, T. Singh, T.J. Trivedi and A. Kumar, Aggregation Behavior of Amino Acid Ionic Liquid Surfactants in Aqueous Media, *J. Phys. Chem. B*, 115 (2011) 13847-13853.

[111] A. Bera, K. Ojha, T. Kumar and A. Mandal, Phase Behavior and Physicochemical Properties of (Sodium Dodecyl Sulfate + Brine + Propan-1-ol + Heptane) Microemulsions, *J. Chem. Eng. Data*, 57 (2012) 1000-1006.

[112] I. Rodriguez-Palmeiro, I. Rodriguez-Escontrela, O. Rodriguez, A. Arce and A. Soto, Characterization and interfacial properties of the surfactant ionic liquid 1-dodecyl-3-methyl imidazolium acetate for enhanced oil recovery, *RSC Adv.*, 5 (2015) 37392-37398.

[113] A. Zeinolabedini Hezave, S. Dorostkar, S. Ayatollahi, M. Nabipour and B. Hemmateenejad, Mechanistic Investigation on

Dynamic Interfacial Tension Between Crude Oil and Ionic Liquid Using Mass Transfer Concept, *J. Dispersion Sci. Technol.*, 35 (2014) 1483-1491.

[114] M.C. Puerto and R.L. Reed, A Three-Parameter Representation of Surfactant/Oil/Brine Interaction, *SPEJ*, 23 (1983) 669-682.

[115] M. Bourrel and R.S. Schechter, *Microemulsions and related systems: formulation, solvency, and physical properties*, Editions Technip, Paris, 2010.

[116] O. Ghosh and C.A. Miller, Liquid-crystalline and microemulsion phase behavior in alcohol-free Aerosol-OT/oil/brine systems, *J. Phys. Chem.*, 91 (1987) 4528-4535.

[117] P.A. Winsor, Hydrotropy, solubilisation and related emulsification processes, *Trans. Faraday Soc.*, 44 (1948) 376-398.

[118] K. Spildo, L. Sun, K. Djurhuus and A. Skauge, A strategy for low cost, effective surfactant injection, *J. Pet. Sci. Eng.*, 117 (2014) 8-14.

USC
UNIVERSIDADE
DE SANTIAGO
DE COMPOSTELA

Appendix A: Publications

USC
UNIVERSIDADE
DE SANTIAGO
DE COMPOSTELA

1- I. Rodríguez-Escontrela, I. Rodríguez-Palmeiro, O. Rodríguez, A. Arce and A. Soto, Phase behavior of the surfactant ionic liquid trihexyltetradecylphosphonium bis(2,4,4-trimethylpentyl)phosphinate with water and dodecane, *Colloids Surf., A,* 480 (2015) 50-59.

2.- I. Rodriguez-Palmeiro, I. Rodriguez-Escontrela, O. Rodriguez, A. Arce and A. Soto, Characterization and interfacial properties of the surfactant ionic liquid 1-dodecyl-3-methyl imidazolium acetate for enhanced oil recovery, RSC Adv., 5 (2015) 37392-37398.

3.- I. Rodríguez-Escontrela, I. Rodríguez-Palmeiro, O. Rodríguez, A. Arce and A. Soto, Liquid–liquid–liquid equilibria for water + $[P_{6\,6\,6\,14}]$[DCA] + dodecane ternary system, *Fluid Phase Equilib.,* 405 (2015) 124-131.

4.- I. Rodríguez-Escontrela, I. Rodríguez-Palmeiro, O. Rodríguez, A. Arce and A. Soto, Characterization and phase behavior of the surfactant ionic liquid tributylmethylphosphonium dodecylsulfate for enhanced oil recovery, *Fluid Phase Equilib.,* 417 (2016) 87-95.

5.- I. Rodríguez-Escontrela, A. Arce, A. Soto, A. Marcilla, M. M. Olaya and J.A. Reyes-Labarta, Correlation of three-liquid-phase equilibria involving ionic liquids, *Phys. Chem. Chem. Phys.*, 18 (2016) 21610-21617.

6.- I. Rodriguez-Escontrela, M. C. Puerto, C. A. Miller, A. Soto, Ionic liquids for low-tension oil recovery processes: Phase behavior tests, *J. Colloid Interface Sci.,* 504 (2017) 404-416.

7.- I. Rodríguez-Palmeiro, I. Rodríguez-Escontrela, O. Rodríguez, S. Reichmann, M. M. Amro, Tributyl(tetradecyl)phosphonium Chloride Ionic Liquid for Surfactant Enhanced Oil Recovery, *Energy Fuels*, 31 (2017), 6758–6765.

USC
UNIVERSIDADE
DE SANTIAGO
DE COMPOSTELA

Appendix B: Resumen
(Summary, in Spanish)

USC
UNIVERSIDADE
DE SANTIAGO
DE COMPOSTELA

Los métodos tradicionales de extracción primaria y secundaria del petróleo extraen aproximadamente la tercera parte del crudo de un yacimiento. A pesar de la necesidad de aumentar el uso de energías renovables, la dependencia actual de los combustibles fósiles como fuente de energía, especialmente del petróleo, es innegable. Pero además, éste es la base de la industria petroquímica que genera miles de compuestos químicos usados en la producción de plásticos, adhesivos, detergentes, tintes, fertilizantes y muchos otros productos. Con la reducción del descubrimiento de nuevos yacimientos, la mejora de las técnicas de recuperación jugará un papel decisivo para poder responder a la demanda de energía en los próximos años y poder mantener nuestro actual estilo de vida.

La extracción terciaria o mejorada del petróleo ("Enhanced Oil Recovery", EOR) consiste en la utilización de medios que aumentan la movilidad del fluido en el yacimiento conjuntamente con los métodos de extracción secundaria (inyección de fluidos para generar un gradiente de presión), permitiendo una extracción mucho más eficaz. Entre los métodos de EOR hay que citar: los métodos térmicos, los métodos de desplazamiento mediante fluido miscible (CO_2 el más utilizado) y los métodos químicos. Estos últimos se consideran los más eficaces, sin embargo su coste es elevado y es necesario mejorar su aplicabilidad puesto que se ven muy afectados por múltiples parámetros: tipo de crudo, temperatura, presión, porosidad, permeabilidad, naturaleza de los productos químicos, necesidad de aditivos, etc.

De los métodos químicos de recuperación del petróleo, el uso de surfactantes es quizás el de mayor potencial. Se basa en la inyección de una disolución acuosa de baja concentración de surfactante dentro de la reserva, con el fin de reducir la tensión interfacial existente entre el agua y el petróleo contenido en los poros de las rocas. De esta forma, se reducen las fuerzas capilares y se mejora la movilidad del crudo atrapado en el yacimiento pudiendo ser arrastrado a la superficie. El control de la movilidad es importante para que el proceso sea efectivo, por eso, habitualmente, la inyección del sistema micelar se combina con la inyección de polímero que aumenta la viscosidad del agua y la eficiencia de barrido, evitando la formación de digitaciones.

Los líquidos iónicos surfactantes (SAILs) constituyen una clase de surfactantes que ha sido recientemente propuesta para mejorar esta aplicación. El uso de SAILs expande las opciones de formulación existentes con los surfactantes tradicionales. La principal ventaja es

que estos compuestos se pueden diseñar de acuerdo a los requerimientos de un yacimiento específico, especialmente para las reservas de petróleo con salinidades y temperaturas elevadas donde el uso de los surfactantes convencionales es poco eficaz. Asimismo, si se seleccionan líquidos iónicos (ILs) líquidos a temperatura ambiente, podrían ser transportados a la reserva sin diluir (de forma pura), algo que es inviable con la mayoría de los surfactantes convencionales. Además, debido a los anillos característicos de muchos ILs, con una gran facilidad para formar enlaces de hidrógeno, la temperatura Krafft de estas sales es frecuentemente más baja que la de los surfactantes comunes similares. Por otro lado, estudios recientes muestran que las disoluciones acuosas de ILs (con y sin hidrocarburo) tienen una alta estabilidad en condiciones extremas de salinidad y/o temperatura.

Una aproximación válida para el estudio de sistemas de interés en la extracción del petróleo, a pesar de que son mezclas complejas (agua, sales, surfactante, componentes del petróleo…), es considerarlos como un sistema pseudo-ternario surfactante + agua/salmuera + hidrocarburo. Así, a temperatura y presión constante, Winsor definió tres tipos de diagramas básicos para estos sistemas: Winsor Tipo I, Tipo II y Tipo III. El diagrama Tipo III comprende una región trifásica rodeada por tres zonas bifásicas y una región monofásica. En lo que concierne a los sistemas cuya composición global se encuentra en la zona trifásica, se separan en tres fases en equilibrio: una fase acuosa y una fase aceitosa que contienen esencialmente agua e hidrocarburo, respectivamente, y una fase intermedia que contiene el surfactante con agua e hidrocarburo solubilizados. En el diagrama Tipo III, las interacciones se equilibran y el surfactante forma lo que se llama la formulación óptima, ya que dicha situación físico-química corresponde a la existencia de una tensión interfacial mínima. La presencia de sal juega un papel clave en el comportamiento de fase de estos sistemas. El incremento de salinidad permite una transición de Winsor Tipo I a Winsor Tipo II, pasando por un sistema óptimo Winsor Tipo III. Por eso, en la definición de una formulación para EOR, es importante determinar la salinidad óptima (salinidad que proporciona un comportamiento de fase Tipo III y una tensión interfacial mínima) para un determinado surfactante. La mezcla de surfactantes es otra posibilidad que está cobrando relevancia últimamente, en ese caso será necesario definir la proporción de surfactantes que a determinada salinidad genera un sistema Winsor Tipo III.

Uno de los grandes desafíos en EOR es encontrar un surfactante o mezcla de surfactantes capaz de generar un sistema Winsor Tipo III con una fase intermedia donde el surfactante solubilice cantidades significativas y equilibradas de agua e hidrocarburo, ya que esto conduce a una tensión interfacial ultra-baja. Por tanto, el estudio del comportamiento de fase de estos sistemas es la primera etapa en la consecución de este objetivo.

Objetivo

El principal objetivo de esta tesis es utilizar ILs con carácter surfactante para obtener formulaciones óptimas que sean capaces de mejorar los métodos químicos de extracción mejorada de petróleo. Para alcanzarlo, se fijan dos objetivos específicos: el primero, con un carácter más fundamental, consiste en estudiar el equilibrio de fases para sistemas ternarios compuestos de agua, alcano e ILs; el segundo, más centrado en la aplicación real, consiste en buscar formulaciones óptimas mediante las herramientas empleadas tradicionalmente en la extracción mejorada de petróleo, evaluando de manera visual el comportamiento de fase de sistemas multicomponente (con presencia de sales).

Experimental

Para la determinación del equilibrio en sistemas agua + SAIL ($[P_{6\,6\,6\,14}][DCA]$, $[P_{6\,6\,6\,14}][(iOc)_2PO_2]$ o $[P_{4\,4\,4\,14}]Cl$) + alcano (*n*-hexano o *n*-dodecano), el estudio se inició con la determinación de las curvas de solubilidad a la temperatura de trabajo mediante el método del punto de niebla. Posteriormente, se determinó el equilibrio líquido-líquido, en celdas termostatizadas especialmente diseñadas para la aplicación. El tiempo de agitación fue de 2 horas, y el de reposo entre 24 y 72 horas. Las composiciones de equilibrio de agua y alcano se determinaron mediante cromatografía de gases (HP 6890) utilizando el método del patrón interno. La composición del IL se estableció por diferencia. Cuando las fases eran prácticamente alcano o agua puros, se utilizó el método de espectroscopia ICP (óptico) para probar que la composición de IL era menor de 0.05 wt%. De una forma similar, cuando el contenido en agua de la fase orgánica era muy pequeño, éste fue determinado mediante valoración (Karl-Fischer).

La densidad y la viscosidad de las fases homogéneas se determinó mediante un densímetro (Anton Paar DMA 5000) con corrección de viscosidad y autocontrol de temperatura y un viscosímetro capilar (Ubbelohde), respectivamente. La medida de las tensiones interfaciales

entre las diferentes fases se llevó a cabo en un tensiómetro de gota giratoria (Kruss Site100).

Además, se emplearon diferentes tipos de microscopía para caracterizar los agregados formados por los SAILs o las microemulsiones. Entre ellos: microscopía electrónica de transmisión (Zeiss Libra 200), microscopía electrónica de transmisión criogénica (Jeol modelo Jem 2010 FEG) y microscopía óptica (Leica TCS SP2). El radio hidrodinámico de los agregados fue medido usando dispersión dinámica de luz (Malvern Zen 3600 ZetaSizer Nano ZS).

En el caso de los SAILs $[P_{4\ 4\ 4\ 14}]Cl$, $[P_{4\,4\,4\,1}][DS]$, $[C_{12}mim]Br$ y $[C_4mim]AOT$, se realizó una evaluación visual del comportamiento de fase en sistemas multicomponentes (en presencia de sal). Se escogió en la mayoría de los casos *n*-octano como crudo modelo, utilizando también en algunos casos *n*-dodecano o butil-benceno y hexil-benceno para bajar la salinidad óptima. Se llevaron a cabo estudios de salinidad usando pipetas selladas. Los escaneos se llevaron a cabo cambiando la salinidad para los surfactantes puros y la relación de surfactantes para una salinidad fija en el caso de las mezclas de surfactantes (SAILs o SAILs con surfactantes convencionales).

Las muestras se agitaron aproximadamente 24 horas a temperatura ambiente y luego se dejaron equilibrar hasta que el volumen de las fases permanecía constante. Los ensayos a temperaturas más elevadas se llevaron a cabo introduciendo las pipetas selladas en un tubo de ensayo con aceite de silicona situado en un calefactor de bloque seco, y fueron agitados a mano hasta que los volúmenes permanecieron contantes. Estos volúmenes sirvieron para calcular los parámetros de solubilización (volumen de agua e hidrocarburo dividido por volumen de surfactante), y con ellos la salinidad o relación de mezcla óptima.

Dado que el SAIL $[P_{4\,4\,4\,1}][DS]$ se sintetizó por primera vez en este trabajo, para la caracterización de su comportamiento de agregación se empleó un tensiómetro (Krüss K11) utilizando el método de la placa Wilhelmy para medir las tensiones superficiales, y un conductivímetro (Basis 30 Crison) para medir la conductividad eléctrica. Para determinar las propiedades físicas se empleó un densímetro Anton Paar DMA 5000 y un reómetro (Anton Para MCR301) para determinar la viscosidad. Las propiedades térmicas de este IL se determinaron empleando un calorímetro diferencial de barrido (TA instruments Q2000) para determinar su temperatura de fusión, y una balanza de análisis termogravimétrico (TA instruments Q500) para determinar su

temperatura de descomposición. El índice de refracción se determinó empleando un refractómetro (Atago RX-5000).

Resultados y discusión

El diagrama de fases para el sistema ternario agua + $[P_{6\,6\,6\,14}][DCA]$ + alcano se determinó (a diferentes temperaturas y presión atmosférica) con *n*-hexano y *n*-dodecano. En ambos casos, los diagramas de fase muestran una región liquido-líquido-líquido que consiste en una fase que es prácticamente alcano, una fase prácticamente agua y una fase intermedia en la que el LI solubiliza agua y alcano. Estos sistemas pueden ser clasificados como Winsor Tipo III y la región trifásica se forma sin la necesidad de añadir co-surfactantes. El sistema trifásico (generado debido a la inmiscibilidad de los tres pares binarios) permanece con el incremento de temperatura. La región trifásica, a una determinada temperatura, es mayor en el caso del *n*-dodecano debido a la mayor inmiscibilidad de este alcano con el IL. El incremento de la temperatura (de 298.15 a 348.15 K en el caso del *n*-dodecano y de 298.15 a 323.15 K en el caso del *n*-hexano) tiene poca influencia sobre el equilibrio.

Se sintetizó un segundo SAIL cambiando el anión. En el caso del $[P_{6\,6\,6\,14}][(iOc)_2PO_2]$, se observó completa miscibilidad con *n*-dodecano. El diagrama de fases obtenido con agua y *n*-dodecano también puede ser clasificado como Winsor Tipo III. Sin embargo, este sistema se diferencia del anterior en que la región bifásica al lado del binario agua + *n*-dodecano no es despreciable y, además, el comportamiento de fase se ve enormemente afectado por la temperatura, disminuyendo el tamaño de la región trifásica al aumentar la temperatura y desapareciendo a 308 K.

Con ambos SAILs, los sistemas Winsor Tipo III se mantuvieron en presencia de sal y se detectó una drástica reducción de la tensión interfacial agua + alcano, aunque lejana a los valores ultra-bajos requeridos en EOR. Se midieron también las densidades y viscosidades de las fases que mostraron valores en concordancia con la composición de las fases.

Se decidió estudiar el IL $[P_{4\,4\,4\,14}]Cl$ debido a su miscibilidad con agua y se determinó el equilibrio líquido-líquido para el sistema ternario agua + $[P_{4\,4\,4\,14}]Cl$ + *n*-dodecano. Sin embargo en este caso el IL resultó ser demasiado hidrofílico, presentando un comportamiento de fase Winsor Tipo I tanto a 298.15 K como a 348.15 K. Este comportamiento se mantuvo en presencia de sal.

Todos los datos de equilibrio fueron satisfactoriamente correlacionados empleando el modelo Non-Random Two Liquid (NRTL).

Para el IL $[P_{4\,4\,4\,1}][DS]$ se obtuvo una concentración micelar crítica de 0.89 mmol·kg^{-1} determinada mediante la medida de la tensión superficial (0.91 por conductimetría). Los parámetros de agregación obtenidos incentivaron su estudio para EOR.

Utilizando *n*-octano o *n*-dodecano como hidrocarburo, los ensayos de salinidad mostraron que el IL $[P_{4\,4\,4\,1}][DS]$ forma una fase viscosa no alcanzando nunca el comportamiento Winsor Tipo II. Con butil-benceno o hexil-benceno, se formaron sistemas Winsor Tipo II a concentraciones muy bajas de sal. El mismo comportamiento se encontró con $[C_4mim]AOT$ y *n*-octano. Se obtuvieron salinidades óptimas muy bajas, con comportamiento Winsor Tipo II en prácticamente todo el intervalo de salinidades. En el caso de los SAILs $[P_{4\,4\,4\,14}]Cl$ y $[C_{12}mim]Br$ con *n*-octano, por el contrario, se obtuvo un comportamiento Winsor Tipo I en todo el rango de salinidades (salinidades óptimas superiores al 15 wt% NaCl).

Como alternativa, se estudiaron sus mezclas o la mezcla de un SAIL con un surfactante tradicional como una opción de diseño para hallar una formulación óptima a una salinidad de una fuerza iónica similar al agua del mar.

Los resultados pusieron de manifiesto que en la mezcla de IL catiónico y aniónico $[C_{12}mim]Br/[C_4mim]AOT$ el comportamiento de fase está influenciado por la gran diferencia de avidez por el agua entre los LIs, que domina las interacciones electroestáticas ente los iones. Se encontró una mezcla óptima en la cual se forma una fase microemulsión con una alta solubilización de hidrocarburo y salmuera, indicando una tensión interfacial suficientemente baja para recuperar petróleo, pero el comportamiento es demasiado sensible a la relación de surfactantes utilizada.

Los ensayos con las mezclas del surfactante tradicional aniónico $IOS_{15\text{-}18}$ y el IL aniónico $[C_4mim]AOT$ revelaron que existe un óptimo cuando las fracciones másicas de uno y de otro son prácticamente iguales, utilizando *n*-octano como hidrocarburo y NaCl como sal. Cuando el IL se reemplaza por el surfactante tradicional (Na-AOT) se observó el mismo comportamiento. Sin embargo, cuando se usa una salmuera con iones divalentes, empleando el SAIL con el anión $[C_4mim]$ se consigue que el comportamiento de la mezcla sea superior, ya que cuando se usa Na-AOT el comportamiento de fase no es

tolerante a sales divalentes y aparecen fases altamente viscosas e indeseables para EOR. Los parámetros de solubilización usando el SAIL son adecuados a 298.15 K pero disminuyen con la temperatura.

Las mezclas de IOS_{15-18} con los SAILs catiónicos $[P_{4\ 4\ 4\ 14}]Cl$ y $[C_{12}mim]Br$, pese a que los ILs y el surfactante convencional individualmente muestran un comportamiento Winsor Tipo I con la salinidad del agua de mar, presentan dos óptimos uno con exceso de IL y otro con exceso de IOS_{15-18} a 298.15K. Como tanto el IOS_{15-18} como los surfactantes catiónicos son hidrofílicos, el surfactante cataniónico producido por su interacción electrostática hace el comportamiento de fase de la mezcla de surfactantes menos hidrofílico que los individuales. En el caso del $[P_{4\ 4\ 4\ 14}]Cl$, cuando se aumenta la temperatura, el segundo óptimo desaparece. En cualquier caso, por razones económicas el óptimo de mayor interés es el que se forma a menor concentración de IL (15 wt%).

Los mejores parámetros de solubilización, desde 298.15 hasta 398.15 K, se obtuvieron con la mezcla $IOS_{15-18}/[C_{12}mim]Br$. Además, la disolución acuosa de mezcla óptima de surfactantes no exhibe separación de fase y contiene agregados de radio hidrodinámico de 20 nm por lo que parece adecuada para su inyección en los pozos. Un comportamiento similar de la fase microemulsión y de la disolución acuosa se halló cuando el IL catiónico fue reemplazado por el surfactante catiónico $C_{12}TAB$. La tensión interfacial entre la formulación óptima, 1 wt% $IOS_{15-18}/[C_{12}mim]Br$ (15 wt% de IL) en salmuera con iones divalentes, y *n*-octano a 25 ºC fue ~0.002 mN/m, un valor algo menor que el obtenido con el sistema IOS_{15-18} /$C_{12}TAB$.

Conclusiones

Los ILs $[P_{6\ 6\ 6\ 14}][DCA]$ y $[P_{6\ 6\ 6\ 14}][(iOc)_2PO_2]$ dieron lugar a sistemas Winsor Tipo III con agua/salmuera y alcano, sin necesidad de añadir ningún co-surfactante, a diferentes temperaturas y presión atmosférica. A pesar de ser el comportamiento buscado en EOR, las microemulsiones formadas presentaron una elevada proporción de líquido iónico y una solubilización muy diferente de agua y alcano, lo que se traduce en una reducción de la tensión interfacial lejana a la requerida en EOR. Además, la falta de solubilidad de estos ILs en agua se añade como problema para emplearlos en extracción mejorada de petróleo.

En el caso del IL $[P_{4\ 4\ 4\ 14}]Cl$, miscible con agua, su comportamiento con agua/salmuera y *n*-dodecano dio lugar a sistemas Winsor Tipo I a

298.15 K y a 348.15 K, lo que en principio también desaconseja su uso en EOR.

A pesar de que estos SAILs no pueden presentarse como una alternativa interesante para EOR, la región trifásica obtenida con agua y alcano hace que sean candidatos para ser usados en aplicaciones que requieren microemulsiones (reacciones químicas, síntesis de nanopartículas, etc.). Además, el hecho de que el equilibrio líquido-líquido junto con el equilibrio líquido-líquido-líquido sea adecuadamente correlacionado con el modelo NRTL facilita su aplicación.

Los ensayos de salinidad mostraron que los SAILs aniónicos $[P_{4\,4\,4\,1}][DS]$ y $[C_4mim]AOT$ son demasiado lipofílicos y los SAILs catiónicos $[P_{4\,4\,4\,14}]Cl$ y $[C_{12}mim]Br$ demasiado hidrofílicos para ser usados solos en EOR.

Con varias de las mezclas de surfactantes estudiadas se consiguieron formulaciones óptimas con *n*-octano y salmuera (salinidad fija similar al agua de mar y conteniendo iones divalentes) adecuadas para recuperaciones a bajas temperaturas. La formulación más prometedora se obtuvo con la mezcla $IOS_{15\text{-}18}/[C_{12}mim]Br$ (~15% $[C_{12}mim]Br$) puesto que tiene parámetros de solubilización adecuados en un amplio intervalo de temperaturas, da lugar a tensiones ultra-bajas, y la disolución acuosa es adecuada para su inyección al no exhibir separación de fase ni problemas de estabilidad. Esta mezcla es de especial interés porque el surfactante $IOS_{15\text{-}18}$, tradicionalmente usado en EOR, a bajas temperaturas y en salmueras duras normalmente precipita.

Como futuro trabajo de investigación se propone llevar a cabo experimentos de inundación ("core flooding") para asegurar que la mezcla óptima se podría inyectar, así como para asegurar su movilidad a través del lecho sin una excesiva retención de surfactante.

La investigación en el uso de SAILs en EOR es todavía muy reciente pero los resultados obtenidos son prometedores especialmente para altas temperaturas y salinidades. La investigación futura debería centrarse en el estudio de mezclas de SAILs y de surfactantes tradicionales con SAILs para mejorar las propiedades de los surfactantes individuales.

USC
UNIVERSIDADE
DE SANTIAGO
DE COMPOSTELA